November 2016

Study of Charge Transport Mechanism in Microbial Nanowires

Ramesh Adhikari
University of Massachusetts - Amherst

STUDY OF CHARGE TRANSPORT MECHANISM IN MICROBIAL NANOWIRES

A Dissertation Presented

by

RAMESH ADHIKARI

Submitted to the Graduate School of the
University of Massachusetts Amherst in partial fulfillment
of the requirements for the degree of

DOCTOR OF PHILOSOPHY

September 2016

Physics

STUDY OF CHARGE TRANSPORT MECHANISM IN MICROBIAL NANOWIRES

A Dissertation Presented

by

RAMESH ADHIKARI

Approved as to style and content by:

Mark T. Tuominen, Chair

Derek R. Lovley, Member

V. Adrian Parsegian, Member

Jun Yan, Member

Rory Miskimen, Department Chair
Physics

ACKNOWLEDGMENTS

As I write this dissertation, I must thank many people who have influenced me directly or indirectly to give a direction to my journey. I would not be in this position today had there been no support, motivation and assistance from so many people that I had privilege to know and learn from. I would like to thank my advisor Prof. Mark T. Tuominen for accepting me to the group and showing me the way forward during my graduate career. Thank you for the motivating discussions and nudges here and there to help me think like a physicist. I would like to thank Prof. Derek R. Lovley for being an unofficial advisor and for involving me in your work of unraveling the mystery of conductive pili. Also, thank you for your support and guidance throughout the process. I would also like to thank Prof. Nikhil S. Malvankar for introducing and enticing me into this exciting field of research. I thank you for your close mentorship and guidance to plan, organize and conduct experiment I was learning to be an experimentalist. I thank Prof. Adrian Parsegian and Prof. Jun Yan for serving in my thesis committee and providing their helpful insights. Thanks to Prof. Parsegian for many insightful discussions during this process.

I would like to thank John Nicholson for teaching me to use many kinds of instruments in the cleanroom, for always being around for discussions and troubleshooting instruments, and of course, his patience. Peng Lin deserves a big thanks for being the first person to go to with problems with any equipment in the cleanroom and suggestions and discussions during nano-fabrication. Thanks to Shuang Pi as well for the help I received in the cleanroom and more importantly tirelessly fabricating nano-imprint lithography devices for my studies on microbial nanowires. Also, thanks

to Hao Jiang and Martin Muthee for their help in cleanroom. Martin deserves another acknowledgment for sharing his carbon nanotubes with me for measurement. Thanks to Lawrence (Larry) Renna for teaching me to perform X-ray diffraction and helping me with acquiring diffraction spectroscopy of the pili samples. Thanks to Yiming Chen and Su-Wei Chang for their help with wire-bonding. I would like to thank Weiguo Huang for sharing his mask holders and teaching me the method of shadow masking to fabricate electrodes on top of nanowire network.

I would like to thank my fellow group members Dan Wang, Wenming Ju and Kun Wang as well as past members Stefan Dickert, Rukhsan Thantirige and Craig Versek for being the people I can always go back to and get help from, suggestions and learn techniques. Thanks to Craig for taking me under his wing during my first summer at UMass and involving me in programming and electrochemical impedance experiments. I would like to thank Walter Pollard and Rick Miastkowski from machine shop for teaching machining. Thanks to Rick for always being available for helping out with machining when needed. Also, I would like to thank Jane Knapp of Physics Department for taking care of all the bureaucracy.

I would like to thank Joy Ward for preparing pili samples and also performing AFM imaging, and paperwork and orders. Also, thanks to Zhiqiang Zhao for his help with AFM imaging. It was also a pleasure working with David Walker, Yang Tan, Ke Xiao, and others in Lovley group. I would like to thank Prof. Eric Martz for teaching the techniques of molecular modeling and help me develop structural understanding of pili.

Special thanks to my parents who have always motivated me to get the best education possible despite themselves never having a chance to attend a school. Also, thanks to my sister and other family members and friends for their continual support. Last, but not least, thanks to my now wife Yelena Kobaliya for being with me since our college days and sharing the pain and joy of this adventure.

ABSTRACT

STUDY OF CHARGE TRANSPORT MECHANISM IN MICROBIAL NANOWIRES

SEPTEMBER 2016

RAMESH ADHIKARI

B.A., BEREA COLLEGE

M.S., UNIVERSITY OF MASSACHUSETTS AMHERST

Ph.D., UNIVERSITY OF MASSACHUSETTS AMHERST

Directed by: Professor Mark T. Tuominen

Conductivity of an individual proteinaceous filaments, called pili or microbial nanowires, produced by wild type *Geobacter sulfurreducens* was measured using a low-noise electrical transport technique. It was shown that the conductivity is diminished if aromatic amino acid residues are removed from the pili. It was demonstrated that the conductivity of *G. sulfurreducens* pili is similar to that of synthetic organic polymers and is related to the respiration rate of the bacteria. Conductivity measurements were performed on microbial nanowires produced by other species of *Geobacter* with a different aromatic amino acid distribution along the wire. Also, measurements on a mutated pili with a higher aromatic residue content is presented. All these studies consistently demonstrated that the aromatic amino acid residues are essential for making conduction along microbial nanowires possible.

Optical studies involving UV-Vis spectroscopy and X-ray diffraction of *G. sulfurreducens* and aromatic residue rich mutant pili are also presented. Denaturation

of cytochromes was observed by lowering pH of the pili solution, implying that it is the pili themselves and not cytochromes attached to them, which are essential for conduction. The optical band gap of wild type pili with different doping level is discussed. Band gap narrowing with increasing doping level was observed. Finally, conductance tuning of wild type pili with field gating is also presented and possible transport mechanism, which can be inferred based on well established free-electron system, is discussed.

TABLE OF CONTENTS

LIST OF TABLES

Table **Page**

LIST OF FIGURES

Figure **Page**

CHAPTER 1

CHARGE TRANSPORT IN BIOLOGY

Charge transport phenomena are fundamental to biological processes. Biological processes such as cell division, DNA replication, RNA transcription, protein synthesis, and metabolism are highly organized, yet involve complex chemical processes which require precise motion of charges throughout the system.[1] These chemical processes are combinations of simpler partial reactions such as proton or atom group transfer, or even more fundamental - electron transfer reactions.[2] Proton or atom transfer reaction involve bond breaking and reorganization for the reactions to complete. During electron transfer reactions, only bond lengths and angles are adjusted as electrons are transferred from one site, called donor, to another site, the acceptor. This seemingly simple process of electron transfer turns out to have a central role in transformation of organic and inorganic compounds in metabolic processes such as photosynthesis and respiration.[3]

From the condensed matter perspective, most of the interest in biological charge transport has been with electron transport because, in addition to being a fundamental process, electron transfer encompasses various physically intriguing and biologically significant phenomena. Studies so far have shown that the electron transport mechanism in biological systems vary significantly from tunneling, hopping, variable range hopping and metallic to coherent transport depending on purpose of the biological systems. Some of the recent developments in understanding of these mechanisms point out that charge transport in biological systems do not necessarily fit the known charge transport mechanisms in condensed matter systems. Over millions of years

these biological systems have been fine tuned in myriad clever ways to ensure efficient means to complete processes. Therefore, charge transport studies in biological systems pose a challenging yet intriguing problem to be addressed.

1.1 Charge Transport in Biology

One of the widely studied charge transport mechanisms in biological systems has been photosynthesis, a widespread and essential biological process that makes complex life-forms on earth possible. During photosynthesis, photon energy from the sun is absorbed as excitons and, through biochemical processes, is stored as ATPs before that energy is used to reduce carbon dioxide and store as chemical energy. As seemingly complex the process is, once the photon is absorbed, the efficiency of photosynthesis is actually about 99%.[4] This is fascinating because condensed matter systems at ambient room temperature do not have such an efficiency of electron transport. Phonon resistance, impurities, defects in crystal structures and grain boundaries introduce disorders leading to resistance for electronic transport. Therefore, the dissipation of electron energy in condensed matter systems is quite significant and hence not nearly as efficient.

This raises questions as to how the complex biological process of photosynthesis can develop such an efficient electron conduction mechanism at ambient temperature. Among various theories that debate on the mechanism of the charge transport, environment assisted quantum transport (ENAQT) theory has been leading the discussions. According to ENAQT theory, an efficient pathway for excitons transport is formed due to thermal dephasing of the localized sites and quantum coherence thus created by delocalized excitons in the disordered system.[5] This is counterintuitive to what is known in condensed matter systems where dephasing the localized sites essentially acts as increasing noise and further deteriorates the conduction through localized sites.

Unlike in photosynthesis, charge transport in other biological systems such as proteins and DNA is not known to be coherent. It has been reported that delocalization of electrons due to the pi-stacking of bases of DNA helixes could make them conductive,[6, 7] even at low temperatures.[8] While there are other reports which suggest that they are insulating.[9, 10, 11] These opposing observations could be due to various artifacts introduced in the experiments such as the detailed nature of electrical contact that can provide either metallic contact or a Schottky barrier, mechanical stress which can disrupt delocalized channel of the charge transport and the DNA environment is exposed which can introduce an ionic channel influencing the conduction.[12] This provides a perspective on the challenge of performing controlled experiments in biological samples and on understanding underlying mechanisms for possible biological function.

Protein is another biological material that has been a topic of investigation of conduction mechanism. Electron transfer through proteins makes it possible for the existence of processes such as photosynthesis, respiration and enzymatic reactions, but the mechanism of the charge transport has not been completely understood.[13] In addition to understanding biological processes, the attraction towards understanding charge transport through proteins also lies in their potential application in molecular electronics.[14] Proteins are complex molecules that have evolved for various physiological processes. This has resulted in proteins becoming fully functional entities which can be viewed as nanometer scale machines for biochemical processes. They offer an alternative to simple molecular systems, such as conjugated organic polymers, as the ones rich in functionalities such as molecular selectivity, long-term stability and their diverse optical, electrical, mechanical, and chemical properties,[14] as well as low cost and toxicity.[15] In addition, proteins have self-assembly properties that surpass that of DNA making them better candidates for self-assembled molecular electronics.[12]

Electron transfer in proteins is possible due to presence of close-packed residues such as aromatic amino acids[16, 17, 18] as their building blocks or the presence of conjugated electron system with metal ions such as in cytochromes or azurine, referred to as metalloproteins.[19, 20] Electron transfer has been reported in both cases for the residues separated as far as 20 Å. From the solid state perspective, electron transfer studies in the protein have been done using various methods involving nanometer-scale single molecule approaches to densely packed bulk structure sandwiched between conducting electrodes.[12, 14]

It has been found that the conduction within the protein is similar to the conjugated organic molecules despite the measurement techniques.[14] This is very exciting because, until a few decades ago, it had been thought that proteins are intrinsically nonconductive.[21] However, most of these measurements were done on the protein molecules of length less than 10 nm. This, along with different structural conformations, and affinity towards other protein filaments creating entangled mesh, present a challenge for devising experimental solid state measurement techniques and electronics.[12]

1.2 Charge transport in pili

In 2005, it was reported that bacteria *Geobacter sulfurreducens* produce long proteinaceous conductivity filaments of nanoscale diameter called pili.[21] These pili hence have been termed microbial nanowires. *Geobacter sulfurreducens* are anaerobic bacteria found in marshy lands such as river banks or lake beds. Electrons generated during metabolic process of the bacteria are channeled out to metal or metal oxides through these nanowires which are about 3 nm in diameter and about 2 μm in length. Hence, proteins in a pilus present a system in which complex peptides are assembled in a specific conformation to form a long conductive pathway. In recent attempts to

understand the mechanism of the charge transport through these microbial nanowires, various physical experiments on biofilms and pili networks have been performed.

Delocalization of the injected charges on pili and inverse temperature dependence of the conductivity of the pili network and biofilm have suggested metallic-like charge transport mechanism in pili.[22, 23] Structural studies from x-ray diffraction and homology modeling have shown that the conduction is possibly due to pi-conjugation of aromatic amino acid residues which form alpha-helical structure at the core of the pili.[24, 25]

While a substantial number of studies have been performed about the charge transport through experimentation on biofilm and pili networks, some mechanistic questions such as intrinsic conductivity of pili, its response to changing environment, and investigating the role of amino acids on the conduction of individual pili were yet to be clarified when I undertook the project. Dependence of the conductivity in response to the environment will not only help us deepen our understanding of the mechanism of the charge transport, but also explore possible application of these microbial nanowires. Furthermore, optical investigation of the pili will provide us with complementary information about the mechanism of the conduction.

In the second chapter of this dissertation, I will be presenting some of the studies that we have performed to better understand the charge transport properties of individual pili and conclusions so far drawn. Conductivity studies of pili from naturally found *Geobacter sulfurreducens* along with aromatic amino acid deficient mutant pili will be presented. In the third chapter, I will present a study on genetically engineered pili from mutated *Geobacter* species along with aromatic residue rich pili from *Geobacter metallireducens* and from *Geobacter uraniireducens*.

In fourth chapter, I will discuss other electronic properties such as carrier density and mobility based on conductivity studies and recent modeling studies of pili. Optical studies will also be presented and the effect of doping on the band gap of

wild type pili and the structural conformation of mutant pili is explored. Finally, in the fifth chapter, I will present the conclusions of the studies performed during my research and discuss suggestions for future work.

CHAPTER 2

CONDUCTIVITY OF INDIVIDUAL MICROBIAL NANOWIRES

2.1 Introduction

Pili produced by *Geobacter sulfurreducens* are conductive wire-like structures of about 3 nm in diameter and about 10-20 μm in length and hence are also termed as microbial nanowires. In order to understand the mechanism of the charge transfer through these nanowires, one of the initial processes of investigation would be studying the response of the nanowire samples to applied electric fields. This also enables us to quantify the electronic properties such as conductivity and mobility values intrinsic to the nanowires.

Previously, studies have been performed to investigate the charge transport mechanism in nanowire biofilm and networks.[22] It was shown that the conductivity of biofilm and network of *G. sulfurreducens* pili is comparable to that of synthetic conjugated metallic nanostructures. The conductivity increased exponentially with decreasing temperature until reaching a crossover temperature after which the conductivity decreased exponentially. This transport phenomenon was ascribed to metallic transport mechanism above the crossover temperature and to disorder induced charge trappings below it. The conductivity of both biofilm and network increased with lowering temperature possibly due to inhibition of thermally generated phonon scatterers. Below some critical temperature, the conductivity decreased possibly due to localization of the charges formed by disorder induced charge traps.

While this approach helped shed some light on the transport mechanism in pili network, it was not a feasible method to estimate the conductivity of an individual

pilus. A network provides numerous possibilities of charge percolation path through the network and also makes it difficult to estimate the number of individual pili and from the specific network geometry. This complicates the process of understanding the conduction mechanism. Recently, charge propagation along a pilus was visualized with electrostatic force microscopy, which suggested that *G. sulfurreducens* pili have conductive properties similar to that of carbon nanotubes,[23] but this method does not directly provide conductivity estimates. Therefore, study of charge transport through the pilus nanowire was deemed necessary.

Various attempts have been made to study single pilus charge transport and to learn about the intrinsic conductivity of a pilus. In fact, the first report of *G. sulfurreducens* producing conductive pili was from the conducting probe atomic force microscopy (CP-AFM) measurement along the diameter of a pilus.[26] Scanning tunneling microscopy (STM) has also been used to probe the nanowire along its diameter which suggested that near the fermi level electronic state of the pili is making them conductive.[27]

However, transport measurements along the diameter of pili does not provide complete picture of conduction through pili. These microbial nanowires are evolved to transfer charges along their length,[28] and it is necessary to investigate the transport along length of the pili in order to understand the conduction mechanism. But, the transport measurement along the length of an individual pilus has not been performed before and intrinsic conductivity of a pilus nanowires has yet been unknown. In this chapter, the charge transport measurements along the length of the pili of conductive *G. sulfurreducens* will be presented and the results are discussed.

Previous conductivity measurements of *G. sulfurreducens* pili along the length employed gold electrode arrays with 50 μm non-conductive gaps between the electrodes.[22, 18] *G. sulfurreducens* pili are typically 10-20 m long and thus individual pili could not bridge the non-conductive gap. However, when pili sheared from cells were placed on

the arrays and air-dried, pili in a physiologically relevant, hydrated state formed a network that spanned the non-conductive gaps. This approach permitted experimental manipulation of the pili to investigate their conductive properties. Measurements on networks of pili in which any associated cytochromes were denatured, ruled out the possibility that electron-hoping between cytochromes could account for electron transport through the pili network. The response of conductivity to temperature and pH were key features suggesting that the pili possess metallic-like conductivity.[22] Furthermore, measurements made with this approach demonstrated that substituting an alanine for key aromatic amino acids in the pili greatly reduced pili conductivity.[18] These results, as well as with X-ray diffraction data and structural modelling consistent with pi-stacking of aromatic amino acids within the pili,[24] have suggested that *G. sulfurreducens* pili possess metallic-like conductivity assisted by aromatic amino acids.[29, 30]

Here, I will describe the use of a low noise nanolectrode platform that makes it possible to measure conductivity along a single pilus. I will present transport measurements along pilus at different pH environment. In addition, in conjuction with observations drawn from modeling, I will discuss about the conduction mechanism though a pilus.

2.2 Methods

Due to the nanoscale dimension of a pilus, it was necessary to produce nanoscale devices to execute conductivity measurements. In addition, a low noise measurement system was also devised. Here, I present the methods of fabrication and sample preparation for experiments.

2.2.1 Electrodes Fabrication

Electrodes for this purpose were fabricated using e-beam lithography. E-beam lithography method uses electron beam at high acceleration voltage to write a designed pattern on a substrate.[31] Commercially available JEOL JSM-7001F Thermal Field Emission Scanning Electron Microscope (SEM) was used as the e-beam writer. Commercially available Design-CAD software was used to design the electrode and stored as a design file in Nanometer Pattern Generation System (NPGS) project. The design file and run file that includes the parameters to determine the dose and exposure were used to control and execute the writing process.

Substrate on which the electrodes were fabricated was prepared by spin coating copolymers on silicon wafer chip with 100 nm thermally grown oxide. Copolymer methyl methacrylate (MMA-E10; MicroChem) was spin-coated first on the silicon dioxide surface at 4000 rpm and then baked at 180 ^{0}C for 5 minutes. This was followed by spin-coating higher molecular weight polymethyl methacrylate (PMMA-A2) at the same speed followed by baking for 5 minutes. Heavier copolymer is coated on the top and lighter on the bottom so that there will be larger undercut which promotes easier liftoff after metallization.[32]

After electrode patterns were written, they were developed with a 1:3 solution of isopropanol (IPA) and methyl isobutyl ketone (MIBK) that leaves trenches of the pattern. Metallization was done by using an e-beam evaporator. First, 10 nm chromium was evaporated in order to provide strong adhesion on oxide surface, followed by 20 nm gold on the top providing us with electrodes with gold surface for contacts. The feature sizes were verified with a Dektak profilometer. Entire fabrication process is summarized in Figure 2.1(a).

An array of gold electrodes, 2 μm wide and 10 μm long, separated by non-conducting gaps of 500 nm (Figure 2.1(b)) was fabricated on n-doped silicon wafer with a 100 nm layer of thermally grown oxide on the surface. The electrodes were

connected to 100×100 μm pads for electrical contacts. Each electrode cluster contained fourteen electrodes(Figure 2.1(c)). Each chip consisted of 3×3 array of the fourteen-electrode clusters.

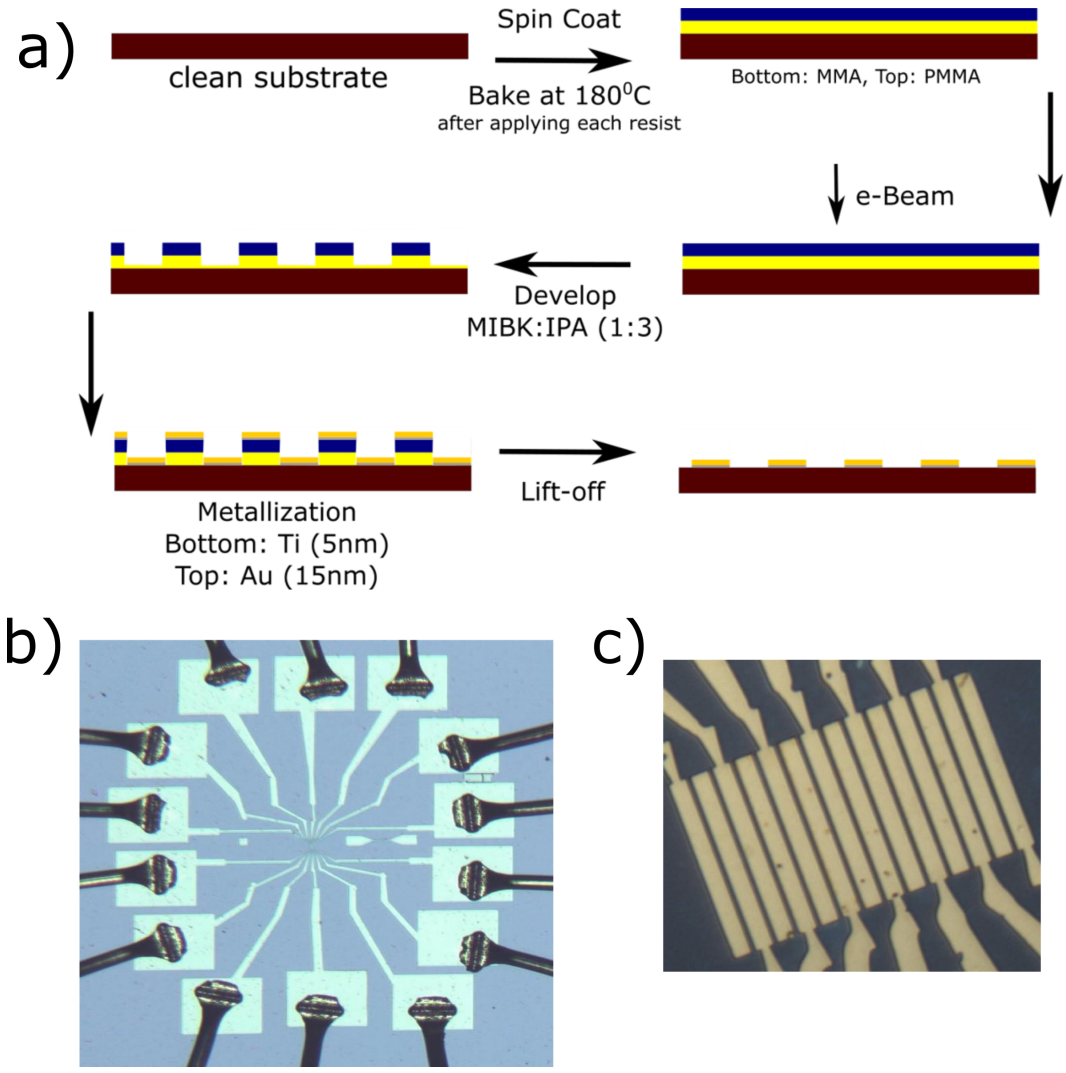

Figure 2.1. a) Process of electrode fabrication using e-beam lithography. b) Electrodes fabricated by e-beam lithography and wire-bonded to connect to circuit. Nine such arrays were fabricated in one chip with e-beam lithography. c) Close-up optical image of the electrodes at the center of each electrode arrays. Electrodes are 10 microns long, 2 microns wide, 30 nm thick, and separated by 500 nm.[33]

2.2.2 Pili Sample Preparation

In-order to study whether it is feasible for a long range charge transfer along the length of pili, we decided to perform transport studies on a single pilus of *G. sulfurreducens*. These pili have six aromatic amino acid residues in their pilin monomer 2.2(a,b). Ideally, X-ray crystallography would provide the best information about the structure of a pilus. Lacking that, in order to get an insight into the structure of a pilus, we have resorted to modeling and simulation. Both homology modeling of *G. sulfurreducens* based on crystallographic pilus structure of *Pseudomonas aeruginosa*, [24] and low energy atomic model[25], suggest that the pilin monomers create helical conductive path along the core of the pilus (Figure2.2d) when docked with other monomers to form a pilus chain.

In addition, the aromatic residues not only form the conducting core, but they are also scattered around the pilus shell. It is yet to be realized if those aromatic amino acids on side-chains have any impact on the conductivity through a pilus. For a conductive pilus, it should be possible for charge to be injected at one end of the pilus and transported along the helical conducting path to the other end due to applied bias. Long range electron transport will be possible if there is a significant $\pi - \pi$ overlap between the helical chain of the aromatic residues promoting delocalization of electron along the pilus[23] or even domain hopping between the delocalized states in the presence of defects and impurities.

Pili from Aro-5 mutant[18] were also chosen to be included in this study. Aro-5 mutants were created by genetically modifying *G. sulfurreducens pili* to lack five of the six aromatic amino acid residues (Figure 2.2(a,c)). Only the phenylalanine residue at the highly conserved region at the amino end of the pilin monomer was left to stay in the monomer. When phenylalanine to alanine mutation on the pilus structure of *G. sulfurreducens* (Figure 2.2e), was performed on the low energy atomic model using Jmol, one obtains Aro-5 pilus structure that retains the helical core of

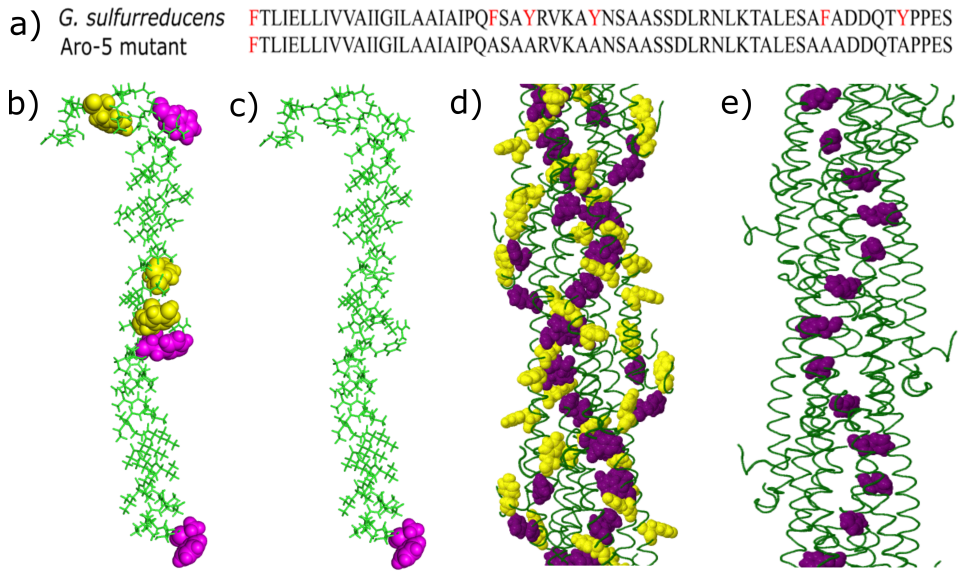

Figure 2.2. a) Amino acid sequence for two pili samples used for the measurement. Residues marked purple and yellow represent aromatic amino acid. *G. sulfurreducens* has six aromatic amino acid residues while Aro-5 mutant has one aromatic amino acid residue. Pilin monomer of *G. sulfurreducens* (b) and Aro-5 mutant (c) represented in wire frame structure. Aromatic residues phenylalanine (magenta) and tyrosine (yellow) are presented as spheres. d) *G. sulfurreducens* pili structure derived from atomic coordinates derived from low energy atomic models.[25] Aromatic residues pheylalanine (purple) and tyrosine (yellow) are represented as spheres while the rest of the amino acid residues are represented as wireframes. e) Aro-5 pilus structure based on *G. sulfurreducens* pilus model.

aromatic amino acid. However, the packing of the aromatic residue is very sparse with the spacing between the residues well over nanometer scale - too large for $\pi - \pi$ overlap. If the aromatic amino acid residues are essential for the conduction through a pilus, Aro-5 pilus should demonstrate significantly diminished transport.

Pili from wild-type *G. sulfurreducens*, and the Aro-5 mutant were removed from live cells and purified in the laboratory as described elsewhere.[22] Growth medium solution (0.2 μl) containing purified pili was drop-cast on a chip with fabricated electrodes. After waiting for 15 minutes to allow pili to settle, the residual solution was withdrawn with a micropipette. Then, a deionized water drop covering the device area was placed on top of the electrode array in order to dissolve any salts. The excess

water was withdrawn after 1 min. The water-rinse process was repeated two more times to ensure that the electrolytes from the growth medium were removed. The samples were gently air dried at room temperature (22°C), which leaves a water layer associated with the pili on the chip. Pili on the electrode array were located with AFM. Occasionally, a single pilus bridging two electrodes was located (Figure 2.2a).

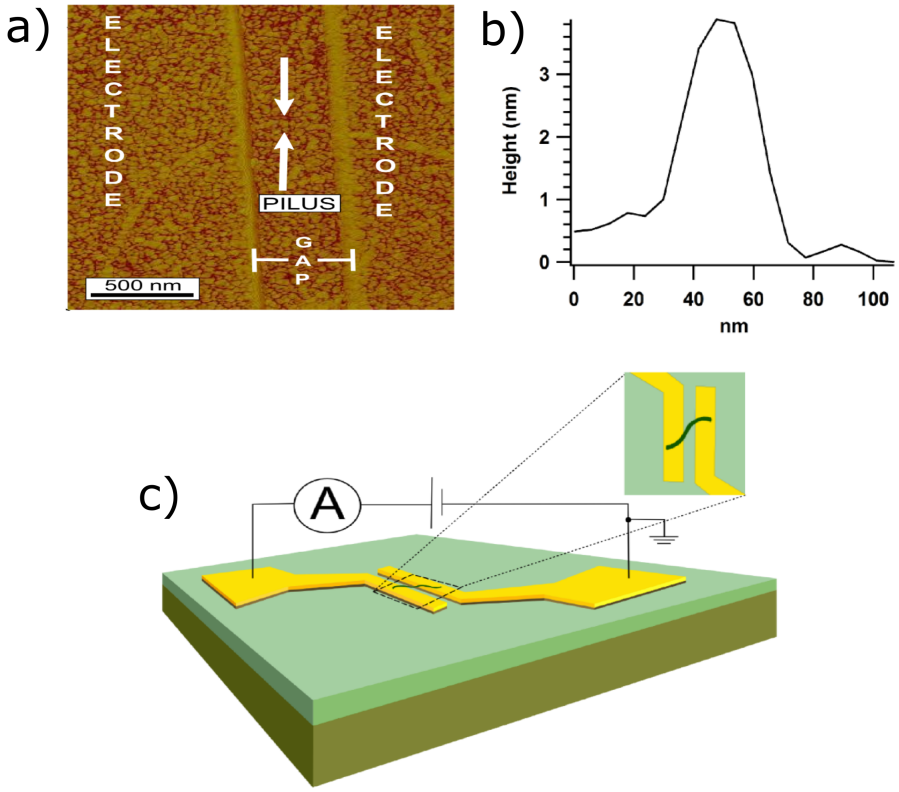

Figure 2.3. a) AFM image of a pilus bridging a pair of electrodes as indicated by arrows. b) Cross sectional height of the bridging pilus. c) Schematic of measurement setup. Electrodes were fabricated on top of thermally grown silicon dioxide.[33]

Cytochromes, which can readily be detected on pili with AFM,[34] were not present on any of the filaments examined, indicating that any cytochromes that may have been associated with the pili[34, 35] were removed as the pili preparations were made. Height measurements (Figure 2.2b)) confirmed that each filament was a pilus, which has a diameter of 3 nm, in contrast to flagellum which has a diameter of 12 nm.[22]

The contact pads corresponding to the two electrodes bridged by the individual pilus were wire bonded with aluminium wire with C103134 West-bond 7400 Ultrasonic Manual Wedge Wirebond. It was connected to a chip holder (130-11FFP, Global Chip Materials, LLC), and the device was placed inside a double-shielded box for high resistance/ low current measurement which will be described below. The circuitry of the system is represented as sketch (Figure 2.2c)). All the measurements were performed in a temperature (22 C) and humidity (55%) controlled cleanroom.

2.2.3 Low Level Current Measurement

Measurements were performed with a Keithley 4200 Semiconductor Characterization System (SCS). Two Source Measure Units (SMUs) of the SCS were equipped with preamplifiers 4100-PA providing the system with capability to measure current signals with resolution of up to 100 aA. These SMUs were connected to the two terminals of the double shielding box with low noise triaxial cable supplied by Keithley. The electronics were controlled with software Keithley Interactive Test Environment (KITE).

Due to low current signal during the measurement, noise to signal ratio was found to be extremely large (Figure 2.4) when measurement was performed with the probe station. This could make current signals for different applied potentials to fall within the range of the uncertainty of each other, making the measurement inconclusive. Therefore, it was deemed necessary for construction of a noise reduction mechanism for low current measurement.

The common practice to remove majority of noise during the electrical measurement is to use a grounded metallic cover, also called as Faraday cage. This essentially shields the device under test from external electrostatic coupling and interference. In addition to this, while measuring a low current/high resistance system, it is necessary to eliminate leakage current which could be of the same magnitude if the impedance

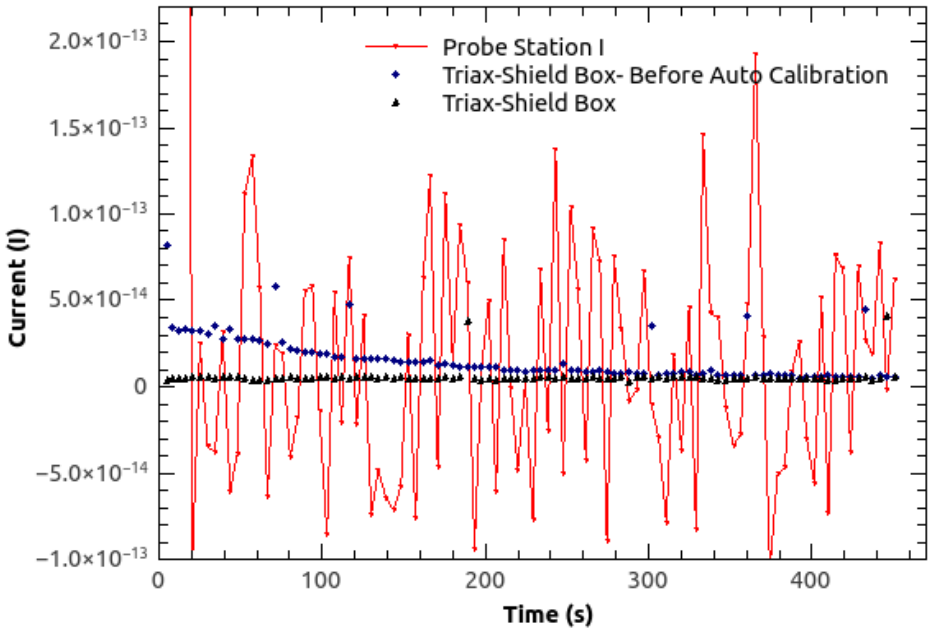

Figure 2.4. Significant noise reduction was observed after using double-shielded box with triaxial cable.

of the device under test is comparable to that of the insulators in the test circuit.[36] The leakage current can be eliminated by introducing guard to the circuitry (Figure 2.4). In the absence of a guard, during the high resistance sample measurement, leakage current can leak into the oxide (RL1) which passes through conductive doped silicon and then back into the circuit through oxide layer (RL2) leading to inaccurate reading of the current through the sample.

When a guard is introduced, an extra layer of a conductor with the potential same as that of the high impedance input is added around the device under test. Since there is no voltage differential across the insulation resistance (RL1, RL2), no leakage current will flow into the circuit leading to accurate current readings though high resistance samples. Further precision can be achieved by adding guards even in the cables, as in triaxial cables, to eliminate the leakage current between the inner high impedance source to external ground which is a problem while using coaxial cables.

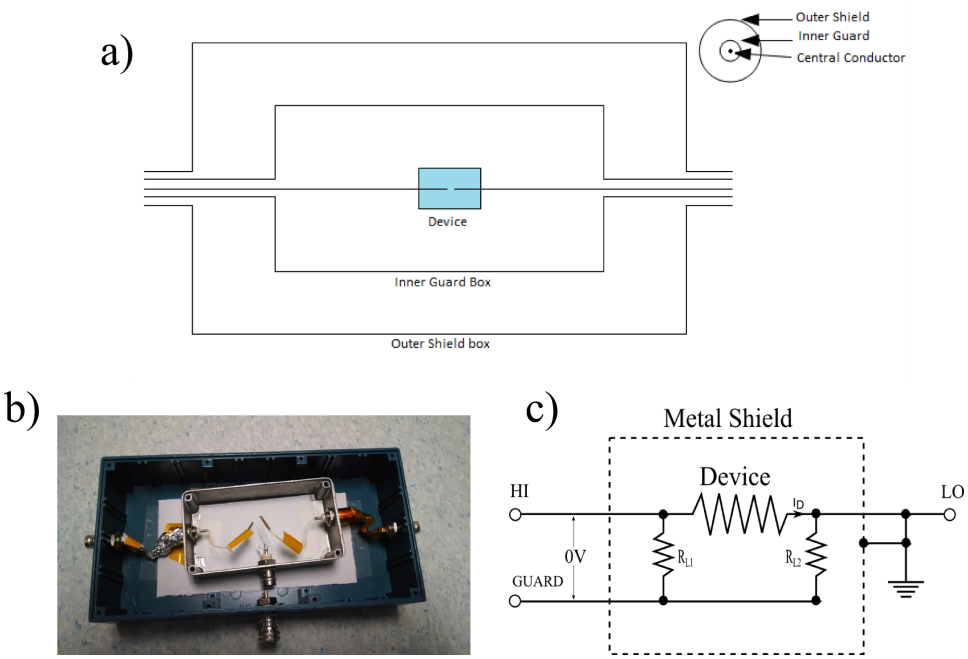

Figure 2.5. Double shielding system for low current measurements. a) Sketch of the shielding system. Outer box is connected to ground of a triaxial cable and inner metal box is connected to low impedance inner guard. b) Image of the shielding system. c) Circuit configuration of the guarded system. In addition to acting as a Faraday cage, the system is designed to help prevent leakage current during high resistance measurements.[33]

With these considerations in mind, a double shielding box was constructed (Figure 2.5b)). As shown in the sketch (Figure 2.5a)), the outer box acted as grounded Faraday cage while the inner box acted as a guard, inside which a sample was placed for the measurement. Triaxial connectors were mounted on the box and triaxial cables were used to connect the shielding box with the measurement unit.

Since we are dealing with high resistance low current measurement, we need to be careful about the data extraction process since small noise, leakage current, and other stray current could affect the measurement values. One of the most common ways to do this sort of measurements is to apply known voltage across the high resistance sample and measure the resulting current. The current is measured by a pico-ammeter since the magnitude of the measured current is very small in this case.

Therefore, it is necessary to avoid leakage current in order to improve the accuracy of the measurement.

The circuit during this measurement is represented in (Figure 2.6a) inset. We can apply a constant voltage (V) from voltage source. Cable resistance (R_c), shunt capacitance (C) and sample resistance (R_s) are involved in the circuit. The shunt capacitance originates from cables, probes, switches and test fixtures.

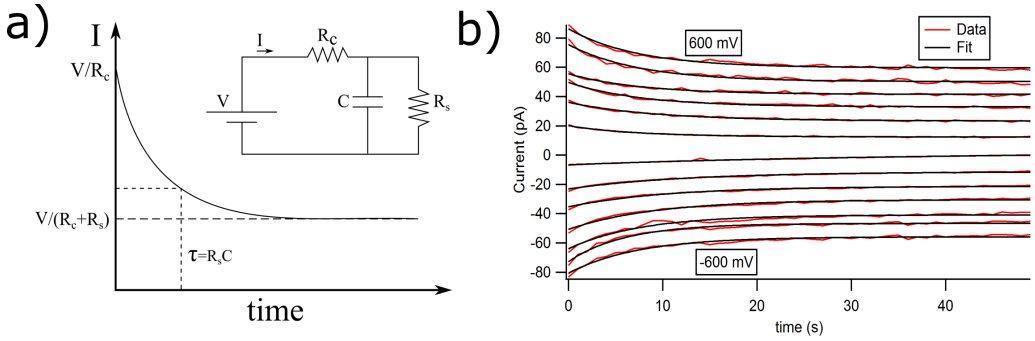

Figure 2.6. a) Expected current over time response for an applied voltage across a pair of electrodes. Current reaches a steady state value after waiting long enough time beyond time constant (τ). Inset is the approximate circuit configuration during measurement which represents parallel RC circuit. b) Steady state current measurement of the wild type pilus. Current values (red) reach steady state over time which can be fitted with exponential offset function (black) to obtain the value of the steady state current [33].

The instant that the voltage source meter is turned on, the current measured essentially comes from cable resistance (V/R_c). In order to measure the accurate current through the sample, it is necessary to wait until the shunt capacitor is charged to its maximum capacity so that there is no current flowing through the part of the circuit involving capacitor but only through the sample. This leads to an exponential decay of the current through the circuit associated with charging of the capacitor and finally a steady state current is achieved as the current measured is the current that is flowing only through the device under test. The time period needed for charging the capacitor and hence the time to achieve a steady state depends on the time constant (τ). The steady state current thus achieved depends on the cable resistance and

sample resistance ($I = V/(R_c + R_s)$). However if $R_s >> R_c$ as in our case, the sample resistance will dominate the current behavior. The value of current through the sample can then be extracted by averaging the steady state current for a given voltage.

2.3 Results and Discussions

2.3.1 Conductivity Measurements

Initial conductivity measurement on an individual nanowire was performed with carbon nanotubes, as a positive control. The Ohmic response (Figure 2.7) of current-voltage (IV) curve and the conductivity of 5927 S/cm were consistent with known properties of carbon nanotubes.[37] After the validation of the experiment process with the carbon nanotubes, measurements were repeated for the microbial nanowires.

During the experiment, various potentials ranging from -0.6V to 0.6V were applied and current response of the sample over time was recorded (Figure 2.5b). As expected, the current recorded had exponentially decaying behavior. Steady state current were acquired for various constant applied voltages. Then, the current voltage (IV) curves (Figure 2.6b) were constructed from the averaging of the steady state values of the current for corresponding applied voltage.

At the physiologically relevant pH 7, individual wild-type pili of *G. sulfurreducens*, spanning the non-conducting gap between two electrodes, exhibited linear, Ohmic behavior (Figure 2.6b). In contrast, the current-voltage response of individual pili from strain Aro-5 was comparable to the response from buffer without pili. This is consistent with the previous finding that the pili from the Aro-5 strain poorly conduct electrons because they lack key aromatic amino acids required for metallic-like conductivity.[23, 18, 24] Conductivity values were calculated from the relation:

$$\sigma = G\left(\frac{l}{\pi r^2}\right) \tag{2.1}$$

where, G is the conductance value acquired from the IV curve, l is the electrode gap (500 nm) and r is the radius of the pilus (1.5 nm). The conductivity of the wild-type pilus measured with this two-probe method was 51 $\pm$ 19 mS/cm (mean $\pm$ standard error of three pili), whereas the conductivity of Aro-5 pili was 38 $\pm$ 1 μS/cm, three orders of magnitude lower than wild-type pili.

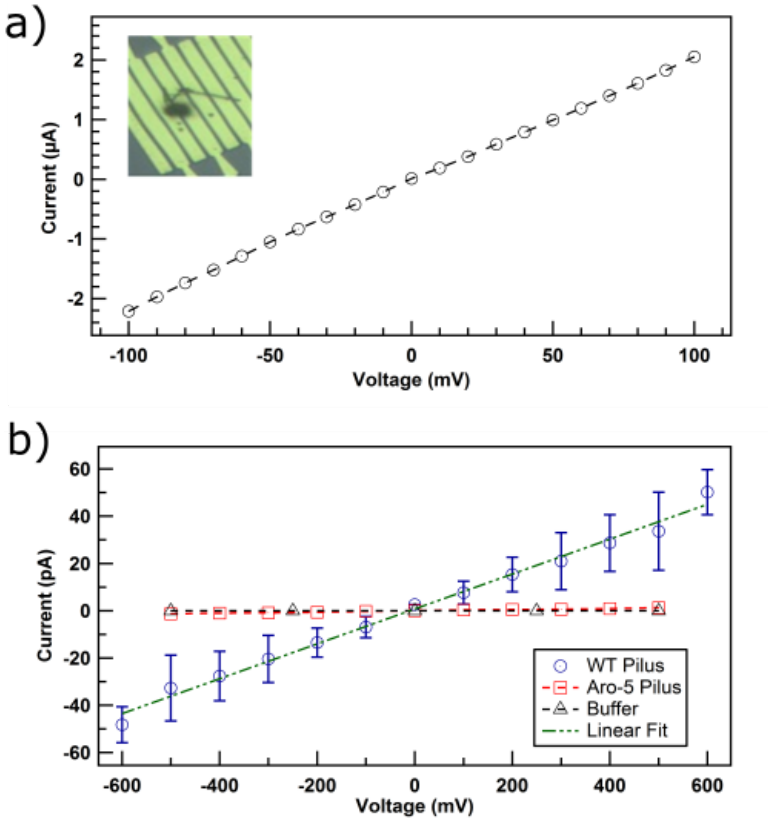

Figure 2.7. Current-voltage responses. (a) Carbon nanotube positive control. Inset is an optical image showing where carbon nanotube bridged across electrodes. (b) Individual *Geobacter sulfurreducens* pili at pH 7 bridging two electrodes with the pilus either from wild-type strain and Aro-5 strain in which key pilus aromatic amino acids are absent.[33]

These results demonstrated that key aromatic amino acids are required for the conductivity of the individual wild-type pili, consistent with the concept that overlapping $\pi - \pi$ orbitals of aromatic amino acids are responsible for the metallic-like conductivity of the pili.[29, 30] Although several computational studies using homol-

ogy modelling concluded that the aromatic amino acids of G. sulfurreducens pili do not stack sufficiently close for metallic like conductivity,[38, 39, 40, 41] homology modelling with a different template predicted tight packing of aromatic amino acids, which was further substantiated with X-ray diffraction data.[24]

2.3.2 pH Dependence of Conductivity

It is well known that the with increasing pH doping, conjugated polymers such as polyanaline and polyacetylene in insulating state start exhibiting semiconducting and even metallic properties.[42, 43] Doping in these conjugated molecules promotes delocalization along the conjugated chains making these polymers highly conducting in highly doped state.

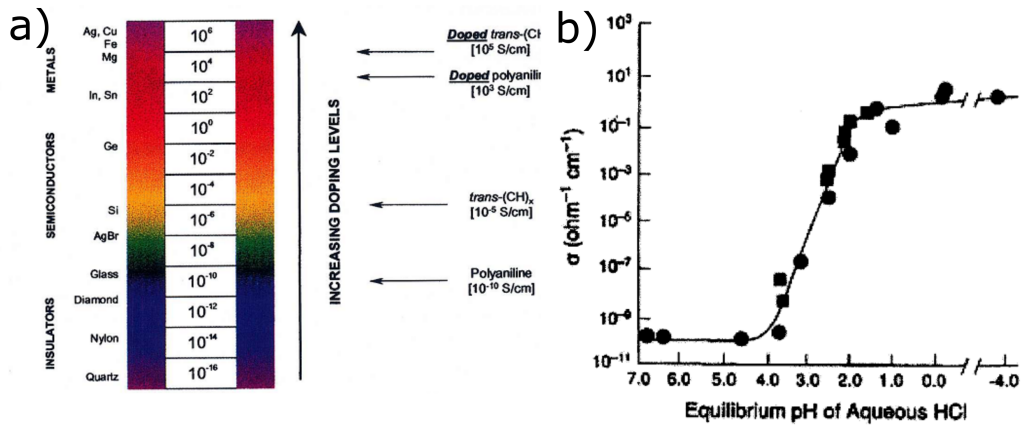

Figure 2.8. Increasing the conductivity of organic polymers by doping. a) Insulating organic polymers can be turned into semiconducting and metallic polymers by improving their molecular conjugation by doping. b) Conductivity of polyaniline as a function of pH of HCl dopant solution. • and ■ represent two different runs of experiments.[43]

In order to investigate if we can observe the increase in the conductivity of microbial nanowires with p-doping by lowering pH, I performed pH dependent study of the conductivity of individual nanowires. In fact, it was demonstrated that for microbial nanowire networks, pH doping by lowering from 10.5 to 2 indeed increased the conductivity by about two orders of magnitude.[22, 24]

For individual nanowires, increasing the pH from 7 to 10.5 dramatically lowered the conductivity of the wild-type pili to 37 $\pm$ 15 S cm^{-1}, whereas decreasing the pH to 2 substantially increased pilus conductivity to 188 $\pm$ 33 mS cm^{-1}(Figure 2.8). The change in conductivity with pH has been attributed to conformational changes that result in greater $\pi - \pi$ stacking of aromatic amino acids at lower pH.[24] This pH response of the individual pilus further confirmed that the measured electronic conductivity is an intrinsic property of the pilus.

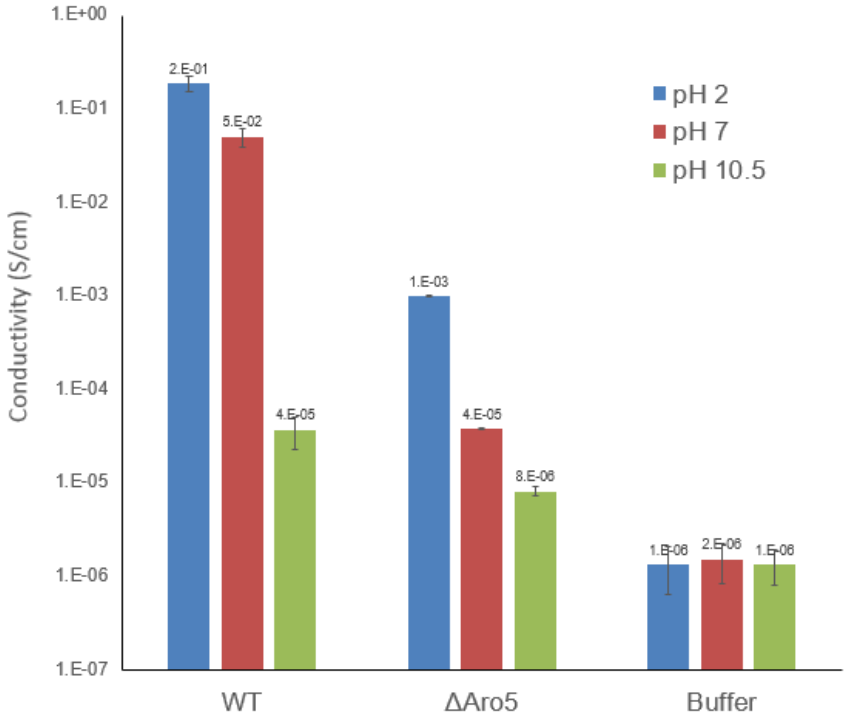

Figure 2.9. pH dependent conductivity of wild-type *G. sulfurreducens* pilus, Aro-5 mutant and corresponding buffer. The buffer conductivity did not significantly change with changes in pH.[33]

An interesting observation was that the conductivity of the Aro-5 mutant increased with lowering pH although it was not as dramatic as for wild type *G. sulfurreducens*. Unlike for wild type pilus, the distance between the helical aromatic amino acid residues at the core of pilus the further than 1.5 nm. At this distance of separation, even with conformational changes, the distance is too large for any kind of $\pi - \pi$

Sample	Conductance (S)	Conductivity (mS/cm)	pH
Wild Type	$5.26 \times 10^{-14} \pm 3.55 \times 10^{-14}$	0.037 ± 0.015	10.5
	$7.22 \times 10^{-11} \pm 2.76 \times 10^{-11}$	51 ± 19	7
	$2.65 \times 10^{-10} \pm 8.28 \times 10^{-11}$	188 ± 34	2
Aro-5	$1.16 \times 10^{-14} \pm 4.80 \times 10^{-15}$	0.0082 ± 0.001	10.5
	$5.43 \times 10^{-14} \pm 2.73 \times 10^{-14}$	0.04 ± 0.001	7
	$1.41 \times 10^{-12} \pm 8.23 \times 10^{-13}$	1 ± 0.03	2

Table 2.1. Experimental values of conductance and corresponding conductivity of various samples. Calculations were performed using equation 2.1.[33]

overlap. However, charge configuration of Aro-5 pili changes as well with lowering pH as more p-carriers are introduced. This implies that not only the conformational changes induced improved $\pi - \pi$ overlap, but also the excess p-type carrier introduced by the chemical doping of the pili also contributes to the charge transport along the pili. I will discuss this phenomena with more details in later part of the chapter. The average conductance and conductivity values calculated from equation 2.1 are presented in Table 2.1.

Other sources of conductive filaments with useful electronic properties may be available in the microbial world because diversity of microbes require electrical connections not only for extracellular electron transfer to insoluble minerals such as Fe(III) oxide, but also for interspecies electron transfer and high density current production in microbial fuel cells.[44, 45] For example, it has been suggested that Acidothiobacillus ferroxidans,[46] and Aeromonas hydrophila[47] have conductive pili, but conductivity was only measured across the diameter of the pili and the pili were fixed with gluturaldehyde, which cross-links proteins, potentially altering their structure and function. An alternative strategy was devised for measuring conductivity along the length of Shewanella oneidensis filaments,[48] but the critical-point drying employed could generate artifacts because outer-surface membranes collapse into structures that look like filaments.[49, 50] Evaluating conductivity along the length

of unfixed pili from these organisms with the method described here will provide a better indication of their likely biological role.

2.3.3 Mechanism based on conductance behavior

In addition to gaining information about quantifiable electronic property like conductivity form the IV measurement, one can also get insight into the possible conduction mechanism based on the behavior of the IV curve. For example, linear IV curve entails ohmic behavior where charge carriers experience uniform potential when they travel through the applied field. While, nonlinear curves imply that the charge carriers experience variable potential during their travel along the field which could be due to disorders in the medium or barriers at the interface. Depending on the size or shape of the potential, one can get insight into whether the material through which charges are transported are insulating, semiconducting in nature or helps us gain insight on the physics of charge transfer at the contact between the sample and electrodes.

Further insight could be gained by studying the differential conductance (dI/dV) response from a device which provides information about the behavior of the electron during transport.[51] From differential conductance curve it is easy to see at what voltages the conductance becomes maximum implying more activity of electrons. The differential conductance is directly proportional to density of states. Behavior of IV curve and the corresponding differential conductance from pili at different pH will be discussed here in order to gain possible mechanistic insight of charge transport during the measurement.

At pH 10.5, asymmetric IV behavior was observed (Figure 2.10). Conductance is higher at negative potential which diminishes at positive potential. Such a rectification behavior has been previously reported for measurements along helical peptide structures and has been attributed to interaction of transporting charge with dipole

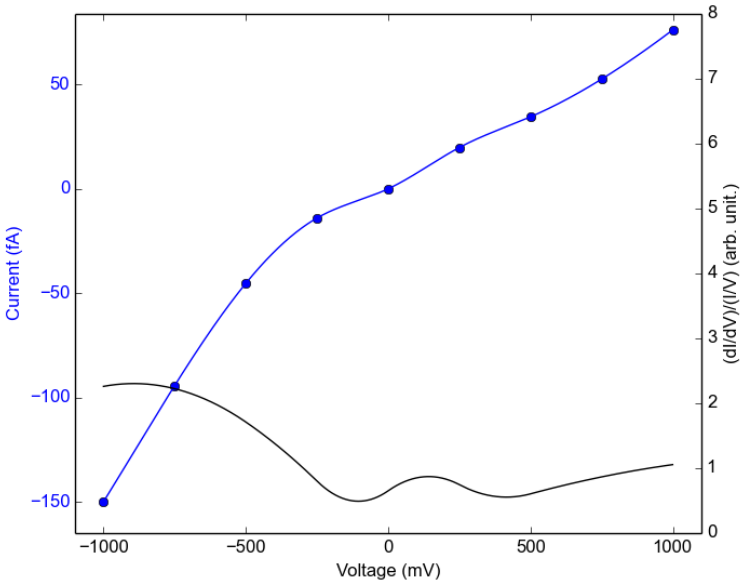

Figure 2.10. IV response and differential conductance for G. sulfurreducens pili in pH 10.5.

moment associated with the peptides.[52, 53, 54] The rectification ratio,[55] defined as:

$$R = \left| \frac{I(V_0)}{I(-V_0)} \right| \tag{2.2}$$

where V_0 is the highest positive bias used, is 0.508 which is similar to previously reported rectification achieved for helical peptides.[53]

Pilin monomers that constitute pili are helical in nature. Peptide units have dipole moment due to opposite polarity of ammonium (NH) and carboxylic (CO) groups. When these peptide units form a helix, a net dipole moment is generated with partial positive charge at the amino end and partial negative charge at the carboxy end (Figure 2.11).[56]

Pilin monomers are composed of the helical structures. Models based on NMR studies [40] of *G. sulfurreducens* pili are presented in Figure 2.12. In addition, the monomers consist of the amino acids in the chain which can retain charges based

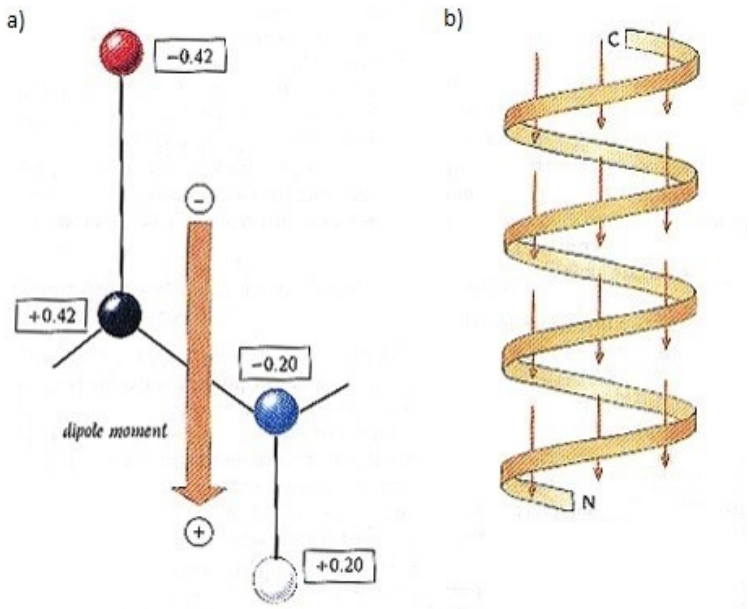

Figure 2.11. a) Dipoles of peptide unit. Approximate functional charges on the atoms of the peptide unit. Color code: Red- Oxygen, Black- Carbon, Blue- Nitrogen. b) Creation of overall dipole moment of helix due to the dipoles of peptide units. Carboxy end is negative and amino end is positive. [56]

on their environment. For example, for a pilin at pH 7, two arginine (Arg, R) and two lysine (Lys, K) are positively charged while three aspartic acid (Asp, D), three glutamic acid (Glu, E), and the C terminus are negatively charged. The dipole created by the charged amino acids as well as helicity of the pilin structure align in parallel to each other.

A pili is composed of 19 pilin monomers.[24] The pilin structures dock in a manner where the hydrophobic N-terminus is at the core of the pili and the C-terminus are at the periphery. Therefore, a pilus has a negatively charged region around the circumference of the pilus and positively charged region towards the inner side (Figure 2.13b). Using the atomic coordinates developed from the low atomic energy model,[25] we can visualize the charge distribution configuration along a pilus (Figure 2.13). At high pH, the net charge in a pilus is negative (Figure 2.14) due to net negative

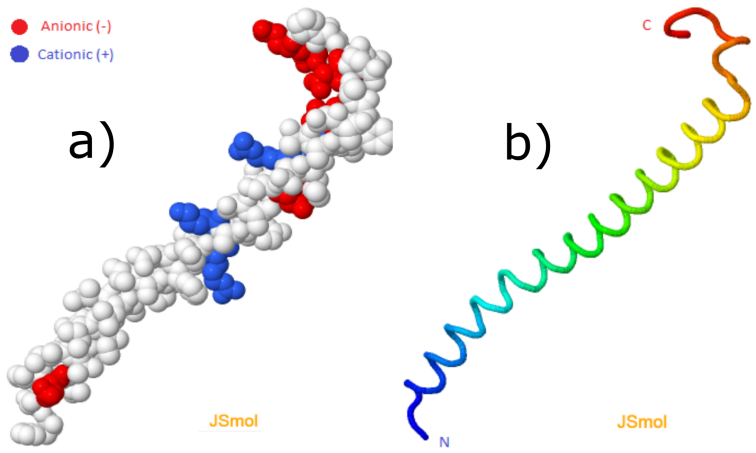

Figure 2.12. Pilin structures based on NMR structures. Pilin monomers are mostly helical with free car a) Location of charged amino acids in a pilin monomer at pH 7. Blue: Positively charged amino acids. Red: Negatively charged amino acids. b) Representation of animo (blue) and carboxy (red) terminal of a helical pili monomer. (Generated using JSmol)

charge in the pilin monomer. At low pH, all the negative amino acid residues are neutralized and result is net positive charge in a pilin monomer and hence a pilus. This charge distribution along the shell of a pilus should definitely play a role in transport measurement using two electrodes since charge injected from electrode to pilus or vice-versa would experience this charge configuration at the interface.

When the IV measurement is performed in a pius at pH 10.5, an asymmetric response (Figure 2.10) is observed. It is clear that a charge carrier faces more than aromatic amino acids in helical conformation close enough for delocalization. When a bias is applied for charge to propagate though pili, it has to pass from the shell of the pili towards the core where it can find conducting path. Provided that the radius of the pili is only 1.5 nm, the distance is short enough for tunneling to be possible. However, in this case, the tunneling barrier towards the central conducting channel is not only physical, but also electrostatic due to the dipole moment of the helices.[57]

One would ideally want only pili on the device during the measurement. In reality, however, even though the sample is air dried, there will still be a thin layer of solution

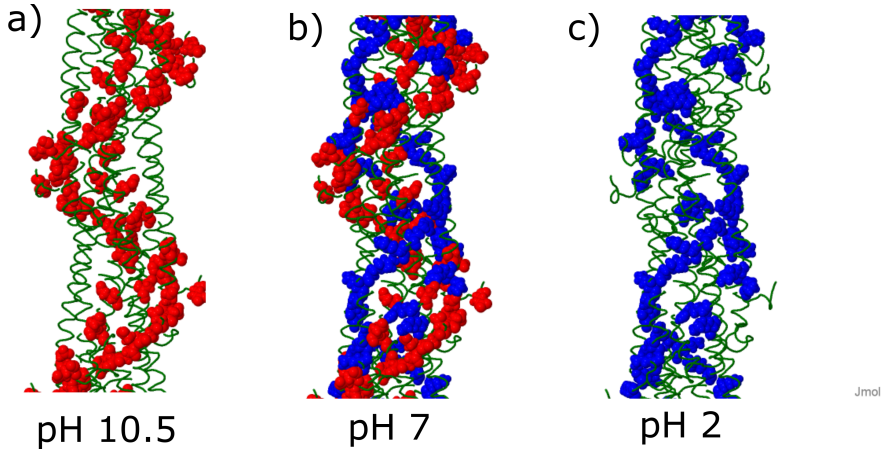

Figure 2.13. Charge configuration along a pilus for different pH environment. With lowering pH the net charge of the pili becomes positive. Positively charged residues are labeled blue and negatively charged residues are labeled red.

present[58] which is enough to affect the properties of the pili. In addition, the pili is a protein structure and they have water associated with them due to the hydrophilic surface. Therefore, it is necessary to account for the environment on the dynamics of the charge transport while probing the IV response.

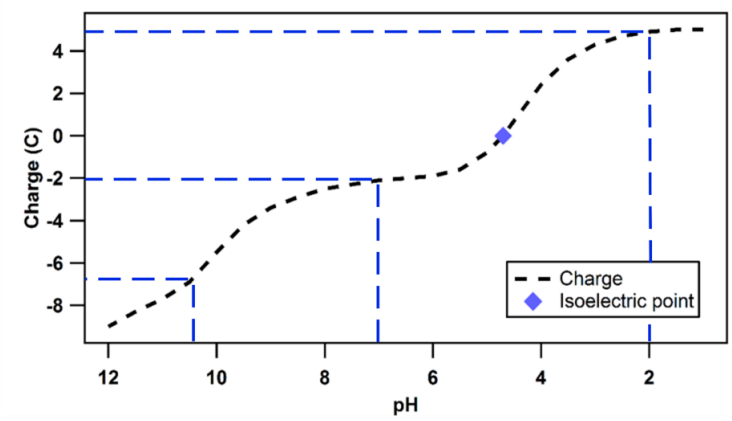

Figure 2.14. Net charge of the pilin monomer as a function of pH. Modeled using protein calculator (protcalc.sourceforge.net/).

At pH 10.5, we can envision pili on electrode as shown in Figure 2.15. When a pilus is laying on top of the electrodes, the negatively charged amino acids lay on the electrode surface. During the measurement, polarity bias of one of the electrodes was

changed while the second electrode was always grounded. Since the pH experiment (Figure 2.9) and previously reported similar result including from solution gated electrical tuning on pili network[22] suggest that the charge carrier in the pili system is of p-type i.e. holes, discussion here will be presented in terms of holes as well.

When a positive bias is applied to an electrode, a hole carrier from the positive terminal needs to travel through the pili in order to reach grounded terminal. Since the shell of the pili is negatively charged, the hole getting injected from positive terminal faces lower barrier due to the negative charge at the interface. After electrode traverses along the pili, as the hole carrier moves from pili to the grounded terminal, the hole experiences higher potential barrier which can impede the transport as shown in Figure 2.15. Due to this barrier created at the grounded electrode interface, hole carriers accumulate at the interface limiting the transport. This explains the lower current during the positive bias in Figure 2.10.

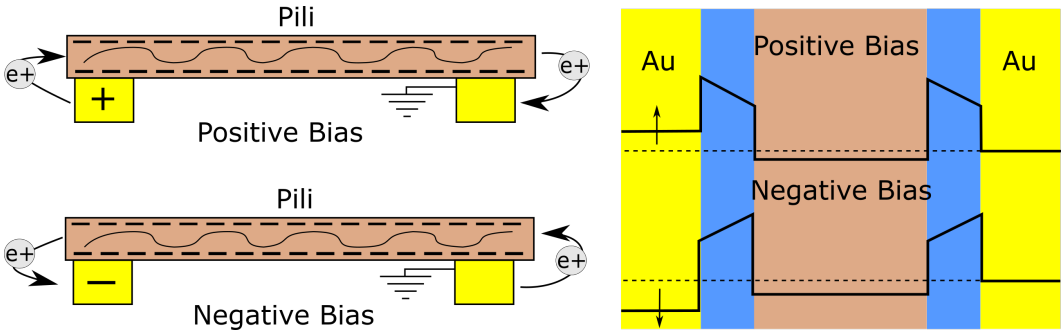

Figure 2.15. Left- Schematics of charge transport for electrode-pili-electrode system at pH 10.5. Right- Energy Band Diagram for the charge transport. Negative bias state provides potential suited for higher conduction than the positive bias system.

On the other hand, when a negative bias is applied to an electrode, a hole carrier from ground needs to travel though the pili to the negative terminal. When a hole is injected from the ground electrode to the pili, the charge carrier faces lower barrier height. Once the hole reaches the aromatic amino acid chain, it travels along the length of the pili due to the field. When the carriers reaches towards the negatively

biased electrode, the charge carrier needs to traverse through negatively charged shell of the pili to the negatively biased electrode. The negative bias of the electrode presents even lower barrier for the hole. This barrier only gets lower as higher biased is applied as shown in Figure 2.15. This promotes charge transport through the electrode-pili-electrode system, as a result of which higher current is achieved with higher barrier.

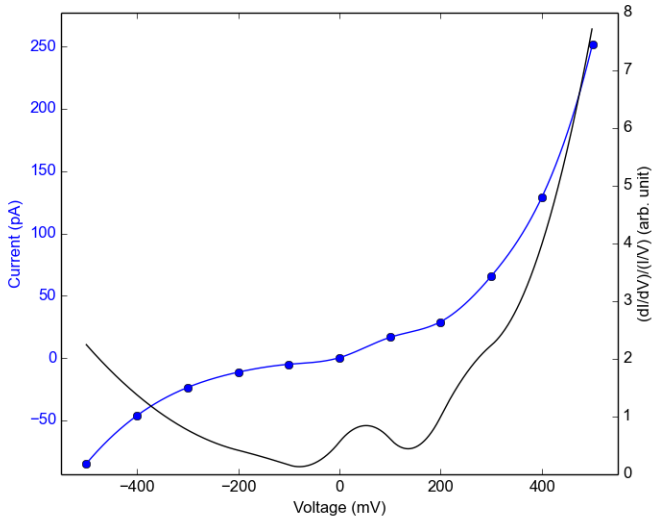

Figure 2.16. a) Blue: Current voltage (IV) response at pH 2. B) Black: Corresponding normalized differential conductance.

A completely reverse effect is observed at pH 2 with asymmetry skewed towards the positive bias. The rectification ratio (Equation 2.2) in this case is 2.97, a much higher value than for pH 10.5. The conductance value at this pH is as much as three orders of magnitude higher than for pH 10.5 implying that charge transport through pili has been vastly improved. However, the assymtery in IV curve at higher voltage means that the carriers are experiencing barriers due to fermi-level mismatch at the interface between pilus and electrodes.

One of the key differences for electrode-pilus-electrode system at pH 2 from pH 10.5 environment is that the charge configuration of pilus has changed from net neg-

ative to net positive. That means, the positive charges populated the shell of the pilus which will interact in exactly the opposite manner compared to the pH 10.5 situation. During positive bias, hole carriers are injected from positive terminal to the pilus. The injected holes travel along the core of the conducting helix of the pilus and get injected into the ground electrode. The barrier experienced by hole carrier during injection from the pili to the ground is shown in Figure 2.17. Therefore the whole process promoted the transport through the pilus when positive bias is applied. Higher is the applied positive bias, higher transport through pilus is achieved.

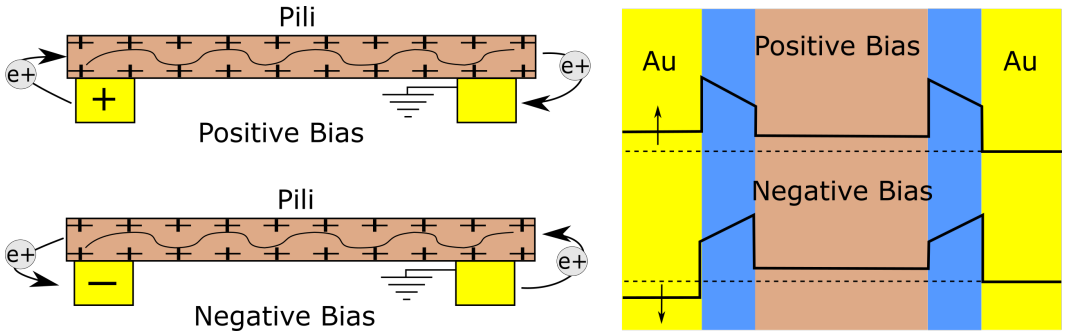

Figure 2.17. Left- Schematics of charge transport for electrode-pili-electrode system at pH 2. Right- Energy Band Diagram for for the charge transport. Negative bias state provides potential suited for higher conduction than the positive bias system.

During negative bias, hole carriers are injected from ground electrodes to the pili which presents a barrier due to positive charges at the shell of pili as shown in Figure 2.17. This barrier would limit the charge injection into the pili even when potential is applied at the negative voltage. The hole carriers will be populated at the interface between pili and ground electrode. If the negative potential is high enough, the carriers can populate to enough numbers that they can move over the barrier leading to conduction. This is observed with the non linear curve which is also present at the negative bias as seen in Figure 2.16.

While the rectification behavior could be issued to charge configuration creating dipole in helices, dipole behavior is expected to be diminished in high pH of 2 where

the concentration of the proton is more than eight orders of magnitude. Net charge of a pilin monomer at this stage is 4.9, and hence only positive charges are retained in the pilus (Figure 2.13c). This makes us speculate that the asymmetry in the IV curve may be due to other interfacial effect at the pili-electrode interface that is other than dipole of pilin helix. This kind of asymmetry is very common in metal-semiconductor-metal system due to mismatching of Fermi level between the semiconductors and metals at the interface. Below I present a case explaining how metal-pili-metal system at higher voltage in pH 2 create schottky barrier at the interface.

For positive bias, the current through pili is very high, but the current diminishes significantly when negative bias is applied. This is equivalent to the metal-pilus-metal system having forward bias when positive voltage is applied and reverse bias when negative voltage is applied. The negative voltage regime was inspected to check if the diminished current is due to Schottky barrier. For Schottky barrier effect, the current-voltage relation is given as:[59]

$$I = AT^2 exp\left(-\frac{\phi_s}{kT}\right) exp\left(\frac{\beta_s}{kT}\sqrt{\frac{V}{d}}\right) \tag{2.3}$$

where, A is the diode area, T is the temperature, β is the Schottky field lowering coefficient given as $2\beta_s = (e^3/\pi\epsilon_s\epsilon_0)^2$, ϕ_s is the interfacial barrier height, V is the applied voltage, d is the distance between the electrodes. Hence, one expects a linear relationship between $ln(I)$ and $V^{1/2}$. This is what is observed (Figure 2.18) at a region of the higher voltage. This kind of behavior is attributed to reverse biased on Schottky barrier.

Unlike for lower and high pH environment, the IV curve at pH 7 (Figure 2.19) is linear and the current is about two fold higher than what was observed for pH 10.5. As shown in Figure 2.13, at pH 7, there is presence of both negative and positive charges associated with amino acids at the outer surface of the pilus. Therefore, at the pilus-electrode interface, both positively and negatively charged amino acids

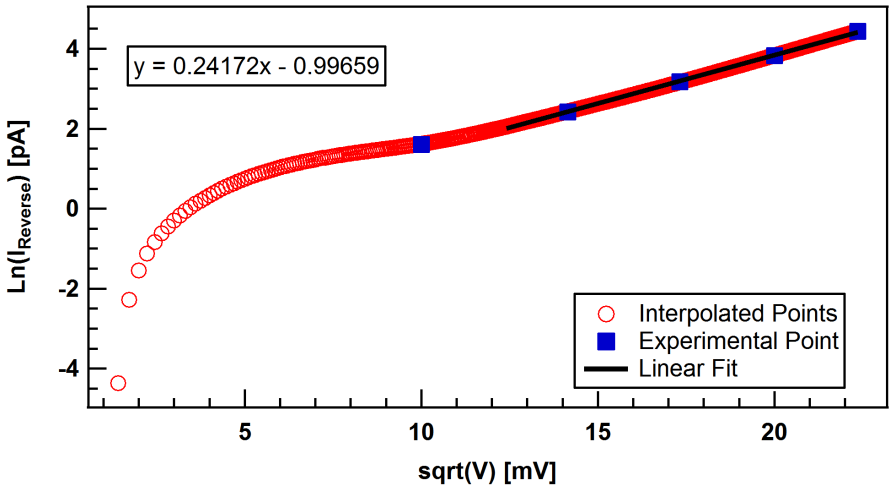

Figure 2.18. $Ln(I)$ vs. $V^{1/2}$ plot show linearity at the higher voltage for reverse bias. Such a behavior is attributed to Schottky barrier.

come to contact. This creates scenario where, from the energy band prespective, the pilus electrode interface could be superposition of energy band at pH 10.5 and pH 2 giving a way to symmetric charge transport with no barrier at the interface due to charge configuration. Only barrier involved is the tunneling barrier at either terminal at pili-electrode interface. This kind of Ohmic behavior has also been observed in controlled experiment where helical peptides were arranged in antiparallel manner in order to cancel out the dipole moment by canceling the charges associated with the helix.[52]

Similar experiment performed with carbon nanotube also resulted in linear response with no noticeable difference in shape of differential conductance for negative or positive potential. This is what we expect of at the room temperature IV measurement of the carbon nanotube.[60] In this situation, only barrier the charge carrier face is the interface during the injection to and from the carbon nanotube.

This brings us back to the introduction in Chapter 1 of this dissertation, where I discussed about various biological processes involved in efficient charge transport, which has not yet been realized in inorganic system. Here, we have a nanowire made

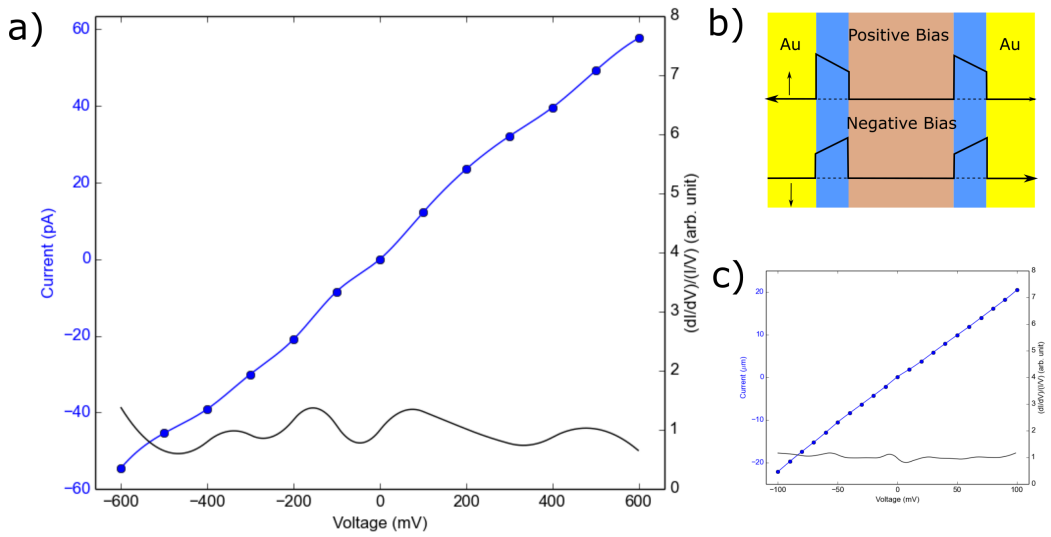

Figure 2.19. a) IV response: Current-voltage (IV) response of the G. sulfurreducens pili in pH 7. Black: Corresponding differential conductance. b) Energy diagram for transport for electrode-pili-electrode system at pH 7. c) IV response of a carbon nanotube (blue) and corresponding differential conductance (black).

up of protein which is designed to conduct electron for long distance. I think it is interesting that for the *G. sulfurreduces*, the contact between electrode and pili is Ohmic at physiologically relevant environment of pH 7. When pH is lowered or increased, the Ohmic contact diminishes introducing barriers at the interface and hence less efficient electron transport.

2.3.4 Conclusions

In summary, the results demonstrate that individual pili of *G. sulfurreducens* are highly conductive. The pilus conductivity of ca. 50 mS/cm is comparable with previously reported conductivity values for nanostructures composed of synthetic organic metals such as polyaniline.[61, 62] *G. sulfurreducens* pili can readily be mass produced in a sustainable manner and they do not contain toxic components. The pili function in water, are highly chemically stable, and their properties can be readily genetically modified. The strong dependence of pilus conductivity on pH and their high aspect

ratio suggests that *G. sulfurreducens* pili might have applications as highly sensitive pH or other environmental sensors.

It was also an interesting observation that the *G. sulfurreducens* pili show ohmic behavior at physiologically relevant environment of pH 7 making the most efficient charge transport through the pili possible. Whether the pH is decreased or increased, potential barriers at the interface with metal are introduced preventing efficient transport.

Increasing conductivity of Aro-5 sample with lowring pH was an interesting finding in this project. Clearly, from the previous studies on network and studies presented on single pilus in this chapter, aromatic amino residues are crucial for the conduction through pili. However, it appears that, in order to explain the conduction to pili, it is necessary to incorporate the involvement of the positively charge amino acids as well. Conformational changes bringing in aromatic residues closer with lowering pH appears to be the major contributor for conduction from our observation that lowring pH from 10.5 to 2, increases the conductivity of *G. sulfurreducens* pilus by about 5000 fold. But, it is notable that for Aro-5 pilus where contribution of aromatic residue is essentially nonexistant the conductivity at pH 2 is about 100 fold higher than the conductivity at pH 10.5. Therefore, it appears that the chemical doping, due to the protons introduced in the pilus by lowering pH and changing the net charge of the pili to positive, does contribute to the conductivity. Therefore, in order to develop a theory for conduction through a pilus, it is essential to incorporate the effect of chemical doping and charged amino acids.

The conductivity measurement technique described here should aid in the search for other conductive filaments in the microbial world, which may have unique properties. Such investigations will not only enhance the understanding of electron transport mechanisms in biological systems, but may also help identify additional biological materials that may have applications in bioelectronics.

CHAPTER 3

ROLE OF AROMATIC AMINO ACIDS IN CONDUCTION ALONG MICROBIAL NANOWIRES

3.1 Introduction

In the previous chapter, I discussed about the conductivity of microbial nanowires produced by *G. sulfurreducens* pilus and Aro-5 mutant. A *G. sulfurreducens* pilus has six aromatic amino acids per pilin monomer while Aro-5 mutant pilus has only one pilin per pilin monomer. We observed that at pH 7, the conductivity of individual *G. sulfurreducens* pilus is 51 ± 11 mS cm^{-1} while individual Aro-5 pilus at that same pH has conductivity of 40 ± 1 μS cm^{-1}. That is about three orders of magnitude higher conductivity for *G. sulfurreducens* pilus than Aro-5 pilus. This provides a clear picture about how aromatic amino acid residues are the integral part of the conductivity through microbial nanowires.

That brings up a question. If one observes significantly lower conductivity of pilus by making them deficient of aromatic residues, one could ask if it is possible to enrich the pilus with the aromatic residues and observe higher conductivity. Higher content of aromatic residues in microbial nanowires implies higher charge accepter sites which should make transport though pilus a lot easier. We went after two approaches to answer this question. One approach was to mutate *G. sulfurreducens* to produce pili with tryptophan, an aromatic residue with double aromatic rings. Another approach was to turn to the nature. It turns out that we can look around for other *Geobacter* species which can produce pili with much higher aromatic residue contents in their pilin monomer. We realized that we can study the conductivity of pili produced from

both of these approaches and get deeper understanding of the of role of aromatic residues in conduction through pili.

The aim of this chapter will be to present the charge transport studies in pilus produced by mutated *G. sulfurreducens* strain producing pili which we termed 'W51W57' and two other naturally occuring *Geobacter* species namely - *G. metallireducens* and *G. uraniireducens*, both of which have higher aromatic residues than *G. sulfurreducens* (Figure 3.1). W51W57 strain produces pili with same length of *G. sulfurreducens* but two aromatic residues are replaced by tryptophan (W). *G. metallireducens* produces pili with short pilin monomer with 59 residues. Among them, 9 are aromatic residues. *G. uraniireducens* produces pilin monomer with 120 residues, 8 of which are aromatic residues.

W51W57 mutant	FTLIELLIVVAIIGILAAIAIPQFSAYRVKAYNSAASSDLRNLKTALESAWADDQTWPPES
G. metallireducens	FTLIELLIVVAIIGILAAIAIPQFAAYRQKAFNSAAESDLKNTKTNLESYYSEHQFYPN
G. uraniireducens	FTLIELLIVVAIIGILAAIAIPQFSKYRIQGFNASGNSDLKNIRTSQESLYAEWQHYGLTQ
	GLATVAGLPGAGKWGVGALVTPTAALPVCIITTDDNNLVPRGLQIPVGNNVTAMATTAA

Figure 3.1. Amino acid sequence for W51W57 mutant, *G. metallireducens* and *G. uraniireducens* piln monomer. Aromatic amino acids are marked in red. *G. metallireducens* has monomer length of 59 with 9 aromatic residues. *G. uraniireducens* pilin monomer is 120 residues long with 8 aromatic residues.

3.2 Methods

One of the early challenges while performing single pili measurements of all these samples was to come up with more efficient method for fabrication of the electrodes. As I presented in the earlier chapter, the conductivity measurements were performed with electrodes fabricated by e-beam lithography. While e-beam lithography process provides versatility of fabricating patterns with any design, the process itself is quite slow. Since e-beam needs to write every single line for the pattern, one needs to spend hours under the scanning electron microscope in order to complete pattern writing. Before that, one needs to go through very careful process of figuring out the dose and

current level of e-beam that is required for writing the desired pattern for electrodes. This involves multiple iterations of writing pattern to optimize the probe current and dose. For nanoscale patterns, these become more important and meticulous as slight increase in beam dose will overlap the pattern features and slight decrease could be too low for photoresist to be cured for development.

Due to all these challenges associated with e-beam lithography, we had to come up with a solution to circumvent time consumption of electrode fabrication process. The idea was that, if we could expedite the fabrication of nano-electrodes, we could spend more time on locating single pili across electrodes under AFM and performing the measurement. One of the solutions would be using Photolithography method. However, there are limitations regarding the resolution of patterns that can be fabricated by this method which is determined by the wavelength of the UV-light used for exposure and accuracy of the lithography system itself. The resolution of photolithography system we have in Conte Cleanroom Lab is about 5 μm which would be too large for our purpose of single pilus studies. The solution was to use nano-imprint lithography (NIL) to address this issue.

3.2.1 Electrode Fabrication with NIL

As the name suggests, nano-imprint lithograhy (NIL) is a method of fabrication process, in which nanoscale imprints for the devices are made using a mold which is followed by etching, metalization, and liftoff (Figure 3.2). The electrodes were fabricated on a heavily doped silicon substrate with 1 μm wet thick thermal oxide with nanoimprint lithography. The substrate was cleaned with a Piranha solution (H_2SO_4 : H_2O_2 = 3 : 1) and a diluted HF solution before patterning. After the cleaning steps, a double layer of resists (50 nm thick poly(methyl-methacrylate) (PMMA) and 60 nm thick UV-curable resist were sequentially spin-coated on the substrate. Circuit patterns including 50 nm nanoelectrodes separated by 50 nm gaps, microscale

fanouts, and contact pads were transferred from a quartz mold to the UV resist with nanoimprint lithography in a homemade imprint chamber. The residual UV-resist layer and the PMMA underlayer were removed in fluorine and oxygen based (CHF3 /O2) reactive ion etching, respectively.[63, 64] Thin films of 5 nm thick titanium and 15 nm thick gold were then deposited in an electron beam evaporator, followed by a liftoff process in acetone with ultrasonication.

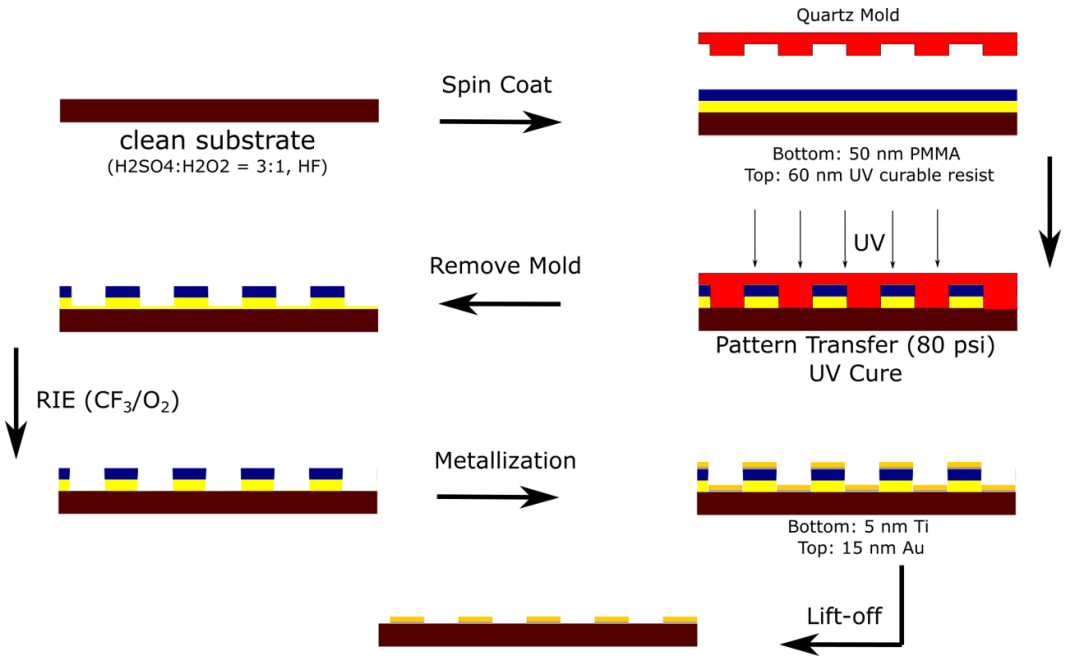

Figure 3.2. Nano-imprint lithography process which can be used for mass production of electrodes by transferring patterns of the mold to fabricate electrodes.

Each set of electrode-contact pad circuitry fabricated was about 2.5mm long and 1.5 mm wide and had 17 individual electrodes. The configuration was visible through optical microscope (Figure 3.3a). In order to ensure that the smallest features were transferred from the mold and no short-circuiting was created, the electrodes at the center of the configuration was imaged with SEM (Figure 3.3b). The SEM images show 50 nm half pitch laminar features. These electrodes fan out to micrometer scale features which fan out to connect contact pads (Figure 3.3c). The pads are 25×25 μm

is size which could be wire bonded or connected to probe station which is connected to the measurement electronics.

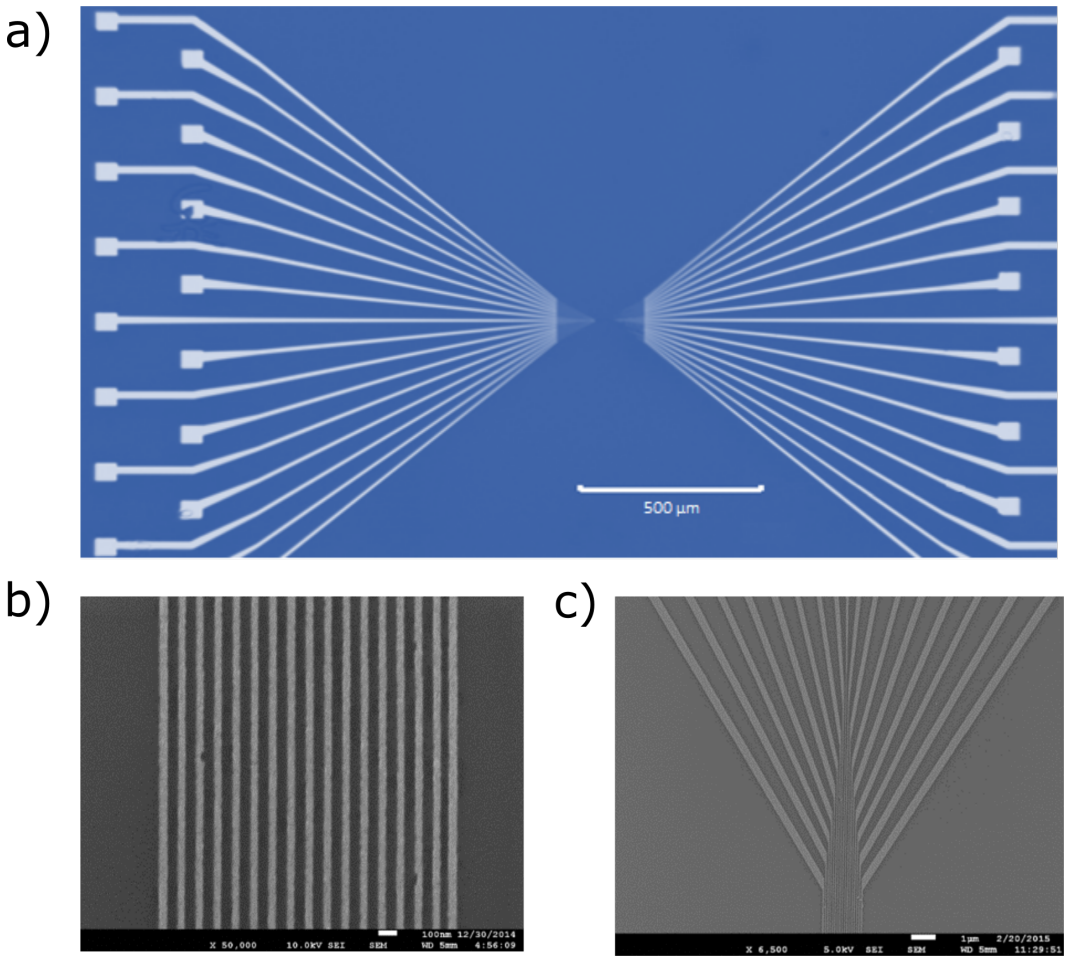

Figure 3.3. Electrodes fabricated by NIL. a) Optical image of fabricated electrode circuit. b) SEM image of the electrodes at the center of the array. Each electrode is 50 nm wide with separation of 50 nm. c) SEM image of fan outs from electrodes to outer pads.

3.2.2 Conductivity Measurements

As described in Chapter 2, pili preparations in ethanolamine buffer (2μl) were drop cast on the electrodes, washed with deionized water and then air dried in desiccator at room temperature (22 ^{0}C) for analysis. Pili on the electrode array were located with atomic force microscopy (Asylum Research). Pilus conductivity was measured with

a Keithley 4200 Semiconductor Characterization System (SCS) in a probe station. The probes (Signatone SE10-T Tungsten) were connected to two Source Measure Units (SMUs) of the SCS equipped with preamplifiers 4100-PA providing the system with capability to measure current signals with resolution of up to 100 aA. Current values were recorded by grounding one of the terminals while the other terminal was set to potentials ranging from -0.5 V to 0.5 V. Constant voltage was applied and current response over time was recorded until the steady state was observed. During the steady state, current through the sample is due to contribution from electronic transport while ionic conduction and leakage current of the system becomes negligible.

Conductivity calculation was performed using $\sigma = G(L/A)$, where G is the conductance value from linear fit of the current-voltage (IV) curve and L is the length of the wire between the electrodes. $A(= \pi r^2)$ is the cross-section area of the nanowire, where r is derived from the height profile of AFM image of pili.

3.3 Conductivity of W51W57 Mutant Pili

3.3.1 Motivation

Various experiments have suggested that tryptophan can help accelerate the charge transport in protein complex and improve the conductivity of the complex. Shih and co-workers [65] reported in 2008 that introducing tryptophan residue as an intermediate electron acceptor between distant metal redox centers enhanced the electron transfer rate by two orders of magnitude. In a study performed on electrical conductivity on peptide networks [66], the peptide network containing phenylalanine and tryptophan exhibited 5 fold higher conductivity than all phenylalanine network. Theoretical calculation in this study suggested that tryptophan-phenylalanine network resembles behavior of conjugated molecules and shows higher conduction than phenylalanine only network.

Regarding pili, once we observed that aromatic residue deficient Aro-5 mutant has severely diminished conductivity, the interest was to investigate if aromatic residues can be increased in pili to improve conduction. The mutation did not affect the amount of production of pili either. This hinted us that *Geobacter* could possibly produce plenty of pili with mutated amino acid contents. Based on the reports of tryptophan mediated electron transfer even for long range in biological systems, we decided to test if it can help improve the conductance through a pilus. Unlike other aromatic residues such as phenylalanin and tyrosine, tryptophan has two conjoint aromatic structures (Figure 3.4a). This helps electrons to delocalize over larger area and makes tryptophan a better candidate to perform as an electron acceptor or a donor. To test this hypothesis, a mutant species with 51^{st} phenylalanine (F) and 57^{th} tyrosine (Y) were replaced with tryptophan (W)(Figure 3.4b)) .

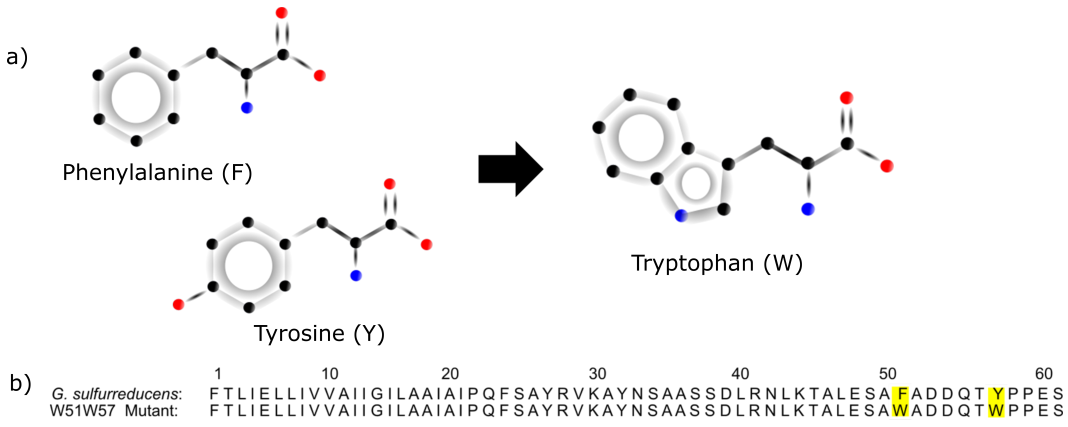

Figure 3.4. a) Aromatic residues with single aromatic ring were replaced with tryptophan (W) with double aromatic rings. Black dot represents carbon, blue represents nitrogen and red represents oxygen. b) Mutation in the pili sequence and consequent change in pili monomer. Changes in amino acid sequence marked in yellow. Phenylalanine (F) at 51st amino acid position and tyrosine (Y) at the 57th position were each replaced with tryptophan (W).

3.3.2 Results and Discussion

In order to mutate *G. sulfurreducens* to produce pili with higher conductivity, genetic mutation was performed with method described by Vargas and colleagues.[18] The strain hence yielded is referred to as W51W57 and was able to produce pili (Figure 3.5a). The pili were harved from the cells, purified (Figure 3.5b), and dropcast on chips with multiple sets of electrodes prepared with NIL.

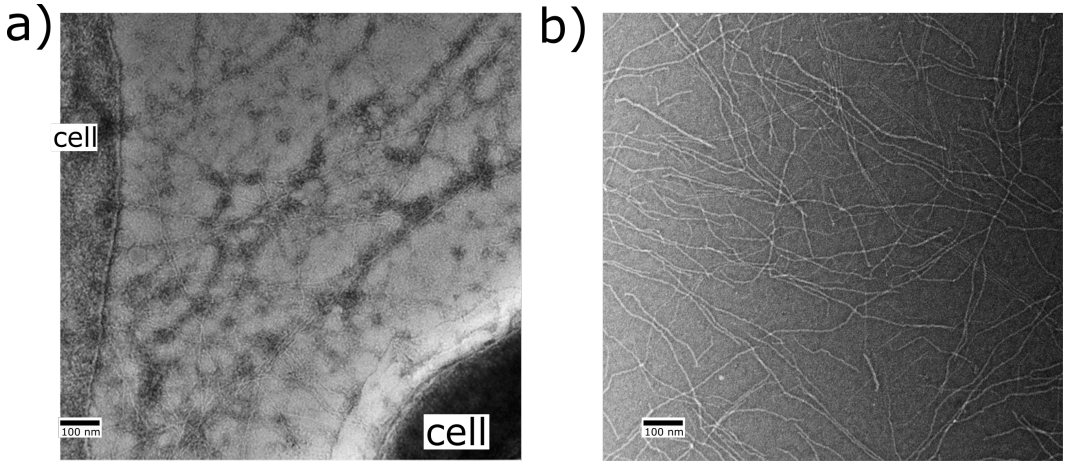

Figure 3.5. a) Transmission electron micrographs of strain W51W57 producing the genetically modified pili. b) The pili harvested from strain W51W57. Scale bars represents 100 nm.[67]

Image of pili was obtained with AFM (Figure 3.6a). When the diameter of the pili was measured, to our surprise, it was only about 1.5 nm (Figure 3.6a,b) which is about half the duameter of pili produced by wild type *G. sulfurreducens*. This implies that there has been significant structural changes of W51W57 pili. Pili are typically assembled by the hydrophobic interaction between the monomers. It is possible that shrinkage in the diameter could be due to the different hydrophobic interaction created between the mutant pili monomer and surrounding water due to the presence of tryptophan. The outermost aromatic structure towards the carboxylic end [24, 25] of a pilin monomer is tyrosine followed by phenylalanine which in this case are replaced by tryptophan. Tryptophan side chain is more hydrophobic than

both tyrosine and phenylalanine.[68] Hence, it could be the reason that causes the pili to collapse towards the long axis causing the diameter to shrink. Detailed structural studies are necessary to evaluate this hypothesis.

An immediate interest this could generate is that this method could be one of the best methods to cost-effectively produce very small diameter nanowires with consistent diameter. There are vast number of ongoing research in materials science on using expensive techniques [69] such as laser ablation, thermal evaporation, chemical vapor deposition, etching[70] or relatively cheaper techniques such as hydrothermal annealing,[69] electrodeposition[71] and chemical synthesis[72] to produce nanowires with high aspect ratio. In addition, there are studies being performed for creating structurally and electronically high aspect ratio nanowires which could open up opportunities for integrated nanoelectronics.[73] Having a method such as genetically mutating *G. sulfurreducens* strain to produce uniform diameter high aspect ratio microbial nanowires will add another dimension to nanowire fabrication process.

There have been various research on combining biological wire-like structures with inorganic material in order to construct inorganic nanowires. DNA is a long strand with diameter of about 2 nm and length up to tens of micrometers.[7, 74] While there has been debate on whether the DNA is intrinsically conductive or not, DNA has found a way into nanotechnology research as an agent to make bottom up approach of nanoscale fabrication easier and cheaper.[75] Taking advantage of its size, stability, topology, functional groups and capacity to self-assemble, it has been shown that DNA can be used as a template to make other organic and inorganic nanowires for possible application in molecular opto-electronics.[76] DNA has been used as a template to construct cadmium selenide nano-rods (22×4.5 nm) which have possible application in polarization sensitive photodetector and micro-emitters,[76] polymer functionalized pi-conjugated DNA nanowires,[76, 77, 78] magnetic nanowires[75], and metallic nanowires based on gold[79, 80] and silver[81] with applications such as nanoscale

metal interconnects, waveguides, and optical sensor chips for single molecule detection.

In other practice of using biomolecules for electronic application, peptide self assembly has been used as promising alternative. Peptides have been assembled into wires, rods and helices with various electronic, optical and mechanical properties that could be of use in bottom-up approach of fabrication of nanostructures. For example, diphenylalanine peptides can self-assemble into highly ordered nano/micro-tubes in which metals can be deposited within hollow cores of the tube and on the outer surface of the tube to form electromagnetic coaxial nanowires.[82] These nanotubes can be used as cost effective method for casting metal nanowires, and etching mask for fabricating silicon nanowires. Arrays of these nanotubes can be used to develop ultra-capacitors for energy storage, microfluidic chips, hydrophobic surfaces, etc.[82]

Peptides can also be genetically modified to act as template for metal nanowires by introducing binding cites for various metals or their oxides.[83] For example, replacing a lysine residue with cysteine in middle region of yeast prion protein SUP35p and octapeptide found in the fiber protein of adenovirus allow gold particles to covalently link with the peptide making nanowires with conductivity comparable to metals such as low resistance and ohmic resistance.[82] Same principle has been applied to TAR-2-Asp peptide which has high affinity to lead to construct lead sensor which responds with higher conduction between the electrons if more lead introduced in the environment.[84]

Other viral proteins have also been functionalized for making inorganic nanowires. Cowpea mosaic virus can be genetically modified to possess cysteine at selected spots have been used as scaffold to construct gold nanowire networks. Biotin was added as recognition system to the viral capsid making the system that would sense the presence of other proteins such as advin, NeutrAvidin, and streptavidin by change in conductance through the network.[85]

With all these practices out there to find out the best method of taking advantages of biomolecules for bottom up approach of nanoscale fabrication, pilus mutation may prove to be one of the most stable ways to get it accomplished. One can think of these microbial nanowires as wires assembled by bacteria with great electronic and mechanical properties. Since, now that we have learned that mutations can be carried out to make smaller microbial nanowires produced by strains such as W5157 mutant, this method can prove to be a great option using them as templates to create inorganic nanowires as well was functionalize them in order to be used as biological or chemical sensors.

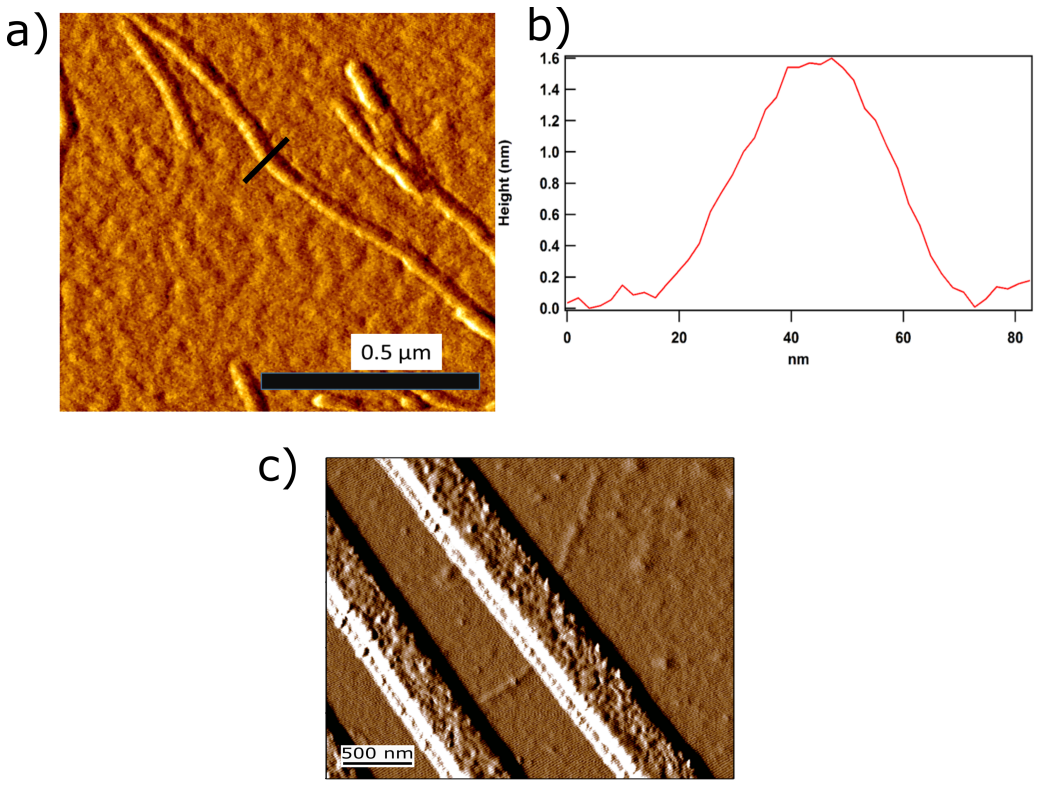

Figure 3.6. a) AFM image of W51W57 pili. The pili appear to be uniformly elongated structures but with diameter of about 1.5 nm (b) which is half the diameter of *G. sulfurreducens* pilus. c) AFM image of W51W57 pilus bridging across NIL electrodes.[67]

In order to perform single pilus conductivity measurements for W51W57 mutant pili, pili in ethanolamine solution were dropcast on NIL electrodes. Single pili bridging electrodes were identified with atomic force microscopy (Figure 3.6 c). Measurement was performed under probe station and process was the same as the measurement process for *G. sulfurreducens* pilus measurement in Chapter 2. The steady state current was recorded for each applied voltage ranging from 0.5 V to -0.5 V.

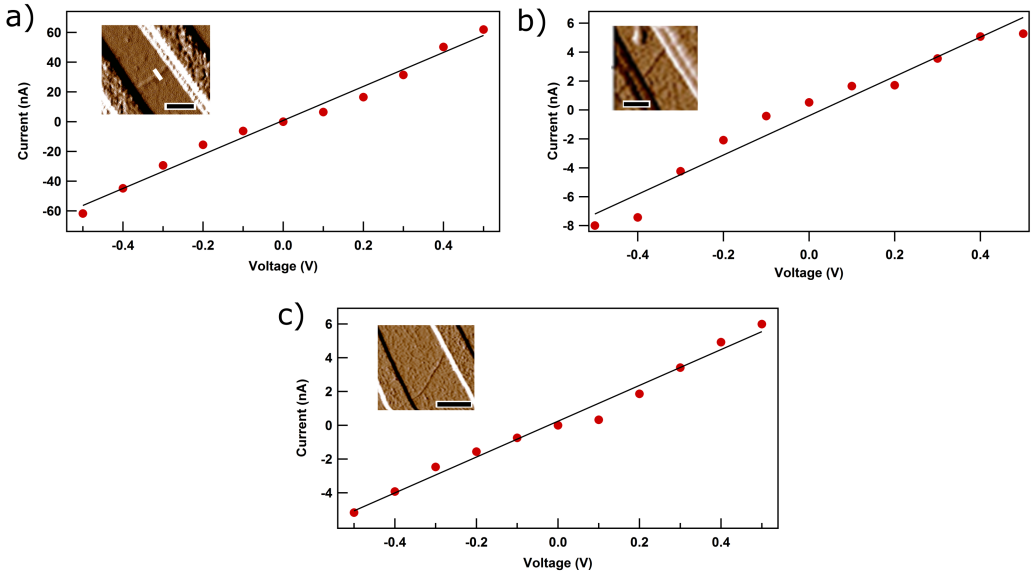

Figure 3.7. Current-voltage(IV) response of mutant W51W57 pilus at pH 2. Three different pilus samples were measured. Insets are the AFM images of the pilus bridging electrodes for each case.[67]

At pH 2, it was observed that the W51W57 pili are very conductive. Three measurements for conductivity of the pili were performed as shown in Figure 3.7. The conductivity for a pili sample was substantially higher than for two other pili. One of the metal-pilus-metal systems that exhibited the highest conductance (Figure 3.7a) had conductivity of about 977 ± 41 S/cm. This conductivity is as much as 5000-fold higher than the previously measured[33] of wild type *G. sulfurreducens* pili at pH 2. The second sample (Figure 3.7b) had conductivity of about 155 ± 8 S/cm and the third sample (Figure 3.7c) exhibited conductivity of 90 ± 4 S/cm. This gives us an

average conductivity of 388 ± 237 S/cm (n=3; mean± standard error) for W51W57 pili conductivity, which in average is 2000-fold higher conductivity than the wild type counterpart.

Since the helical aromatic core has a radius of less than a nanometer, we believe that this conformational changes created due to hydrophobic interactions with monomer would not destroy the $\pi - \pi$ interaction. Rather, due to tryptophan coming closer to the core could promote the pi-stacking. This could explain the higher conductivity of these mutant pili.

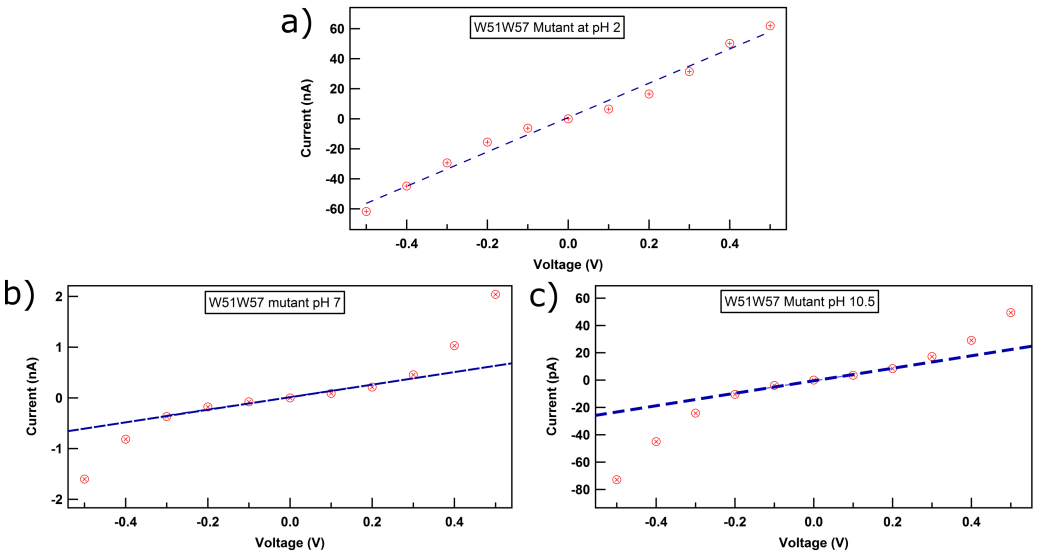

Figure 3.8. Current-voltage (IV) response of W51W57 pilus at a) pH 2, b) pH 7 and c) pH 10.5. Conductivity values were extracted from the linear part of the IV curve.

For pH 7, we observe linear Ohmic response at lower voltage (Figure 3.8b) and non-linear regime at higher voltages. The average conductivity calculated for the linear regime from the three samples is 10.5±1.5 S/cm which is about 200-fold higher than the conductivity of the wild type sample at this pH environment. For high pH of 10.5 (Figure 3.8c), the non-linearity is higher compared to the sample at pH 7. The average conductivity value at this pH is 0.32±0.12 S/cm. This value is about three orders of magnitude higher than the conductivity of wild type at this pH.

Two things are important to be noted here. One is the increasing conductivity of pilus with lowering pH as seen for other pilus samples. This phenomenon appears to be the same for W51W57 pili as well. The conductivity values for different pH are presented in Figure 3.9a) while the buffer samples do not show any significant changes. As discussed in Chapter 2, this phenomenon could be attributed to the increased packing of the aromatic amino acids at lower pH [24] as well as due to the contributions of the charged amino acids for charge transfer.[33] Second observation is the massive change in the magnitude of the conductivity of pili recorded for the mutant with tryptophan, making it comparable to other nanowires (Figure 3.9b).

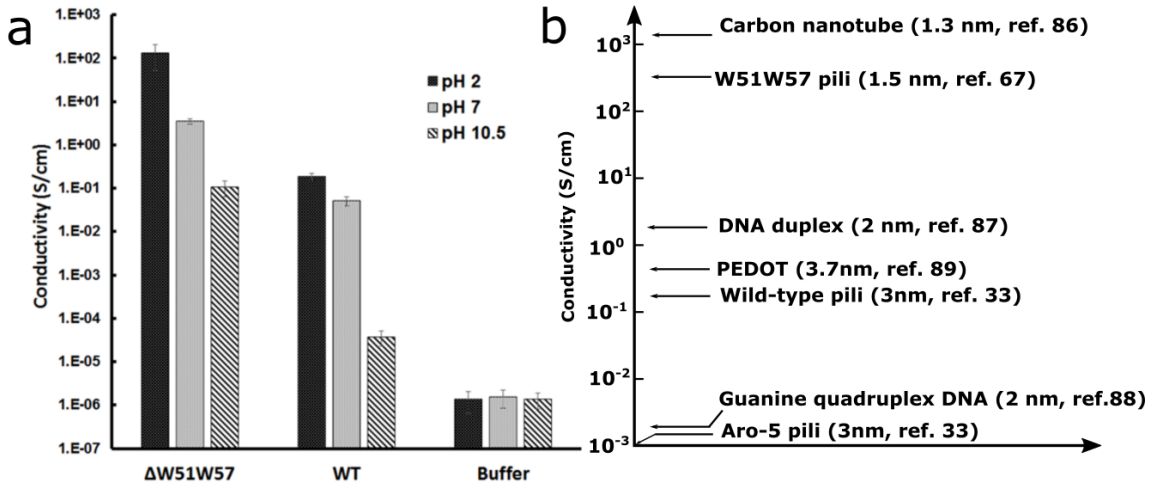

Figure 3.9. a) Dependence of conductivity of W51W57 mutant pili on varying pH environment in comparison with wild type pili. Buffer samples show no change in conductivity with pH. b) Conductivity of W51W57 mutant pili compared to various organic and biological nanowires of similar dimension.[67]

An important consideration for the practicality of microbial nanowires is whether they can match the conductivity of other organic conductive materials. When compared with other materials of similar diameter, the conductivity of the W51W57 pili prepared at pH 2 is somewhat lower than that of carbon nanotubes[86], but is substantially more conductive than DNA[87, 88] or PEDOT (poly(3,4-ethylenedioxythiophene)) nanowires[89] (Figure 3.9b).

In summary, these results demonstrate the potential of synthesizing electrically conductive, non-toxic nanowires with a sustainable biological process fueled with inexpensive renewable substrates. The simultaneous reduction in diameter and increase in conductivity associated with genetic modification reported here demonstrate just some of the possibilities for improving the properties of electrically conductive pili. Based on studies with other proteins, it is likely that the pili can be modified to enhance binding of a diversity of materials[90, 91] or conjugation with polymers[92]. The ability to mass-produce such thin conductive filaments with consistent uniform diameters, morphology, and composition with simple renewable feedstocks could be an attractive option for nanowire synthesis.

3.4 Conductivity of *G. metallireducens* Pili

G. metallireducens is one of the naturally occurring *Geobacter* species with larger amino acid residues in its monomer. The PilA genes of *G. metallireducens* were expressed in *G. sulfurreducens* with the method described by Vargas and colleagues.[18] The strain produced abundant pili (Figure 3.10a) and were purified (Figure 3.10b) to be used for measurement.

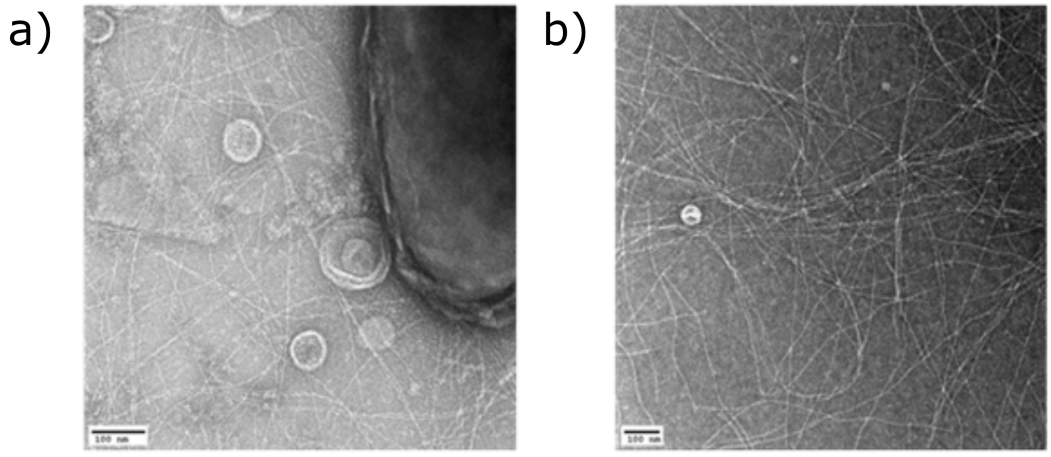

Figure 3.10. TEM image of a) pili produced by *G. metallireducens* expressed in *G. sulfurreducens*, b) Purified harvested pili. (Credit: Joy E. Ward)

The purified pili solution was dropcast on NIL electrodes and washed with DI water as explained in preparation methods for other pili already discussed. AFM imaging was performed to locate a pilus bridging electrodes (Figure 3.11a). The diameter of the pili was about 3 nm (Figure 3.11b), similar to that of *G. sulfurreducens*. Current-voltage(IV) response measurements were performed in a probe station with Keithley 4200 SCS Paramteric Analyzer. Constant potential ranging from -0.02V to 0.02 V was applied on the sample and steady state current was recorded for pili in both pH 7 and pH 2 environment (Figure 3.11c,d).

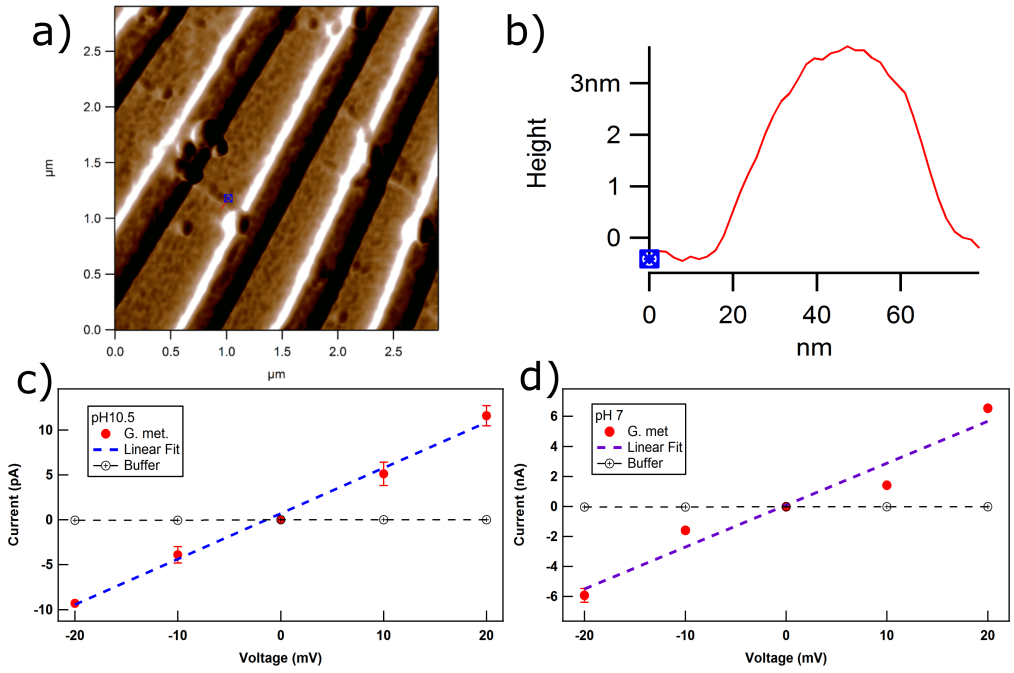

Figure 3.11. a) *G. metallireducens* pili bridging electrodes. b) Height profile of the pili. c) IV response of *G. metallireducens* at pH 10.5 and d) pH 7. The average value of the current from three measurements are represented as datapoints while standard error is represented as error bar.

Conductivity of the *G. metallireducens* pili was calculated to be 277 ± 19 S/cm at pH 7 while at pH 10.5 it was 0.503 ± 0.067 S/cm. Both of these conductivity values are higher than that of *G. sulfurreducens* pili and even W51W57 pili as well. The pH

7 conductivity is about 27 fold higher than that of W51W57 mutant and about 5000 fold higher than *G. sulfurreducens*.

As shown in Figure 3.1, *G. metallireducens* pilin monomer, which contains 59 amino acids is shorter than *G. sulfurreducens* pilin monomer which contains 61 amino acids. In addition, *G. metallireducens* has 9 aromatic residues in a pilin monomer while *G. sulfurreducens* has 6 aromatic residues in a pilin monomer. This shorter monomer length with higher number of the aromatic residues seems to make the pili very conductive. Observation of higher conductivity of this pili and larger number of the aromatic amino acid content implies that the aromatic residues indeed contribute to the conduction through the pili.

The discovery of conductive pili in *G. metallireducens* is consistent with its requirement for pili for Direct Interspecies Electron Transport(DIET) and its ability to produce high current densities[93]. Expressing the more highly conductive *G. metallireducens* pili in *G. sulfurreducens* did not increase the ability of bacteria to reduce Fe(III) oxide faster or to produce higher current densities than the control *G. sulfurreducens* strain expressing the wild-type pili. There are many steps in *G. sulfurreducens*, most of which are poorly defined and understood, between the uptake of acetate as an electron donor and the final step of electron transfer to an extracellular electron acceptor. The results presented here suggest that the conductivity of the wild-type *G. sulfurreducens* pili is not the limiting step.

3.5 Conductivity of *G. uraniireducens* Pili

G. urannireducens biofilm exhibit low current densities and poor Fe(III) oxide reduction. This suggests that their pili could be poorly conductive. Their pili possess a distinctive length of pilin monomer and distribution of aromatic residue in the pili (Figure 3.1). A pilin monomer constitutes 120 amino residues which is almost double the length of *G. sulfurreducens*. On the other hand, *G. uraniireducens* has

8 aromatic residues while *G. sulfurreducens* has 6 aromatic residues. However, the aromatic residues in *G. uraniireducens* pili are existent within the first half of the pilin monomer towards amino end. The half of pilin towards carboxylic end does not have a single aromatic amino residue. When these pilin monomers come together to form a pilus, it seems impossible for aromatic residue to form any continuous aromatic residues. In addition, the lack of aromatic residues towards the carboxylic end also suggests that it would be difficult for the aromatic residues towards shell of pili to facilitate charge transport across the radius of the pili and hence demonstrating low conductivity.

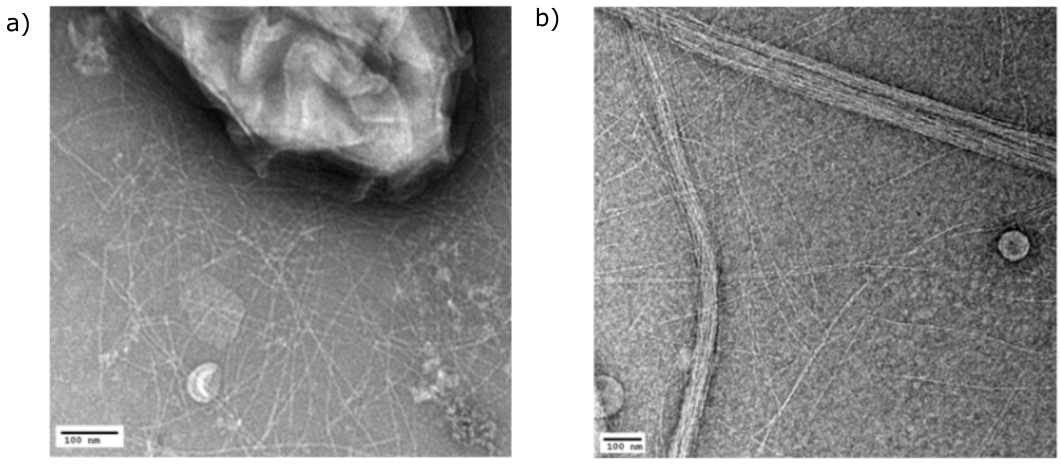

Figure 3.12. TEM image of a) pili produced by *G. uraniireducens* expressed in *G. sulfurreducens*, b) Purified harvested pili. [94]

In order to directly evaluate the conductivity of the *G. uraniireducens* pili, preparations of pili sheared from the *G. uraniireducens* cells (Figure 3.12) were placed on a NIL nanoelectrode array mentioned earlier in the chapter. AFM revealed pili bridging several of the electrodes (Figure 3.13a). The diameter of the pili was $3nm$ (Figure 3.13b), comparable to that of the *G. sulfurreducens*. The current-voltage response of pili bridging two electrodes was linear, implying an ohmic effect (Figure 3.13c). The conductivity of the pili at pH 7 was 0.3 ± 0.09 mS/cm (mean $\pm$ standard deviation;

n=3), which is more than two orders of magnitude lower than the previously reported [33] conductivity of *G. sulfurreducens* pili at pH 7 (Figure 3.13d).

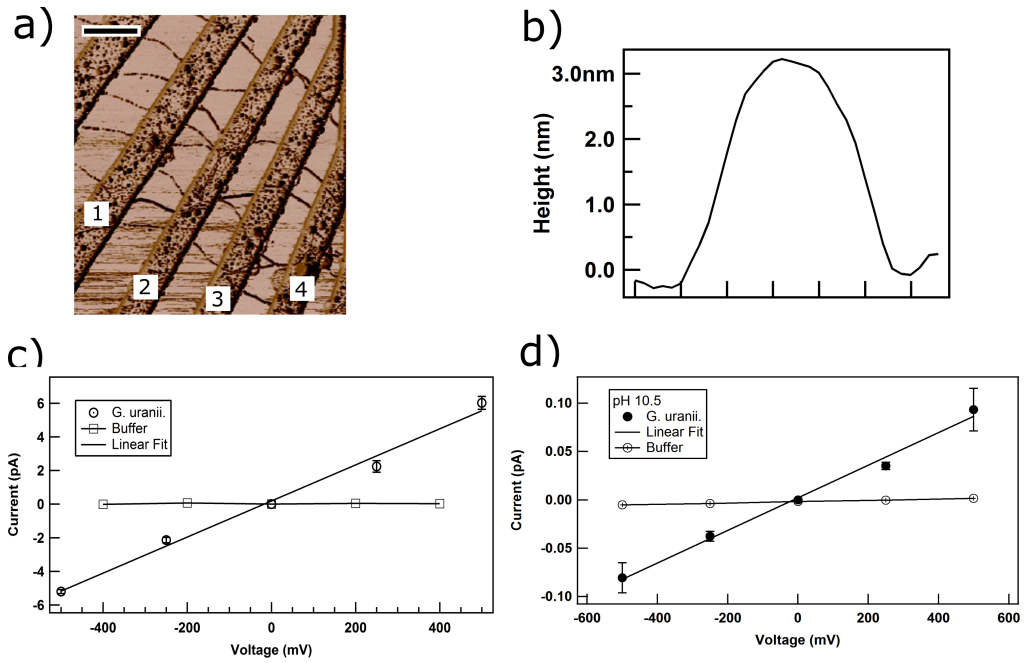

Figure 3.13. Conductivity of *G. uraniireducens* pili. a) AFM image of the *G. uraniireducens* pili bridging electrodes. Electrode pairs 1-2, 2-3 and 3-4 were used for the conductivity measurements. The scale bar represents 500 nm. b) Diameter (height) of the G. uraniireducens pili. c) Current-voltage response of the pili at pH 7 and d) pH 10.5. The average value of the current from three measurements are represented as data points while the standard error is represented as the error bar.[94]

The conductivity of the *G. uraniireducens* was calculated as the same manner as explained above. In order to account for the multiple pili bridging across the electrodes, we treated them to be equivalent to the multiple resistors in parallel. Assuming that all the pili have the same resistance, the equivalent resistance of n number of pili across electrodes would $R_{eq} = R/n$, where R is individual resistance of the wire. This implies that the equivalent conductance would be $G_{eq} = n \cdot G$, where G is conductance of an individual pili. Therefore, conductance of an individual pilus can be derived from the equivalent conductance extracted from the linear fit of

the IV graph and dividing the value by the number of pili bridging the electrodes as observed in the AFM images.

3.6 Relationship between Aromatic Residues and Conduction

In this manner, I completed single pili conductivity study for five different samples - *G. sulfurreducens*, *G. metallireducens*, *G. uraniireducens*, W51W57 mutant and Aro-5 mutant. Even though all of these pili are produced by bacteria of genus *Geobacter* and related mutants, they provide pili with varying morphology and aromatic amino acid residue distributions. Since aromatic amino acids appear to be the main contributor of the conductivity through the pili, an obvious measure is to observe how the relationship between the presence of the aromatic amino acid residues correlates with conductivity of pili.

As shown in Figure 3.14, we observe that the conductivity of the pilus is higher for samples with higher number of aromatic residues. The number of aromatic residues is higher for the samples towards the left side of the graph. One outlier is *G. uraniireducens* pilus which has same number of aromatic residues in pilin monomer as that of W51W57 mutant and higher than *G. sulfurreducens* (Table 3.1). In addition, the same *G. uraniireducens* has pilin longer than any of the other species or mutants under study. It is almost twice as long as the wild type *G. sulfurreducens* pili. On the other hand, highly conductive *G. metallireducens* has shortest length among all the pili we have studied. This suggests that consideration for some combination of number of aromatic residues in pilin monomer and length of pili is needed for understanding the transport through pili.

One of the measures to look at the relationship is to normalize the aromatic residue content in a pili and visualize its correlation with pili. Since aromatic number and monomer length are variable, one can normalize the aromatic residue content with

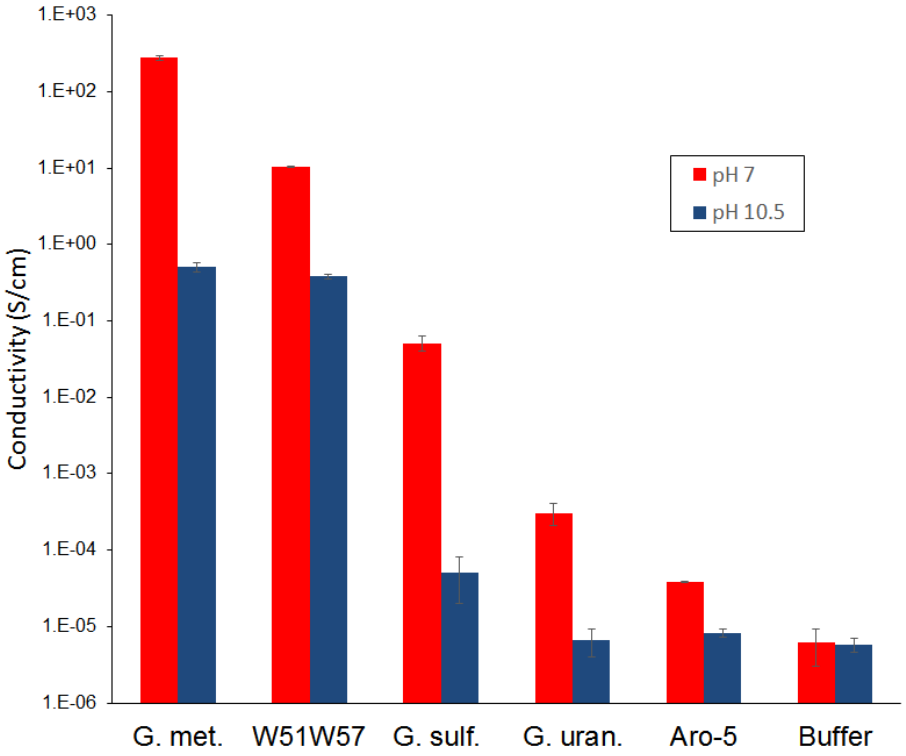

Figure 3.14. Conductivity for various *Geobacter* species and mutants. The increasing conductivity of the pilus from right to left seems to co-relate with higher aromatic residues and shorter pilin monomer.

respect to the monomer length and derive the aromatic residue density (ρ_{Aro}). Table 3.1 contains the data for aromatic residue density and conductivity of various pili for which individual pilus measurements were made.

When the conductivity of pili was plotted (Figure 3.15) with aromatic residue density ($n = N/L$) an interesting phenomenon was observed except for Aro-5 mutant. Aro-5 mutant has only one aromatic residue in pilin monomer and hence the aromatic amino acids are too far away to contribute to conduction through pili. When we look at the conductivity of other pili samples, the exponential relationship is very pronounced. It appears that there is a presence of threshold density of aromatics before the aromatic residues become dense enough to be relevant for conductivity

Sample	N	L	$\rho_{\mathbf{Aro}}$	σ-pH 7(S/cm)	σ-pH 10.5(S/cm)
G. met.	9	59	0.153	277±18.9	0.503±0.067
W51W57	8	61	0.13	10.3±0.084	0.383±0.025
G. sulf.	6	61	0.098	0.051±0.019	$(5.1 \pm 3.10) \times 10^{-5}$
G. urani.	8	120	0.067	$(3.1 \pm 0.95) \times 10^{-4}$	$(6.53 \pm 2.58) \times 10^{-6}$
Aro-5	1	61	0.016	$(4 \pm 0.1) \times 10^{-5}$	$(8.20 \pm 1) \times 10^{-6}$

Table 3.1. Relationship between conductivity and aromatic residues. N represents the number of aromatic residues in a pilin monomer, L is pilin length i.e. number of amino acids in a pilin, ρ_{Aro} is density of aromatic residue (L/N), and σ represents conductivity.

through pili. Therefore, as shown in Figure 3.15, two regimes of conduction are observed.

Below threshold near residue density of 0.06 residue per unit length, it appears that the conductivity is dominated by dopant induced carriers. The conductivity improvement is not very significant with increase in residue density, but the values are larger for pH 7 samples compared to the same nanowires in pH 10.5. This suggests that increase in carrier density and charge configuration in pili are dominant mode of conduction below threshold aromatic residue density. Above the threshold, the conductivity values of pili increase exponentially with the aromatic residue density. This suggests that at this regime, the interplay between increased carrier density and doping due to lowering pH and contribution of aromatic residue is evident. Lowering pH improves the conductivity and the observation is similar to conduction at pre-threshold regime. However, aromatic residue density appears to have significant affect on the conductivity of pili.

This dependence is studied by fitting post-threshold regime in log-linear plot in Figure 3.15 with linear function. For pH 7, the linear curve fits the data points quite well and the function is $ln(\sigma) = 160.52n - 18.76$. After working out for expression for conductivity, one can achieve:

$$\sigma = 7.12 \times 10^{-9} \cdot e^{160.52n} \tag{3.1}$$

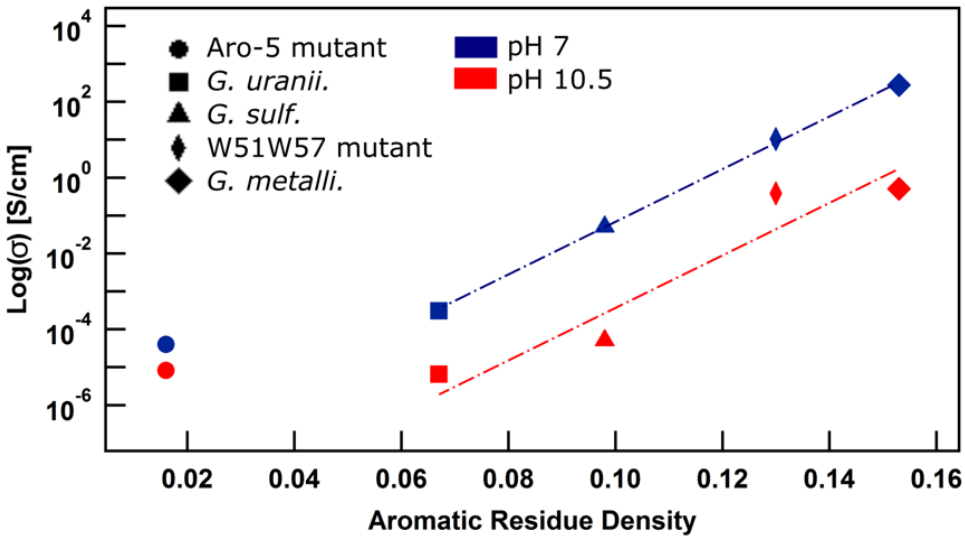

Figure 3.15. Relationship between pili conductivity *vs.* the aromatic residue density. The graph shows exponential relationship between the aromatic residue density and conductivity. pH 7 and pH 10.5 data have been presented.

where, n is the aromatic residue density which is the ratio of number of aromatic residues in a monomer (N) and the length of the monomer (L). Similarly for pH 10.5, linear fit to post-threshold regime is $ln(\sigma) = 149.12n - 22.57$. Hence, the expression for conductivity is:

$$\sigma = 1.58 \times 10^{-10} \cdot e^{149.12n} \tag{3.2}$$

The value of coefficient of the exponential function is 45 fold higher for pH 7 samples compared to pH 10.5 samples. This value is possibly determined by the parameters involving charge configuration within pili and doping of pili induced by pH.

On the other hand, the rate of increase in the logarithm of the conductivity of pili sample is proportional to the aromatic residue density. The observation of exponential growth in conductivity with residue suggests of the possibility of constructing highly

conductive microbial nanowires by increasing density of aromatic residue within pilin monomer.

As shown in Figure 2.2 of the second chapter, there are two kinds of distributions of aromatic residues on a pilus. Some aromatic residues, closer towards the amino end of the monomer, come together to form conducting helical structure. Other aromatic residues which are found closer towards carboxylic end are distributed over the body and periphery of a pilus. So far, only the relevance of the aromatic residues forming helical conducting path have been brought to attention when discussing about charge transport through pili. However, looking at the exponential dependence of conductivity of the pili with the aromatic residue density, it appears that not only the aromatic residues that form the helical conducting core of the pili, but other aromatic residues in the pilus also play a role in conduction mechanism.

This observation may also be an effect observed due to two probe measurement where not only the conduction through the pili plays a role in the acquired signal, but also the contact interface between a pilus and electrodes. When a pilus rests on electrodes after dropcasting, it is expected that when a potential is applied, the charge carrier that gets injected from electrode to pili would tunnel though the shell of the pili and gets transported along the helical conducting chain. For example, in case of W51W57 mutant when last two aromatic residues were replaced with tryptophan, the high conductivity observed could be due to electron transfer facilitated by the tryptophan at the interface between pili and electrodes in addition to tryptophan residues facilitating transport along the length of the pili. Following the same narrative for *G. uraniireducens* pili, the long aromatic residue deficient carboxylic end may create a non-conductive layer around the pili making it much difficult for electron to be transferred between aromatic residues at core to the electrode at the surface. While at the same time the long pilin monomer with aromatic residue deficient sec-

tion could from large separations of the aromatic residues at core of a pilus. Both of these cases would severely limit transport along the pili.

3.7 Conclusion

It is clear that number of aromatic residues in pilin monomer dictates the conduction though pili, unless if the aromatic rich monomer also have long aromatic residue deficient part to it. One of the interesting findings from this project is that even within *Geobacter* species there are diversities in the conduction mechanism of the pili for different species. This variation in the conductivity comes from the diversity in amino acid sequence and length which determined the density of the aromatic residues in pili. It appears that despite the length of the pili sequence, the sample that has higher aromatic residue density makes more conductive pili.

Another interesting finding is that we can tune the conductivity of pili by genetically mutating the pili to incorporate more aromatic residues. This kind of "genetic doping" opens up new ways into making novel materials according to out need. An obvious question that follows is what is the limit of conductivity of pili? That will depend on how many amino acid residues can be switched with aromatic residues by mutation while still getting the bacteria to produce pili.

It was also interesting to find out that when we introduced tryptophan through mutation in pili, the diameter shrunk in half to about 1.5 nm. This diameter is narrower than DNA. It turns out that we stumbled into method of creating very small but uniform diameter nanowires which has been drawing lot of interest in materials science for nanoelectronics. While we do not understand what made this pili to shrink in diameter, this phenomenon in conjunction with cross-linking armino residues introduced by genetic mutation could lead to a number of studies of using these kinds of pili as template for construction of extremely narrow diameter metallic or semiconducting nanowires and sensor application.

CHAPTER 4

TRANSPORT PROPERTIES OF MICROBIAL NANOWIRES

4.1 Introduction

In addition to the conductivity of pili, information about other transport properties such as mobility, charge density, and band gap can help us develop insight on mechanism of transport in microbial nanowires. Some of this information can be gained from the conductivity measurements, while various other electrical and optical probing methods can be applied to gain addition information about the transport properties. Based on the experimental results presented in the earlier chapters, and other new experiments various transport parameters will be calculated and quantified. Also, some possible device applications will be suggested in this chapter.

4.2 Respiration Rate

When we measured the conductivity of pili, we applied a potential across the pili bridging electrodes and measured the current response. In its environment, *G. sulfurreducens* itself generates potential inside the cell so that electric field gradient is created along the pili and charge is transported along the pili. In other words, when *G. sulfurreducens* respires in order to support its metabolism, it creates a potential bias with respect to the surrounding electron acceptors, generating current along the pili. If we know the potential bias created in a *Geobacter* cell, with the information about the conductivity of pilus, we can calculate the electron transfer rate along the pilus which will be equivalent to the respiration rate.

In order for the conductivity of a pilus to have physiological relevance, the conductivity must be sufficient to transfer electrons at rates that can support respiration. The electron transfer rate (Γ) along a pilus can be calculated as:

$$\Gamma = \frac{I}{e} = \frac{\sigma \cdot A \cdot V}{e \cdot l} \tag{4.1}$$

where, I is the current through the e-pili at the redox potential (V) over the pilus length [95], σ is conductivity, A is the cross sectional area of the pilus, and e is the fundamental electronic charge.

The maximum rate for *G. sulfurreducens* electron transfer to electrodes or Fe (III) is about 8 mA/mg protein.[96] A cell contains about 10^{-13} g of protein. This provides rate equivalent to approximately 5×10^6 electrons/sec per cell. The electron carrier(s) that transfer electrons to the *G. sulfurreducens* e-pili is as yet unknown. However, the periplasmic, multi-heme c-type cytochrome PpcA is a likely candidate because it is one of the most abundant proteins in *G. sulfurreducens* and is considered to be an important intermediary in electron transport from the inner membrane to outer surface electron transport components.[97]

Furthermore, PpcA is a conservative choice for estimating e-pili conduction rates because its mid-point potential of $-170mV$ is more positive than the mid-point potentials of other potential electron carriers.[98] Maximum rates of electron transfer to electrodes were documented at +240 mV,[96] yielding a V (voltage difference along the e-pilus [+240 mV - ($-$170mV)]) of 410 mV. *G. sulfurreducens* pilus can extend up to 20 μm. Over this length the rate of electron flux through an individual pilus at a 410 mV potential difference is estimated (Equation 4.1) to be 4 $\times 10^6$ electrons/sec. Therefore, flux along a single pilus would be nearly sufficient to account for the long-range electron transport requirements of *G. sulfurreducens* at maximum respiration rates. *G. sulfurreducens* cells typically express more than 20 e-pili,[26, 99] and thus a single cells full complement of pili should be able to accommodate rates of elec-

tron transport well in excess of the cell's need for extracellular electron transfer to electrodes.

A lack of reliable information on the potential of poorly crystalline Fe (III) oxide, which is the only source of Fe(III) oxide that *G. sulfurreducens* can reduce, makes it difficult to make comparable calculations for Fe (III) oxide reduction. In a similar manner, there is no information on the electron-accepting proteins involved in direct interspecies electron transfer. However, even at a minimal potential difference of 100 mV, a single pilus can transport 1×10^6 electrons/sec per cell over 20 μm. Given that rates of Fe (III) oxide reduction and interspecies electron transfer are slow compared to maximal current production rates, and the fact that Fe (III) oxides and electron-accepting cells [100] are often much closer to the cell than 20 μm, it is likely that the multiple e-pili of *G. sulfurreducens* can also readily accommodate extracellular electron transport to Fe (III) oxides or other cells.

The pili from *G. uraniireducens* are about 1000 times less conductive than *G. sulfurreducens*. That would provide respiration rate estimation at the order of 10^3 electrons per second per cell. This will require more than 300 pili to support maximum rates of electron transport which is not realistic. However, it has been proposed that these species circumvent this limitation by releasing compounds that can serve as an electron shuttle between the outer surface of the cell and electron acceptors around them.[94] This is reducing mechanism which enables microbes *Shewanella oneidensis* and *Geothrix fermentans* reduce Fe(III) oxides despite the lack of conductive pili.[101, 102]

On the other hand, *G. metallireducens* produces conductive pili just like *G. sulfurreducens*. It is not certain as to whether their pili would provide any more advantage to the bacteria since conductivity through *G. sulfurreducens* is enough for maintaining respiration. However, higher conductivity may be beneficial during direct interspecies electron transfer (DIET) and its ability to produce high cur-

rent density.[103] *G. metallireducens* is capable of directly donating electrons to *Methanosaeta* or *Methanosarcina* species for carbon dioxide reduction to methane.[104, 105]

4.3 Charge Mobility of an Individual Pili

One of the parameters that can be calculated based on the recent low atomic energy model of *G. sulfurreducens* pili is charge carrier density. In lack of full detailed molecular structure information of the pili (from, for example, x-ray scattering techniques), modeling can be used to estimate the size of the unit cells and the number of carriers in a unit cell. I will be using parameters developed in the low energy atomic model based modeling of *G. sulfurreducens* developed by Xiao and colleagues.[25] Since aromatic residues form helical conducting core, one unit cell can be defined as the axial rise occurred when the aromatic residue make one complete turn. The axial rise per turn is about 10 Å, with about six residues per turn.[25] Radius of pili according to the model was about 17 Å, similar to the experimental value. Using these parameters, the volume charge density in a unit cell can be calculated as:

$$\rho = \frac{N}{\pi r^2 z} = 6.5 \times 10^{20} cm^{-3} \tag{4.2}$$

where, N (=6) is the number of aromatic residues per unit cell, r (=1.5 nm) is the radius of pili and z (=10.5 Å) is the length of the unit cell. This charge carrier density is quite large and is a common phenomenon among organic conductors. For example, polyaniline has charge carrier density of 2.7×10^{21} cm^{-3} in fully HCL doped state.[106] In contrast, the charge carrier density of inorganic nanowires are orders of magnitude lower. For example, carrier concentration for indium-arsenide(InAs) nanowires is in the order of 10^{18} cm^{-3} [107] and for gallium nanowire is in the order of 10^{13} cm^{-3} [107] and for silicon nanowire is 10^{10} cm^{-3}.[108]

The carrier density calculated here is a good estimate for the physiologically relevant environment i.e. at around pH 7 while the solution is neutral. The modeling from which the parameters have been derived does not include the effect of the environment. It has been shown that the carrier density for conjugated systems like polyanaline increase exponentially with increasing pH due to increase in protonation.[106] It is not properly understood how changes in the pH would affect the charge carrier density of a pilus. Since conductivity of a material is dependent on its carrier density, understanding the behavior of carrier density with different doping levels would help understand charge transport in pili.

One of the projects that could be undertaken is to understand how the changes in pH changes charge carrier density in pili. The relationship between pH and and proton concentration is: pH = -log[H^+]. Every unit increase in pH represents an order increase in concentration of proton in solution. It is not understood as to how this would affect the carrier concentration in pili itself. Studies have been performed in polyaniline to understand the effect of pH on carrier density from molecular modeling and simulation.[106] This work has demonstrated that the carrier density in polyaniline can increase by 1000 fold for two unit increase in pH. Eventually, it was demonstrated that the conductivity in polyaniline is exponentially dependent on charge carrier density which is similar to the observation I have presented in Figure 3.15.

Conductivity, mobility, and carrier density are related quantities. A thorough experimental studies would be necessary to truly understand the relationship between these parameters. Here, I will use one of the widely used relationships that will help us estimate the carrier mobility from known quantities. Using the experimental conductivity value (σ) in conjunction with the charge carrier density (ρ) calculated in equation 4.2, one can calculate the mobility of the pili.

$$\sigma = e \cdot \rho \cdot \mu \Rightarrow \mu = \frac{\sigma}{e \cdot \rho} = 3.58 \times 10^{-4} cm^2 V^{-1} s^{-1} \tag{4.3}$$

where e is the elementary charge. This carrier mobility is on par with its organic counterparts[109, 110] and much lower than inorganic counterparts such as silicon which can be doped with arsenic or boron to provide mobility of up to the scale of 10^5 $\mathrm{cm^2V^{-1}s^{-1}}$.[111]

For application in electronic devices and to potentially replace silicon, germanium and other inorganic semiconductors as active materials, it is necessary that the carrier mobility to be increased. There have been various studies on strategies to improve mobility of organic polymers.[112, 113] Carrier mobility is easily affected by molecular ordering, grain sizes, boundaries, and impurities.[113] Organic semiconductors in their crystalline form such as pentacene crystalline thin films (40 $\mathrm{cm^2V^{-1}s^{-1}}$) and rubrene single crystals (43 $\mathrm{cm^2V^{-1}s^{-1}}$) have high mobility. For conjugated polymers, however, the 10 $\mathrm{cm^2V^{-1}s^{-1}}$ has been the highest mobility achieved. Poor packing and lack of microscopic order have been a setback for achieving higher mobility in polymers.[114] Due to the similar polymeric structure, the low mobility in microbial nanowires produced by *G. sulfurreducens* could also be due to environmental or structural disorders.

As discussed in previous chapters, the conductivity of the microbial nanowires can be increased by orders of magnitude by proton doping. At this point we do not understand how the carrier concentration, mobility, and the conductivity in the microbial nanowires are related. An interesting study would be investigating the effect of doping on the carrier mobility or density. This would not only help us better understand the mechanism of charge transport in microbial nanowires, but also help develop methodologies to improve mobility for possible application in electronics.

4.4 Optical Studies of Microbial Nanowires

4.4.1 X-ray Diffraction

High resolution X-ray crystallography would provide the information about the structure of the microbial nanowires which would vastly improve our understanding of charge transport mechanism through these nanowires. However, obtaining X-ray crystallography of protein structures is very challenging due to unpredictable nature of the protein and low success rate of crystallization.[115] For X-ray crystallography, the protein must be purified, crystallized and must defract to sufficient resolution. The success rate of the crystallization is so low that greater than 60% of the overall cost of the structure determination efforts are due to failed attempts.[116]

NMR is another method for understanding structure of protein, but it requires large volume of target to be produced with very high concentration.[116] There has been NMR study on *G. sulfurreducens* pilin.[117] However, the study demonstrated that the pilin monomer in solution could have 18 different conformations towards its carboxylic end. This has proven to be a challenge in developing the best estimate of the pilus structure. There have been homology based modeling[24] and low energy atomic model[25] of pilus derived from NMR pilin structure. While these structures have provided best estimates of the structure of entire pilus, knowing the exact structure has been a challenge.

Despite the technical difficulties of performing X-ray crystallization, one can perform X-ray diffraction experiments on the pili and get some information, especially if any order is improved in the sample despite the random distribution and alignment of pili in the network. A study performed on highly purified polyaniline has shown that when the structural defects of the sample were reduced, the X-ray diffraction peak at 20^0 corresponding to face-to-face stacking distance between phenyl ring improved.[118] The samples with higher peak at 25^0 also had improved conduction compared to the samples with very low intensity peak at that angle. The reduction in

the conductivity and X-ray peak were attributed to combination of molecular-scale disorder and structural inhomogeneities at mesoscopic length scales. This creates disorder-induced localization of the charge carriers and impedes carrier transport and shortens mean free path.

A similar observation has been reported for *G. sulfurreducens* pili. Quite remarkably pH 2, the X-ray diffraction peak had 100-fold increase in the intensity compared to that of peak for pili in pH 10.5 environment.[24] On the other hand, as discussed in this dissertation and other publications[22, 33], the conductivity of the pili increases with lowering pH. Like in the case of the polyaniline, it appears that with lowering pH more order is created within pili due to the charge interaction of amino acids with excess proton in the environment. This conformational change appears to essentially improve the pi-stacking between the aromatic amino acid residues.

As described in Chapter 3, the conductivity of the mutant W51W57 pili also increases with lowering pH. Therefore, I decided to investigate if this increase can also be attributed to the conformational changes with better pi-stacking of the aromatic residues.

During X-ray diffraction, an X-ray is shined on the sample and reflected ray is detected. The rays that are reflected have different phases compared to each other and the highest intensity would be detected due to constructive interference if the phase difference between the reflected beam is multiple of wavelength. The phase that gives constructive interference is achieved by changing the incident angle. From this observation, one can calculate the atomic spacing. This phenomenon is mathematically described by Bragg's law:

$$n\lambda = 2dsin(\theta) \tag{4.4}$$

where, n is an integer, λ is wavelength of the incident wave, d is the spacing between atomic layers in the crystals, and θ is the angle of incident. This explanation fits well

for crystalline structures. However, in our case since we are dealing with protenacious nanowire structure that has plenty of disorders and structural non-uniformity, we expect that X-ray diffraction would show no peak. However, if there is consistent occurrence of $\pi - \pi$ stacking in the network, it should be observed as peak in X-ray diffraction.

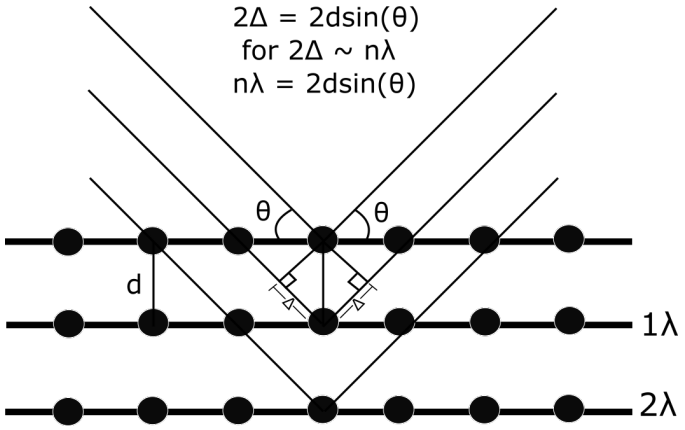

Figure 4.1. Sketch representing X-ray diffraction process. The intensity of the reflected beam depends on constructive interference which occurs if the phase difference is a multiple of wavelength.

X-ray diffraction (XRD) was performed with a PANalytical X'Pert X-ray diffraction platform. Cu K_α X-ray source was used which generated radiation of 1.54 Å. Pili solutions (10 μl) at pH 10.5, 7 and 2 were dropcast onto glass slides and air dried to form a film. A film from buffer was also constructed, x-ray diffraction performed and subtracted from the X-ray data from pili network samples. The X-ray diffraction patterns have been presented in Figure 4.2 The X-ray diffraction showed three distinct peaks at angles (2θ) of 23^0, 32.7^0 and 46.8^0 corresponding to spacing of 3.8 Å, 2.7 Å, and 1.9 Å.

These three peaks have again been presented separately in Figure 4.3. Figure 4.3a) is the first diffraction peak at 23^0 corresponding to the spacing of 3.8 Å, which is towards the upper limit of the $\pi - \pi$ interaction.[119] It is clear that there is no intensity peak at this angle at pH 10.5 implying to existence of any order. At pH 7,

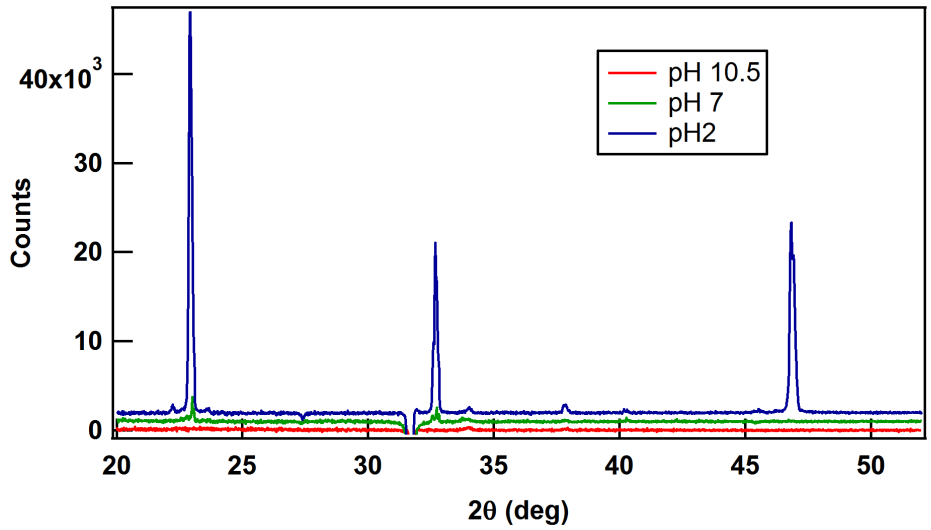

Figure 4.2. X-ray diffraction of W51W57 mutant pili at different pH. Three distinct peaks are observed at 23^0, 32.7^0 and 46.8^0 for pH 2. Only first two peaks are observed for pH 7 and no peaks were observed for pH 10.5.

the peak is generated which is magnified by orders of magnitude at pH 2. This means that like in the case of *G. sulfurreducens* pili, there is structural changes happening with lowering pH which is developing order related to $\pi - \pi$ interaction in the pili network.

Interestingly, two other peaks at higher angles were also observed for pH 2. At $2\theta = 32.7^0$, peak was observed for pH 2 and pH 7 samples while no peak was observed for pH 10.5 sample (Figure 4.3b). This peak is associated with spacing of 2.7 Å. The XRD peak at $2\theta = 46.8^0$ is second order diffraction of the peak at $2\theta = 23^0$. This higher order diffraction could be due to higher degree molecular ordering of aromatic residues at pH 2 and is not visible for other measurements at lower pH.

Conformational changes due to lowering pH have possibly to do with the charge interaction between charged amino acids and pili environment. When pH is lowered, the net charge in the pili becomes positive as shown in Figure 2.14. At the same time, more protons are introduced in the environment. Coulomb interaction due to this charge configuration could push pilin monomers towards the long axis of a pilus

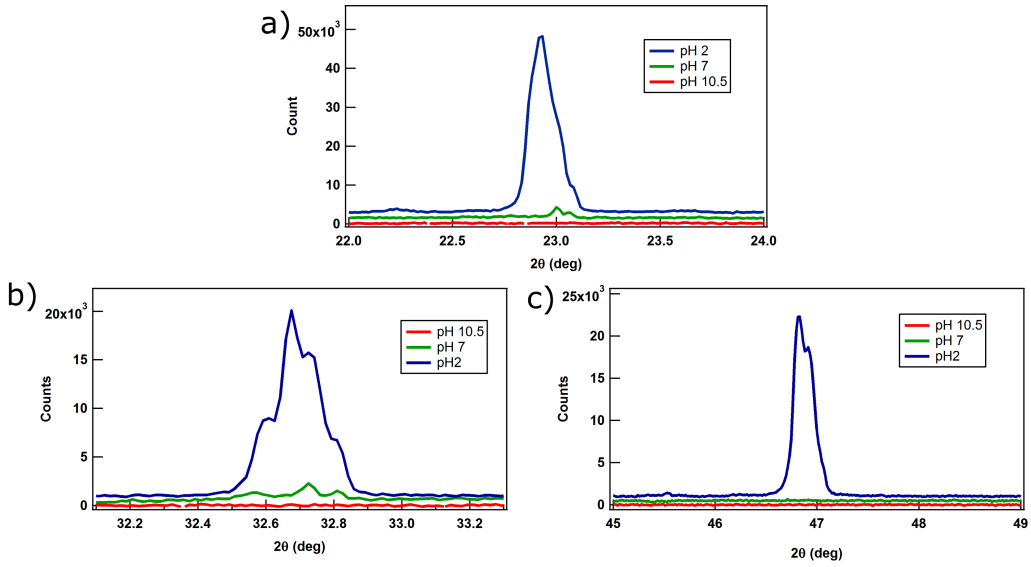

Figure 4.3. Zoomed-in version of three peaks observed in the XRD spectrum displayed in Figure 4.2 Peak is observed for pili in pH 2 environment. Peak was observed at only two higher angles for pH 7 samples. No peak was observed for pH 10.5 sample.

bringing the aromatic residues together. Of course, the changes do not need to be large; a change of a fraction of an Angstrom can make a large difference in extent of stacking of aromatic residues.

When we discuss about $\pi - \pi$ interaction or π stacking, it is important to understand the configuration of the aromatic rings. For $\pi - \pi$ interaction to occur, the aromatic rings need to be in different parallel planes. One of the configurations is the face-to-face alignment. This is the kind of alignment of aromatic rings and hence the interchain π-stacking suggested for transport in polyaniline.[118] In pili network, however, due to the circular nature of the cross section of pili, it may not be possible for such stacking of aromatic residues to occur between different chains. Even though the carboxylic end of the pili are free to bend, it may not be possible for sustained pi-stacking among the peripheral aromatic residues of different pili.

If we refer back to the structure of a pilus, the aromatic residue form conducting helical core of the pili where the aromatic residues could be close enough for π-

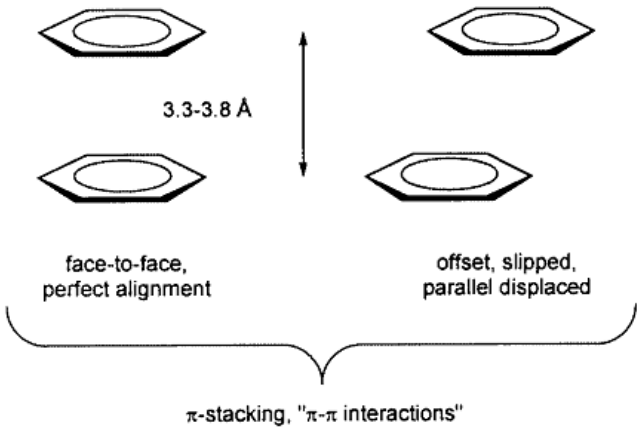

Figure 4.4. Possible alignment configuration of aromatic rings during $\pi - \pi$ interaction. Aromatic residues in a pilus most likely have parallel displaced configuration. Image adapted from [119].

stacking. The possible stacking in this case could be aromatic rings having parallel displaced stacking as shown in Figure 4.4. Therefore, the x-ray peak observed could be attributed to the parallel displaced π-stacking of aromatic rings within each pilus, unlike in the case of polyaniline where the peak is attributed to pi-stacking between aromatic rings of different polyaniline polymer.

This may explain the reason the pili networks have much lower conductivity than single pilus itself. Within a pilus, $\pi - \pi$ interaction between aromatic residues facilitates the transport along the length. But for the network, charge needs to tunnel from the conducting core of a pilus to another. Add that to the contact resistance between the pili in network, the resistance of the network would be much higher.

4.4.2 UV-Vis Spectroscopy

UV-Vis spectroscopy was performed with SHIMADZU 3600 UV-Vis NIR Spectrometer. 600 ml of ethanolamine buffer solution at different pH was prepared in quartz cuevettes. 10 μl of *G. sulfurreducens* pili solution was added to the buffer solutions and let stay overnight.

We observed a large absorption peak at about 408 nm which has been associated with OmcS c-type cytochrome.[120] We observed that the absorbance peak decreases with increasing in pH which is possibly due to denaturation of the c-type cytochrome. On the other hand, the absorbance peaks related to aromatic residues increase with lowering pH. Aromatic residues in wild type samples are tyrosine and phenylalanine with absorption at 275 nm and 258 nm respectively.[121] At around the region where aromatic residues show UV absorption peak, hyperchromic effect is observed. This kind of effect could be possible due to extended conjugation within aromatic residues in pili.

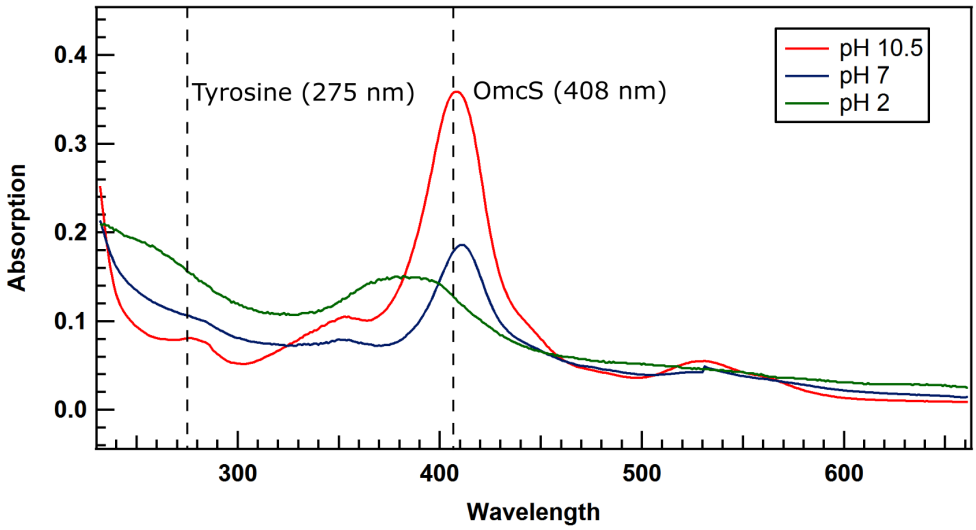

Figure 4.5. UV-Vis response from wild type *G. sulfurreducens* show that cytochrome denatures with lowering pH. Also, the absorption from aromatic amino acid increases with increases in longer wavelength.

There are some reports suggesting that c-type cytochrome is responsible for conduction through microbial nanowires. However, the experimental observation is that lowering pH is denaturing the c-type cytochrome while from conductivity measurements reported in earier chapters, the conductivity of pili increases with lowering pH. This suggests that the conductivity of the pili is intrinsic. Since c-type cytochromes

are metalloproteins with delocalized electrons, it is possible that cytochromes could assist charge transport in biofilm. However, they are not necessary for conduction through pili.

4.4.3 Optical Band Gap Studies

Based on the optical absorption, one can estimate the band gap of the material. It is rooted in the idea that the lowest band gap between highest occupied molecular orbital (HOMO) and lowest unoccupied molecular orbital (LUMO) would be observed at absorption at the lowest energy. The relationship between incident photon energy and absorption coefficient, also known as Tauc model, is:[122, 123, 124]

$$\alpha\hbar\omega = C(\hbar\omega - E_{bandgap})^P \tag{4.5}$$

where, α is the absorption coefficient which is related to optical absorbance, $\hbar\omega$ is the incident photon energy, C is a constant, $E_{bandgap}$ is the optical band-gap energy and P is the bandgap transition dependent exponent. The values for P is 1/2 for direct allowed, 3/2 for direct forbidden, 2 for indirect allowed and 3 for indirect forbidden transitions.[125, 124]

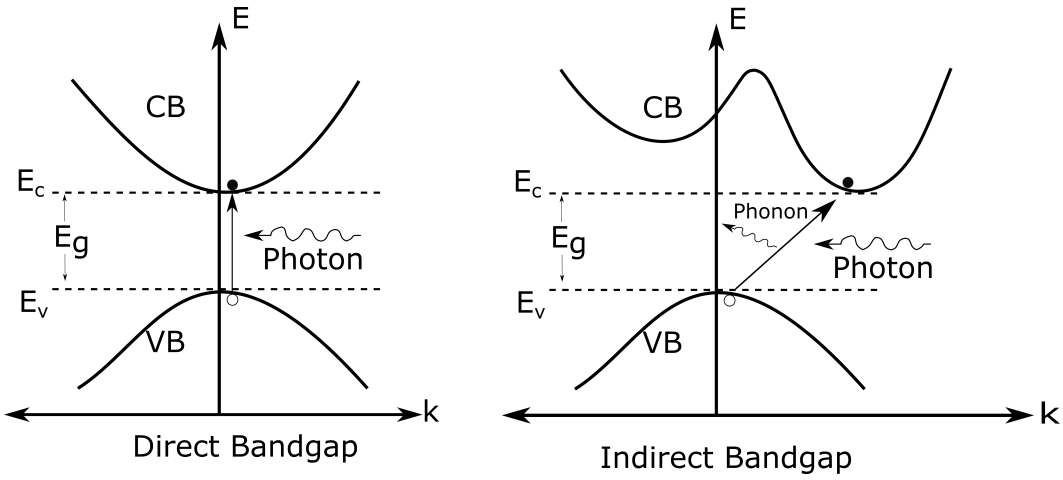

Figure 4.6. Photon absorption in direct and indirect bandgap transitions.

Among the allowed band gaps, for direct band gap, the maxima of the valance band and minima of the conduction band occur at the same wavevector i.e. momentum. For indirect bandgap, the maxima of the valance band and the minima of the conduction band have different momenum (Figure 4.6). For making indirect transition possible, photon energy needs to be higher than that of the band gap so that electron can not only absorb the photon energy, but also gain momentum for transition to conduction band. However, most of the indirect transitions happen at lower energy with two-step process involving photon and phonon interactions. Photons have relatively large energy and low momentum whereas phonons have relatively lower energy but larger momentum. Therefore, during the transition, the first step is the interaction with photon which provides the energy for carrier excitation and second is due to phonon interaction which provides momentum for carrier to reach conduction band.[126]

In order to calculate the band gap in *G. sulfurreducens* pili, we generate Tauc plots by plotting $(\alpha h\omega)^{1/p}$ versus photon energy $(h\omega)$. The band gaps were obtained from abscissa intercept by extrapolating linear portion of the absorption curve. Evaluations for indirect (Figure 4.7) and direct (Figure 4.8) band gaps were performed. At abscissa intercept, $(\alpha h\omega)^{1/p} = 0$ and hence, the bandgap of the material would be $E_{bandgap} = \omega\hbar$.

Tauc plot for indirect bandgap is presented in Figure 4.7. Left side of the panel have optical absorbance from 1.5 to 5.2 eV while the left panel is zoomed in image towards the linear plot region. Indirect bandgap hence calculated was 1.93 for pH 10.5, 1.48 for pH 7 and 0.0.54 for pH 2 pili solution. Values for direct bandgap were higher than the indirect band gap. Direct bandgap was 2.11 at pH 10.5, 2.04 at pH 7 and 1.92 at pH 2.

One of the conclusions that we can draw from observation of smaller indirect bandgaps for pili is that they will not be able to demonstrate photoluminescence

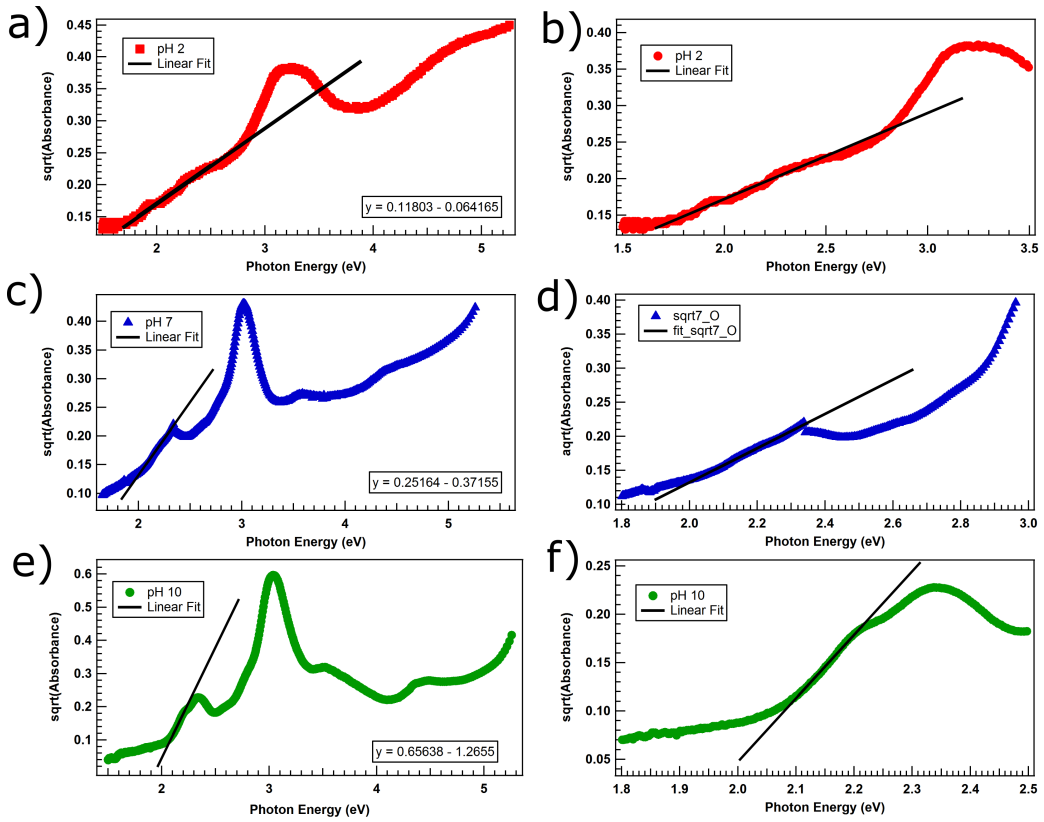

Figure 4.7. Tauc plot of optical absorption with respect to the incident photon energy. Left panel is the zoomed in version of the right panel.a) and b) are for pH 2, c) and d) are for pH 7, and e) and f) are for pH 10.5 pili solution.

because indirect bandgap materials do not have efficient electron-hole recombination process. As mentioned above, indirect transition involves two step process which includes phonon interactions while direct transition only involves photon. Photoluminiscence occurs when excited electron in conduction band transitions back to the valance band and electron-hole recombination occurs. In case of presence of the impurities and defects in the materials, the recombination process is non-radiative since the the electron's energy will be transferred to the impurities and defects.

Ideally, for direct bandgap materials, just like during absorption process, since no phonons are involved the electron-hole recombination energy is radiated out as photon and hence luminiscence is observed. However, for indirect bandgap material, the recombination process undergoes longer radiative lifetime due to involvement of both

photons and phonons and hence possesses relatively small efficiency due to competition with nonradiative combination.[127] Therefore, only materials with smaller direct bandgap are used for light emitting devices. There have been numerous researches on photoluminiscece of organic polymers and their applications in light emitting devices to the extent that organic light emitting devices are now even commercially available. However, it appears that microbial nanowires will not be a good candidate for such studies.

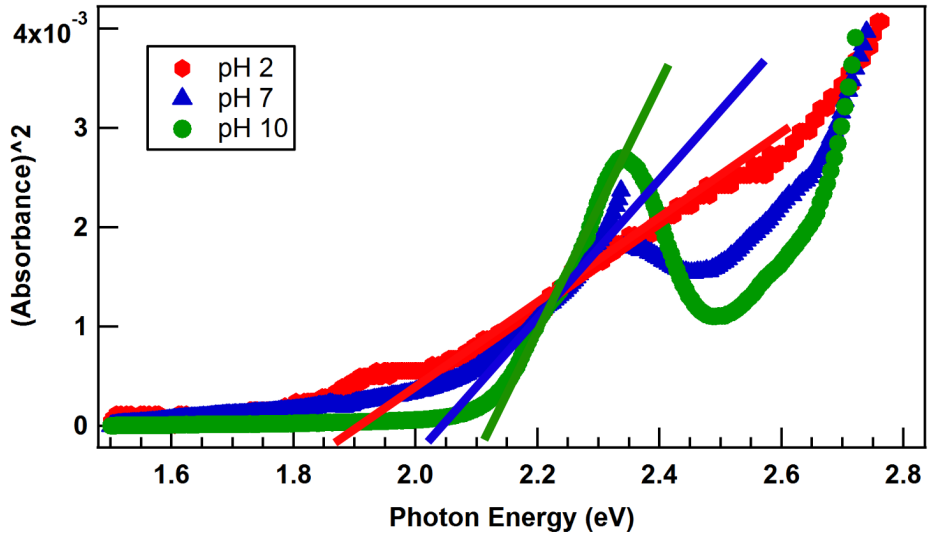

Figure 4.8. Tauc plot of optical absorption with respect to the incident photon energy for direct band gap.

We observe that both direct and indirect bandgaps decrease with lowering pH of pili solution. This lowering of the bandgap with lowering of pH suggests that doping induced bandgap narrowing occurs in microbial nanowires as well. This is a well known phenomena in semiconductors and various models have been developed to explain the phenomena. [128]

According to one of the models, at high dopant concentration of about 10^{18} cm^{-3} an impurity band is formed. When the concentration is further increased, the band becomes shallower and eventually gets absorbed into the conduction or valance band

making the gap smaller. For degenerate materials at doping level of about 10^{21} cm^{-3}, the interdoping spacing becomes comparable to the wavepacket size of thermal carriers. This causes tailing of the edge of the conduction and valance bands bringing the gap closer.[128]

There have also been models based on the electrostatic interactions between majority and minority carriers. Energy minimization happens by creating electron hole pairs because they are electrostatically bound to one another. The reduction in the energy of the minority-majority carrier complex depends on the majority carrier concentration and has been calculated by integrating electrostatic field energy of the system over entire space. The relation hence developed for the bandgap reduction is:[128]

$$\Delta E_g = \frac{3q^2}{16\pi\epsilon} \cdot \sqrt{\frac{q^2 N}{\epsilon k T}} \tag{4.6}$$

which suggests that the bandgap is proportional to the square root of the majority carrier doping concentration (N). Here, q is the charge of an electron, ϵ is the permittivity of space, k is the Boltzman's constant and T is the temperature.

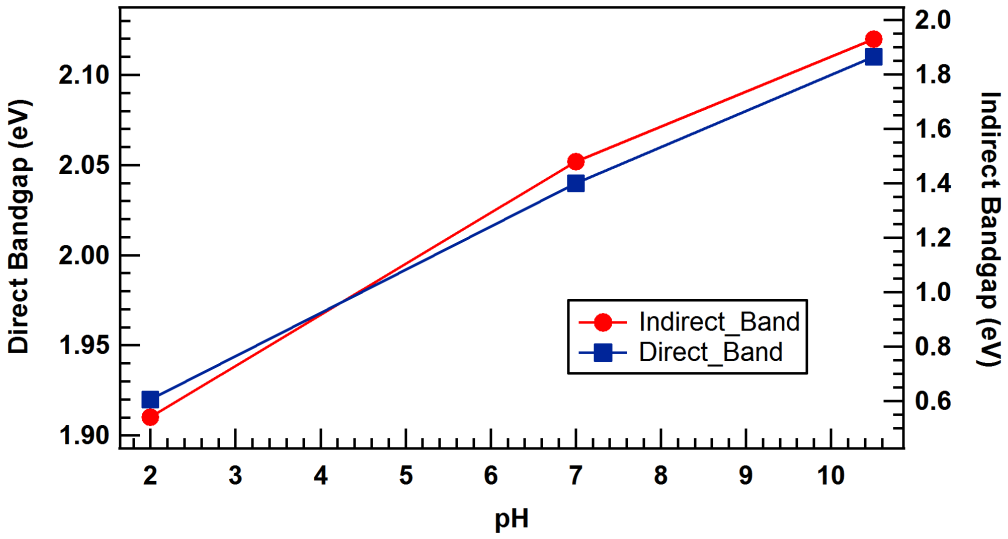

Figure 4.9. Effect of pH on direct and indirect band gaps.

A more thorough derivation was developed later which included, in addition to carrier-interactions, the scattering of the free carriers from ionized impurities from doping giving rise to a downward shift of the conduction band.[129] Most recently, Shaker and colleagues [130] have presented a simple yet general model to explain the observation of the band gap due to doping in semiconductor materials. Their model is based on the idea that an energy gap is essentially separation energy of an electron-hole pair. When hole and/or electron concentration is increased, it is favorable for the separation distance of an electron-hole pair to become smaller and hence band narrowing occurs.

Using this principle and simply using Coulomb's law, the general expression for change in energy gap can be written using Coulomb's potential as:

$$\Delta E_g = \frac{q}{4\pi\epsilon_0\epsilon_r}\left(\frac{1}{a_{he}} - \frac{1}{a_i}\right) \tag{4.7}$$

where, a_{he} is the distance of separation of an electron hole pair after doping and a_i is the same quantity for the same material before doping. Among other quantities, q is the charge of an electron, ϵ_0 is the permittivity of a free space and ϵ_r is the relative permittivity of the material under study.

In order to apply this principle for material under study it is necessary to know the majority carrier and the the microscopic distribution of the dopant in the material. For example, for a n-type semiconductor with doping concentration N, and electron concentration n dominated the hole concentration is p. Electron would form a three dimensional matrix and holes would occupy the center of some cubes. At his configuration the the electron-hole spacing is about half the diagonal of the cube, and the relationship can be written as $a_{he} = \sqrt{3}a_{ee}/2$. Plugging in this value in 4.7, the band gap narrowing is derived as:

$$\Delta E_g = \frac{q}{2\sqrt{3}\pi\epsilon_0\epsilon_r}(n^{1/3} - n_i^{1/3}) \tag{4.8}$$

Therefore, in order to compare the theory with the experimental observation presented in Figure 4.9, one needs to know the carrier concentration before and after doping. As mentioned in the previous section, at this point we do not have a complete understanding of how increasing pH changes the carrier density. This makes it difficult to check if this theory is valid for the pili system any more than the fact that the theory clearly shows that the band gap narrowing is higher for higher carrier concentration.

Another possible reason that can explain the band gap narrowing in microbial nanowires could be the alignment of the aromatic residues within pili. As shown in the XRD spectra, the intensity of pi-stacking peak increases with lowering pH. This could be the consequence of increasing the order of aromatic residues within pili. This conformational change is possibly due to the lowering of torsion angle between the different aromatic residues. Evolution of the electronic properties due to changes in torsion angle between adjacent aromatic rings have been studies in the case of organic polymers such as poluparaphenylene, polypyrole, and polythiophere. [131] The band gaps in these polymers decrease as the torsion angle between the aromatic residues decreases. For example, in the theoretical calculation performed by Bredas, et. al. [131], the band gap for polythiophene can be reduced from 5.22 at perpendicular conformation (90^0 torsion angle) to 2.19 at coplanar conformation (0^0 torsion angle).

4.5 Field Gated Transport in Microbial Nanowires

Transport through organic materials have been known to be tuned by applying field, and based on this principle, tremendous research efforts have been put into studying transistor behavior in conjugated polymer and small-molecule organic semiconductors. Molecules in organic polymers are held together by a weaker bond such as van der Waals bond unlike in case of their inorganic counterparts where cova-

lent bonds keep the materials rigid providing better charge conduction path. Due to this difference in the makeup, the organic materials tend to have transport behavior which is intermediate between conventional low mobility hopping transport in amorphous glasses and high mobility band transport in covalently bonded single crystals.[132] Organic semiconductors have not found commercial applications as organic light emitting devices (OLEDs) and transistor behaviors from these materials have been applied to generate e-paper displays, simple circuits, and chemical and biological sensors.[132]

Malvankar and colleagues [22] demonstrated that it was possible to gate pili bofilm and tune the conductivity. The gating was performed with electrolyte and about two orders of magnitude change in conduction through the biofilm was observed. Therefore, it was necessary to experiment if it was possible to construct solid state field effect transistor with pili network. Field effect transistor measurements are one of the most common transport measurements which not only provide insight into transport mechanism, but also provide an idea about possible applications.

4.5.1 Sample Preparation and Measurement

The transistor setup was build using shadow masking process which has been used for fabricating devices with polymers as active material.[133] First, pili solution (10μl) was dropcast on silicon chip with 1000 nm thermally grown oxide and let air dry. Then, TEM grid (Figure 4.10a) as mask was attached to the chip and metalization was performed with deposition of 20 nm gold with e-beam evaporation. The result was 25×25 μm electrodes over the area covered by TEM grid (Figure 4.10b). AFM imaging of the sample hence prepared displays the gold electrodes and pili network as shown in Figure 4.10c.

Measurement was performed by using probe station connected to Keithley 4200-SCS Parametric Analyzer with circuit configuration as shown in Figure 4.10d. Drain-

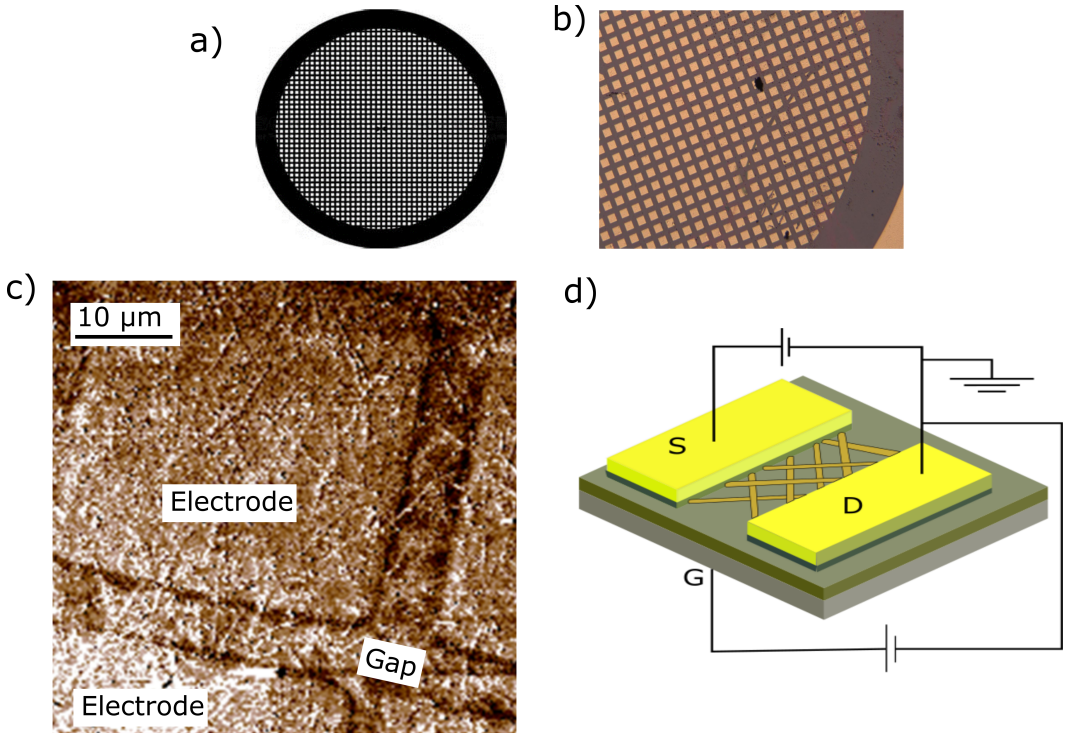

Figure 4.10. Electrodes deposition using shadow mask. a) TEM grid which is used as mask. b) Optical image of substrate with deposited electrodes on dropcast pili network. c) AFM image of electrodes and network of pili. d) Sketch of the transistor measurement setup.

source voltage of the ranged from negative to positive 10 V. Highly doped semiconductor base underneath thermally grown oxide was used as gate. The gate was created by scratching off the thermal oxide at the edge of the chip and applying silver paint to prevent oxidation of the doped semiconductor. Gate voltage of negative to positive 10 V was applied during the measurement. The sketch of the measurement setup is presented in Figure 4.10d.

4.5.2 Results and Discussion

The drain-source response to drain-source voltage and gate voltage hence obtained is presented in Figure 4.11. Linear drain-source IV behavior implies that the contact between pili network and electrodes was ohmic. We observe two different regimes in field effect transport. For the drain-source voltage between -8 V to 8V, the conduction

though the pili network is highest for -10 V gate voltage. For 10 V gate, the conduction through the network is minimum. For the drain-source voltage above 8V or below -8 V, the pili network starts to conduct irrespective of the gate voltage applied.

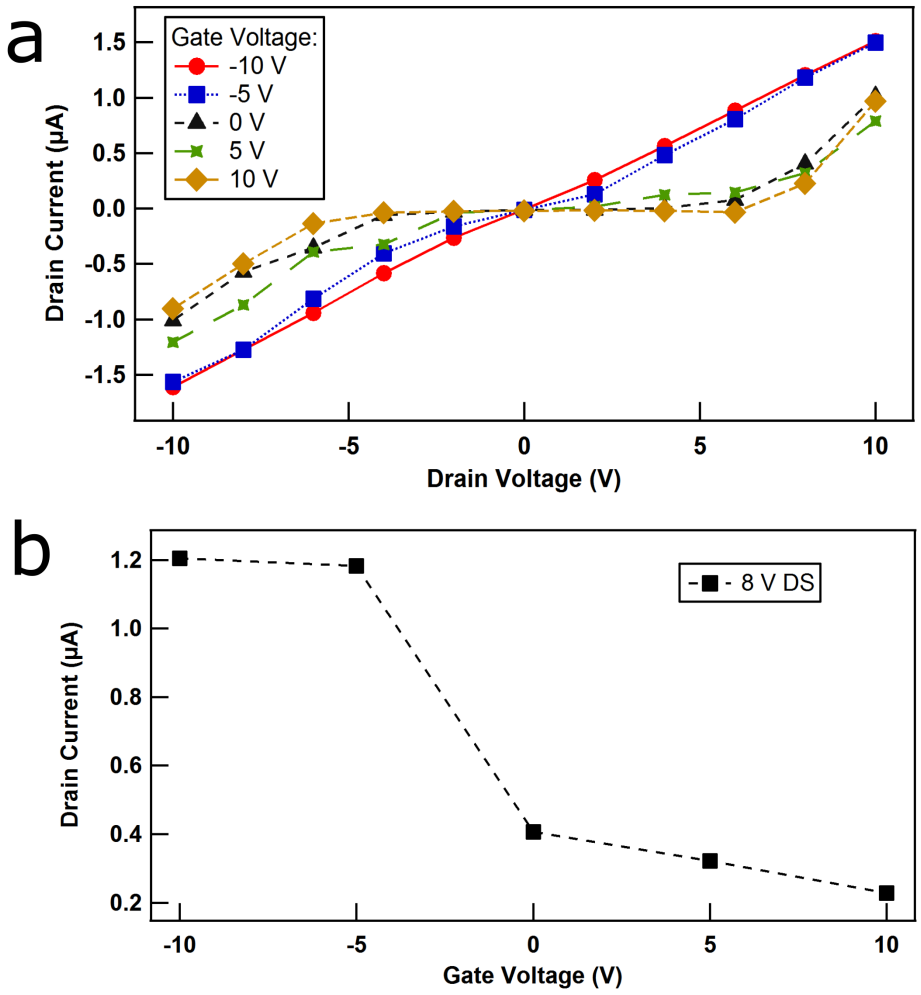

Figure 4.11. Gate induced tuning of conductance through pili newtork. a) Drain-source current response for drain-source voltage for various applied gate voltage. b) Drain current at 8 V drain-source bias for applied gate voltage.

In the regime between 6V to -6V, the phenomena is similar to any other transistor behavior. When negative bias is applied to the gate, the carriers are depleted due to growth in depletion region and hence there is no conduction through the pili membrane. However, when high enough bias is applied, the the depletion zone breaks

down letting the current pass through the active material which in this case is the pili network. This behavior is similar to that of p-type semiconductor.

One of the parameter that can be derived form the experimental observation above is carrier mobility. Mobility is the measure of the drift velocity of the carriers per unit applied electric field. Mobility and charge carrier density are the two parameters that dictate the conductivity of any material. The mobility value for for a transistor can be calculated as [134]:

$$\mu = \frac{L}{ZC_{OX}V_{DS}} \cdot \left.\frac{\partial I_D}{\partial V_{GS}}\right|_{V_{DS}=const} \tag{4.9}$$

where, L is length of channel, Z is the width of the channel, C_{OX} is oxide capacitance per unit area, V_{DS} is drain source voltage, I_D is drain current and V_{GS} is gate source voltage. The term $\partial I_D/\partial V_{GS}$ is also known as transconductance (g_m).

The oxide capacitance per unit area, C_{ox}, is ϵ_{ox}/t_{ox}, where ϵ_{ox} is oxide permittivity, which for silicon dioxide is $3.9\times8.85\times10^{-14}$ F/cm. The transconductance at the linear regime is about 1.5×10^{-7} A/V. The mobility hence calculated for this device is 2.7×10^{-5} $\mathrm{cm^2V^{-1}s^{-1}}$. This value is about an order of magnitude lower than the value obtained in Equation 4.3 based on single pilus measurements. Another parameter that can be calculated from the Figure 4.11b is on/off current ratio ($I_{on/off}$) which is the ratio of the current during "on"-state of the transistor and "off"-state of the transistor. This ratio for the pili transistor was about 30.

The mobility value obtained for pili transistor device is common among other organic field effect transistors since organic molecules are poorly hold together by weak van der Wall bond and not crystalline. Molecular engineering such as generating densely packed film by evaporating than in solutions, purifying the organic semiconductors and developing single molecule organic crystals are some of the practices that are used to fabricate organic field effect transistors with higher carrier mobility. [135]

The low mobility of the transistor device fabricated here possibly has to do with the purity of the pili network film as well as the molecular ordering - or rather disordering in the pili network which is a common issues regarding with organic field effect transistors. The pili in the film were not equally distributed across the device. However, during the calculation of mobility was performed with assumption that all the dimension such as channel length and width was filled with uniformly distributed dense pili. Therefore, the mobility value reported above is underestimated. In addition, the pili solution contains ethanolamine and other biomaterials and hence making the pili network full of impurities.

Secondly, from the molecular perspective, the low mobility could also have been contribution of lack of better stacking of aromatic residues because the pili solution was at high pH of 10.5. It has been demonstrated that the 0.17 Åwider crystal packing deom 3.28 Åto 3.43 Åof a pentacene derivative lowered the mobility by 45 fold.[136] As described above and elsewhere [24, 22] pH 10.5 the aromatic packing in pili is very minimal which increases with lowering pH. Therefore, we may be able to achieve much larger mobility values if the the study is performed for pili networks at lower pH where we expect conformational changes in pili bringing aromatic residue closer together.

It has also been reported that for pi-stacking systems, the mobility is low for 1-D pi-stacked material and much higher for 2-D π-stacking materials. For example,[135] vapor deposited film of triisopropyl silyl (TIPS) penatacene derivative with strong two-dimensional face-to-face interactions showed hole mobility of 0.4 $cm^2V^{-1}s^{-1}$. For film deposition under similar condition, the highest mobility for 1-D π-stacked material was less than 0.001 $cm^2V^{-1}s^{-1}$. This is 400 fold difference in mobility of pentacene derivatives due to difference in one or two dimensional transport.

Even though the aromatic residues are scattered along the pili, it is believed that the transport happens through the helical structure formed by aromatic residues at

the core of the pili. Hence, it is possible that even in network, the conduction though pili possibly could be dominated by 1-D transport along the length of the pili which would provide low mobility since the carriers transport is subject to be impeded by disorders along the chain.

The interesting part of the observation described in this section is field modulated conduction of microbial nanowires. If the charge transport in microbial nanowires are occurring via π-orbital conjugation giving rise to a metallic system, an obvious question is how can one observe an effect like conventional semiconductors.

Studies in conjugation polymer has suggested that this phenomena could be due to inhomogeneity within the microbial nanowires and ions in the system.[137] These nanowires are susceptible for structural defects which provide sites for mobile ions. The mobile ions can move from within the defects to the outer debye layer in the network film due to the applied external field. In addition, the ions also produce additional screening field. Therefore, the modulation of the ionic concentration in disordered regions within nanowires maybe the determining factor for transistor like effect in microbial nanowire network. Below, I will use the theory to understand the field gated transport mechanism in pili.

As I have discussed earlier in this chapter, the carrier density is in the order of $10^{20} cm^{-3}$. However, it is well-known that electric field cannot be used for turning the conductance of materials with higher carrier density, for examples - metals because carriers in their high concentrations are effective in screening of the external field. Screening length (r_e) for a degenerate electron gas is:[138]

$$\frac{1}{r_e^2} = N(E_F)\frac{e^2}{\epsilon\epsilon_0} \tag{4.10}$$

where, $N(E_F)$ is the electron density of the states at the Fermi Level, $e = 1.6 \times 10^{-19} C$ is the fundamental electronic charge, ϵ is relative dielectric constant of the microbial nanowire and $\epsilon_0 = 8.85 \times 10^{-12} F/m$ is the vacuum permittivity.

There has been various experimental and computational studies on investigating dielectric constant of proteins which have been granted range of values across the literature since it depends on charge configuration, structure and amino acid sequence. We use $\epsilon = 3$, which is the value obtained from NMR studies for protein in solution.[139] This value may be the best representation of the dielectric constant of the protein because they were obtained from the analysis of the NMR chemical shift perturbations instead of other methods such as analysis of pK_a which are thermodynamic variables and are contaminated by non-electrostatic factors.

Charge carrier concentration (ρ) as calculated in section 4.3 is $6.5 \times 10^{20} cm^{-3}$. Fermi energy, if we assume a free electron gas model, is given as:

$$E_F = \frac{\hbar^2}{2m}\left(\frac{3\pi^2 N}{V}\right)^{2/3} = \frac{\hbar^2}{2m}\left(3\pi^2\rho\right)^{2/3} \tag{4.11}$$

which calculates out to be $0.25eV$. Here, $\hbar = 1 \times 10^{-34} Js$ is reduced Plank's constant and m is the mass of an electron/carrier. Therefore, the density of states at the Fermi level is $N(E_F) \approx \rho/E_F = 2.6 \times 10^{21} cm^{-3}(eV)^{-1}$. Hence, the screening length calculated using equation 4.10 is 2.53 Å. A pili has diameter of about 30 AA. Therefore, the screening length is about an order smaller than even the diameter of a single pili. This is phenomena similar to that of metals where the screening length is only a few angstrom and hence applied field does not affect the transport.[138]

In addition to the screening length, one can calculate the screening time in order to understand how fast the screening occurs due to applied field. Making the assumption that charge redistribution during the screening process occurs due to diffusion of charge carrier, the characteristic screening time (t_e) can be estimated as:[140]

$$r_e = \sqrt{Dt_e} \Rightarrow t_e = \frac{r_e^2}{D} \tag{4.12}$$

where, D is the diffusion coefficient. Now, using Einstein relation:

$$D = \frac{\mu kT}{e} \tag{4.13}$$

where, $k = 1.38 m^2 kg/s^2 K$ is Boltzmann constant. Using the value of mobility ($\mu = 3.58 \times 10^{-4} cm^2 V^{-1} s^{s-1}$) calulcated in section 3.3, room temperature ($T = 295K$) in which the experiment was performed, and value for fundamental electronic charge (e), the diffusion value calculated is $9.11 \times 10^{-10} m^2/s$. Using Equation 4.12, the screening time calculated is $7.03 \times 10^{-11} s$.

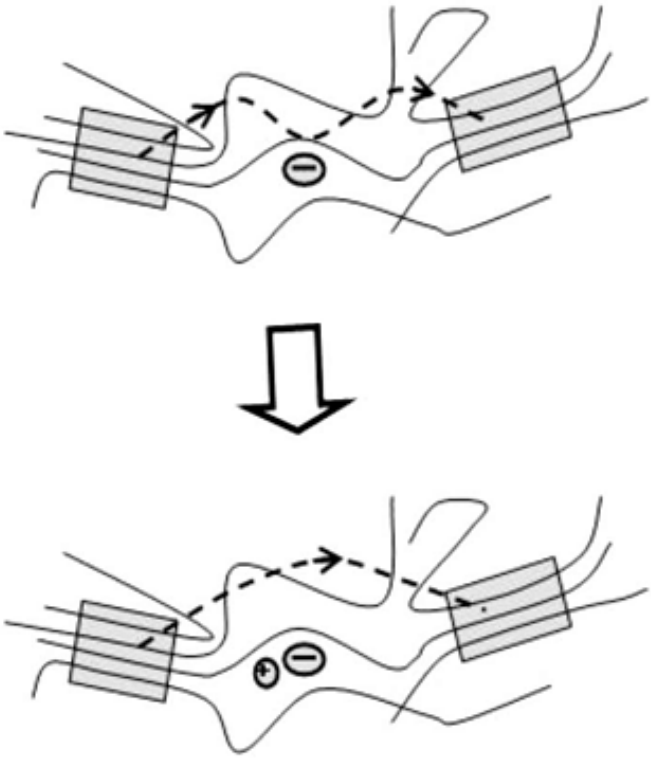

Figure 4.12. Suppression of hopping across delocalized regimes by electric field modulated ion content in disordered region. [138]

Hence, screening length in microbial nanowires is very small, about 10 times smaller than the diameter of the pili itself, and it occurs in about 10 fs. This analysis brings to the conclusion that not even most of the carriers in pili experience the external field and hence we cannot expect the mechanism of field induced depletion layers determine the conduction as in semiconductors.

This kind of observation is prevalent in metallic polymers as well, which have very high carrier density but yet, one can observe transistor effect with them. Prigodion and colleagues [138, 140, 141] have been working on a theoretical model which may explain this behavior based on modulation of carrier mobility based on applied gate voltage. I will attempt to explain the observation in microbial nanowires based on their theory for conducting polymers.

If there is no structural defect in microbial nanowires, due to close packing of aromatic residues, they can act as a continuous metallic nanowires. However, in reality, unlike inorganic systems that are strongly bonded together with covalent bonds, organic systems are more flexible and due to their quasi-1D nature, more susceptible to structural defects. Therefore, one can think of a microbial nanowire as wire with ordered regions where charge delocalization is possible seperated by disordered regions at multiple locations along the wire. For a charge to be transported from one end of the wire to another, the carrier needs to hop through localized charged states in the disordered regions. The ability of a carrier to hop through these disordered regions determines the dc transport through the wire.[141]

When positive gate voltage is applied, the positive ions are displaced from the substrate surface towards the disordered regions of the nanowire. The charge acceptors in the disordered regions are hence compensated. In this manner, the hopping sites at the disordered regions are removed making the Fermi level more localized within the ordered metallic region and hence decreasing the conductivity. [138]

4.6 Conclusions

Microbial nanowires in our study show electronic characteristics similar to other organic semiconductors. The values such as charge carrier density and mobility are similar to any other polymer systems. With high charge carrier density, if more studies are performed to improve mobility and current on-off radio of the pili, such

as purification, addition of more aromatic residues or doping, we may be able to use these microbial nanowires for bio-nanoelectronics for sensing applications or even as molecular wires. Another interesting study would be studying charge carrier density for various doping level and understand its effect in conductivity.

X-ray diffraction of mutated W51W57 pili show that even for this pili, lowering pH increases the peak at 3.8 Å. This distance is within range for $\pi - \pi$ interaction. The highly conductive nature of this pili make it an interesting candidate for studies of charge carrier density and mobility. The constricted diameter of the mutant pili possibly means that the charge carrier density would be higher than in wild type counterparts and mobility is possibly improved as well. Further structural studies and transport studies would be necessary for understanding transport mechanism through mutant pili.

It appears that the pili network in solution represents indirect band-gap material. This suggests that microbial nanowires may not be ideal candidate for photoelectronic devices due inefficiencies in transition associated with indirect band-gap materials. It is possible to observe the gating effect in microbial network in solid-state transistor setup. The gating effect despite the high carrier density of nanowires is possibly due to the interaction of localized sites in disordered regions with ions in the solution.

CHAPTER 5

CONCLUSION AND FUTURE WORKS

5.1 Conclusion

Hence, it has been demonstrated in this dissertation that microbial nanowires demonstrate a great potential as as nanoscale conductors. In the first chapter, it was demonstrated that individual microbial nanowires are able to transport charges over a long distance. A very sensitive noise reduction set-up was developed and used for the transport measurements. In addition, it was also demonstrated that aromatic amino acids are essential for long range transport through a pilus by performing transport studies on a pilus where five of six aromatic residues were replaced by a non-aromatic amino acid residue.

In the second chapter, it was demonstrated that genetically manipulated pili, where more aromatic residues are introduced become highly conductive. Replacing single aromatic ring residues such as phenylalanine and tyrosine by double aromatic ring tryptophan increased conductivity of the nanowires by about three orders of magnitude. At the same time, the diameter of the wire shrunk by about half, possibly due to higher hydrophobicity of tryptophan residues. Furthermore, it was also demonstrated that another naturally occuring *Geobacter* species, *G. metallireducens* also generates highly conductive pili which is composed on pilin monomers highly rich in aromatic residues. However, another species *G. sulfurreducens* produces pili with lot less denser aromatic residues and its pili are very poor conductors. Based on these studies, it was realized that conductivity of a microbial nanowire is exponentially related to the aromatic amino acid density in the pili.

In the third chapter, I discussed the transport parameters for microbial nanowires derived from the conductivity studies and other optical and electronic measurements. *G. sulfurreducens* nanowires have charge large carrier density and small carrier mobility similar to that of organic semiconductors. It was observed that *G. sulfurreducens* nanowires are indirect bandgap material and the band gap can be lowered with higher doping. X-ray study of mutant pili demonstrated that $\pi - \pi$ interaction is still doping promoted, like in wild type pili.

5.2 Future Works

From the projects I have been involved, I have been able to demonstrate that long range solid state charge propagation is possible through microbial nanowires. Working with a team of microbiologists, we were able to demonstrate that it is possible to genetically modify microbial nanowires to make them rich in aromatic residues and hence significantly improving conduction. Results from all of the projects implied that aromatic residues are an essential component of conduction in microbial nanowires. These studies suggested that these nanowires have electronic behavior similar to that of organic polymers which are currently being studied for their potential to replace silicon-based devices.

Organic semiconductors have come a long way with developments in improvement of crucial electronic property - carrier mobility of higher than 1 $cm^2V^{-1}s^{-1}$. Study of microbial nanowires is still in its nascent phase and further works involving molecular engineering processes such as genetic modification, doping, purification, and development of assembly processes could dramatically improve their performance. The amount of work that can be performed on these microbial nanwoires at this point is unfathomable. My hope is that from some of the studies suggested below we will provide another step towards achieving more coherent understanding on the transport

properties of microbial nanowires and hopefully realize applications and properties that may have been unthought of previously.

5.2.1 Contactless Conductivity Study

Contact interface between the material under study and electrodes can influence the transport measurements due to fermi level mismatching or due to poor contact which affect measurement of true intrinsic electronic parameters such as conductivity and mobility. Contactless conductivity measurement of λ-DNA has been reported.[142] The conductivity of the sample was evaluated by measuring the loss of quality factor of highly sensitive resonant cavities. The quality factor Q of the cavity is inversely proportional to the loss W which is related to the conductivity as provided by the relation:

$$W = \frac{1}{3} V \sigma E_0^2 \tag{5.1}$$

where the factor $1/3$ is due to geometrial average of random orientations of conducting sample with respect of the direction of the applied uniform electric field, V is the volume of the conducting medium, σ is real part of the complex conductivity, and E_0 is the time averaged applied ac-field at the position of the sample. There are also studies reported where terahertz time-domain spectroscopy (THz-TDS) technique has been used to study conductivity of materials and understanding carrier dynamics.[143] These kinds of contactless studies on pili nanowires for various samples could help us learn about the intrinsic charge transport properties and dynamics.

5.2.2 Interchain and intrachain conductivity contribution in pili network

Performing single pili measurement is a tedious process especially when one has to depend on statistical randomness for positioning a single pili bridging across the electrodes. On the other hand, conduction through a network depends on conductivity of pili nanowires, i.e. intrachain conductivity, as well as conduction across the nanowires

i.e. interchain conductivity. Interchain and intrachain transition rates can differ by orders of magnitude and hence AC conductivity studies can be performed understand the transport properties of a polymer chain.[144] For weakly coupled chains, the charge transfer rate (Γ_{inter}) between different chains is low. The conductivity ($\sigma(\omega)$) at frequencies $\omega >> \Gamma_{inter}$ is dominated by charge transport processes within single polymer chains. Since impurities cause charge localization in 1D chain, the intrachain conductivity for very low frequency as well as temperature is zero. However, for room temperature photon-assisted hopping is present within the chain. Based on this principle, Reedijik[144] and colleagues have developed a model to quantify parameters such as transfer rates, localization lengths, drift velocity and interchain and intrachain conductivity values.

Rather easier inter- or intrachain charge dynamics studies can be achieved by using optical infrared measurements. If high quality film can be prepared from the pili network, high-precision reflectance studies can be performed to study parallel and perpendicular contributions to the optical constants.[145] Perpendicular conduction would be due to contribution of inter-chain charge transfer while parallel component of the conduction would be due to charge transfer along the length of the nanowires. However, the challenge for this method is ability to prepare high quality aligned pili samples. If that is achieved, one could go further and perform optical spectra study to observe if metallic behavior can be obtained for pure pili sample.[146]

5.2.3 Mechanical and Electromechanical Properties of Microbial Nanowires

Understanding the electrical properties of these microbial nanowires is only one side of the coin. It is necessary to understand the mechanical properties of these nanowires so that the scope of their application is properly understood. These nanowires might be subject to nonideal environments and, if they are to be used in devices, they need to have robust mechanical properties so that they can be ma-

nipulated per need. At the nanoscale, mechanical properties of the materials improve dramatically or at least retain the bulk properties. For example, germanium wafers are known to be brittle and difficult to handle even though germanium has a higher mobility compared to silicon. However, germanium nanowires show elastic moduli that is comparable to the bulk, their mechanical strength is significantly larger than any bulk semiconductor material.[147]

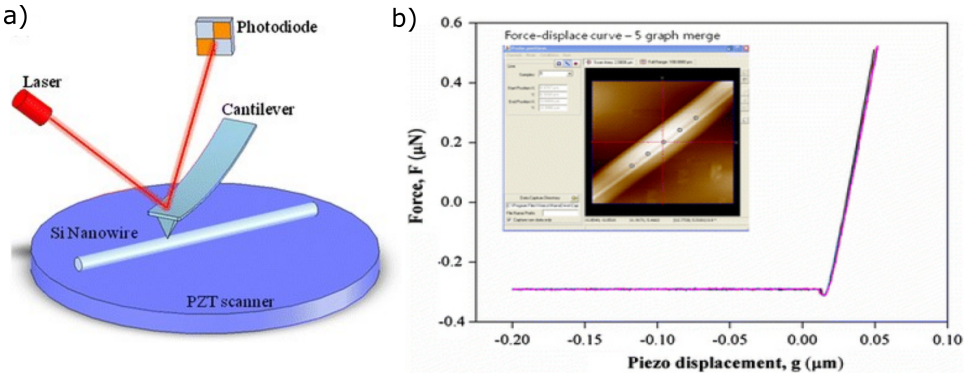

Figure 5.1. Mechanical porperties of nanowires: a) Schematics of AFM nanoindentation of silicon nanowires. b) Force-piezo displacement curves from five different points on a silicon nanowire (inset).[148]

The experiment for studying mechanical properties of nanowires can be performed with AFM nanoindentation.[148] In this method, once the nanowire is located a mechanical force is applied using AFM canitlever and indentation response of the nanowire. Force applied and loading rate should be chosen in order to achieve indentation response in linear regime so that classical Hertz theory can be applied. Advantage of this method is that one does not need to manipulate the nanowires; once the nanowire is located, one can perform the measurement. Once, the curve of mechanical force on the nanowire (k_{NW}) for different applied force (F) is applied, it can be fitted with relationship derived from Hertz theory as:

$$k_{NW} = (6E^{*2}RF)^{1/3} \tag{5.2}$$

where, E^* is the effective Young's modulus and R is the AFM tip radius. From curve fitting the experimental data, one can extract Young's modulus and hence quantify mechanical properties of the nanowires.

5.2.4 Temperature Dependent Transport Studies

Temperature dependent transport studies are crucial in obtaining deeper insight into conduction mechanism of a given system. Yet, for microbial nanowire systems, temperature dependent studies are very limited. The first report of temperature dependent studies was presented by Malvankar and colleagues.[22] Exponentially increasing conductivity with lowering temperature until a crossover point was observed in this study. In this range, this behavior was similar to what is observed in a metallic system. Below the temperature of about 270 K, the conductivity decreases exponentially similar to hopping transport phenomena. Thermally activated charge transport was reported in recent studies on a single *G. sulfurreducens* nanowires, but the study was performed for only two temperatures - at room temperature and at 77 K.[149] A rather thorough study would be temperature dependent conductivity study of a single microbial nanowires for a range of temperature. In addition, mobility studies can also be formed as a function of temperature. Temperature studies also needs to be done regarding highly conductive *G. sulfurreducens* pili and W51W57 mutant pili.

Temperature dependent transistor studies could also help elucidate conjecture presented in the Chapter 4 of this dissertation. One can acquire the data for a range of temperature and plot the temperature dependent resistance at different gate voltages to compare the experimental results with chain-linked granular model.[138] This can help in understanding the relationship of dependence of temperature on applied gate voltage and the degree of compensation and hence check the validity of the current conjecture of disordered induced gating effect.

5.2.5 Optical Band Gap Studies

Optical response of *G. sulfurreducens* pili presented in this dissertation show that those pili are semiconducting in nature. Lowering the band gap with increasing doping is a promising result which means that it is possible to control the band-gap of this material by changing the doping amount. Lower indirect band gap than the direct band gap means that the wild type pili may not be ideally suitable for applications in optoelectronic devices, but it will be interesting to study the band gaps and their response to conductive pili from *G. sulfurreducens* and W51W57 mutants and explore their possible application in optoelectronics.

5.2.6 Environmental Effect on Mobility

Microbial nanowires are essentially molecular nanowires. In bulk materials, transport properties are dominated by the properties of the bulk and the surface effects such as effect of interaction with the environment is not dominant. However for a quasi 1D systems such as the microbial nanowire, charge in the nanowire can easily interact with charges in the surroundings. Understanding the charge interaction of the molecular systems and enhancing their charge transport properties has always been of interest in material science to lead a way forward to potential practical application, for example, in sensors.

Among various systems with studies of the environmental effect on the transport properties, systems involving graphene has provided an excellent platform due to their robust mechanical properties and excellent charge transport properties. It has been shown that in a graphene field effect transistor system, the carrier mobility can be increased up to 3 orders of magnitude by exposing the graphene in different solvents with dielectric constant varying over 2 orders of magnitude.[150] Furthermore, exposure to polar and non-polar dielectric solution has opposite effect.[151] Polar solutions generate an ion-electron interaction and disrupt the charge carriers of the

system while non-polar solutions help lower the ion-electron interaction and hence provide higher carrier mobility.

It will be interesting to investigate if a similar enhancement in charge mobility and conductivity by introducing various dielectric solutions on microbial nanowires devices. It has been reported in the chapter one that the conductivity of a pili is similar to polyaniline nanowire, a well-known conjugated polymer. Furthermore it has also been shown that by changing the pH of the pili environment, it is possible to increase the conductivity of the pili by 3 orders of magnitude.

Therefore, it will be interesting to study the changes in the conductivity and mobility of the pili in various dielectric environment. Studies should be done in the environment with varying dielectric constant and various polarity. This will provide us with more mechanistic insight of how the charges through pili interact with the environment in addition to possibly achieving better conductance than in a physiological environment.

5.2.7 Self-assembly of Microbial Nanowires

One of the biggest challenges in device fabrication with nanowires is having control over their assembly for devices fabrication. In order to construct complex networks for applications such as nanoelectronics, spintronics, optoelectronics, sensors and thermoelectric devices, it is necessary to have control over the assembly of the nanowires.[152] Among the practices to assemble the nanowires using external stimulus such as electric and magnetic fields can be used to assemble nanowires and could possibly tried with microbial nanowires.

5.2.7.1 Response to a Magnetic Field

It has been shown that a magnetic field can used used to align organic conductor such as polyaniline.[153] The alignment was created during the synthesis of the nanowire and it was shown that nanowires network synthesized in the magnetic field

demonstrated conduction about 1.85 times higher than the sample prepared without magnetic field. The higher conduction was due to aligning of nanowires along the field direction instead of random distribution.

It has also been reported that diphenylalanine peptide structures can be aligned along the magnetic field.[154] The alignment has been attributed to magnetic torque due to diamagnetic anisotropy of the aromatic rings of phenylalanine. It will be intriguing to investigate if this behavior of aromatic residues can be taken into advantage in assembling microbial nanowires. It has been previously suggested that one could study the effect of the magnetic field on the assembly of microbial nanowires.[155] I believe this project has large implications in device physics and should be investigated.

5.2.7.2 Dielectrophoresis

Using AC-dielectrophoresis, on-site deposition of nanowires can be accomplished. There are extinsive studies on using this method to deposit carbon nanotubes on nanoelectrodes.[156] For this method one can also devise wiring schemes based on capacitive coupling between the substrate and the electrodes and gain control over number of deposited nanotubes in a given contact. Dielectrophoresis has also been used to manipulate DNA either by using electrodes[157] or even without electrodes [158]. Field gradient induces dipole moment in DNA causing it to aggregate where the field is high and hence essentially traps DNA strands.

Studies have also been performed to align peptide nanotubes across electrodes using dielectrophoresis paving the way towards integration of bionanostructures in nanoscale devices.[159] It could be possible that microbial nanowires can be deposited in controlled manner using this technique for their possible device applications.

BIBLIOGRAPHY

[1] G. Vattay, D. Salahub, I. Csabai, A. Nassimi, and S.A. Kaufmann. Quantum criticality at the origin of life. *Journal of Physics: Conference Series*, 626(1):012023, 2015.

[2] A.M. Kuznetsov and J. Ulstrup. *Electron Transfer in Chemistry and Biology: An Introduction to the Theory*. John Wiley and Sons Ltd, 1999.

[3] H. Sigel and A. Sigel. *Electron transfer reactions in metalloproteins: Metal ions in biological systems*, volume 27. CRC Press, 1991.

[4] R.E. Blankenship. *Molecular mechanisms of photosynthesis*. John Wiley and Sons Ltd, 2 edition, 2014.

[5] M. Mohseni, P. Rebentrost, S. Lloyd, and A.A. Guzik. Environment-assisted quantum walks in photosynthetic energy transfer. *The Journal of Chemical Physics*, 129:174106, 2008.

[6] T.Y. Astakhova, V.N. Likhachev, and G.A. Vinogradov. Long-range charge transfer in biopolymers. *Russian Chemical Reviews*, 81(11):994–1010, 2012.

[7] H.W. Fink and C. Schonenberger. Electrical conduction through dna molecules. *Nature*, 398:407–410, 1999.

[8] A.Y. Kasumov, M. Kociak, S. Guerona nd B. Reulet, V.T. Volkov, D.V. Klinov, and H. Bouchiat. Proximity-induced superconductivity in dna. *Nature*, 291:280–282, 2001.

[9] E. Braun, Y. Eichen, U. Sivan, and G. Ben-Yoseph. Dna-templated assembly and electrode attachment of a conducting silver wire. *Nature*, 391:775–778, 1998.

[10] D. Porath, A. Bezryadin, S.d. Vries, and C. Dekker. Direct measurement of electrical transport through dna molecules. *Nature*, 403:635–638, 2000.

[11] C. Gomez-Navarro, F. moreno Herrero, P.J.d. Pablo, J. Gomez-Herrero, and A.M.Baro. Contactless experiments on individual dna molecules show no evidence for molecular wire behavior. *PNAS*, 99(13):8484–8487, 2002.

[12] M.W. Shinwari, M.J. Deen, E.B. Starikov, and G. Cuniberti. Electrical conductance in biological molecules. *Advanced Functional Materials*, 20:1865–1883, 2010.

[13] J. Gao, P. Muller, M. Wang, S. Eckhardt, M. Lauz, K.M. Fromm, and B. Giese. Electron transfer in peptides: The influence of charged amino acids. *Angewandte Chemie International Edition*, 50(8):1926–1930, 2011.

[14] N. Amdursky, D. Marchak, L. Sepunaru, I. Pecht, M. Sheves, and D. Cahen. Electron transfer via proteins. *Advanced Materials*, 26:7142–7161, 2014.

[15] C.A.E. Hauser and S. Zhang. Nanotechnology: Peptides as biological semiconductors. *Nature*, 468:516–517, 2010.

[16] M. Cordes, A. Kottgen, C. Jasper, O. Jacques, H. Boudebous, and B. Giese. Influence of amino acid side chains on long-distance electron transfer in peptides: Electron hopping via stepping stones. *Angew. Chem. Int. Ed.*, 47:3461–3463, 2008.

[17] C. Aubert, M.H. Vos, P. Mathis, A.P.M. Eker, and K. Brettel. Intraprotein radical transfer during photoactivation of dna photolyase. *Nature*, 405:586–590, 2000.

[18] M. Vargas, N.S. Malvankar, P.L. Tremblay, C. Leang, J. A. Smith, P. Patel, O. Synoeyenbos-West, K.P. Nevin, and D.R. Lovley. Aromatic amino acids required for pili conductivity and long-range extracellular electron transport in geobacter sulfurreducens. *mBio*, 4(2):e00105–13, 2013.

[19] H.B. Gray and J.R. Winkler. Long-range electron transfer. *PNAS*, 102(10):3534–3539, 2005.

[20] J.R. Winkler and H.B. Gray. Electron flow through metalloproteins. *Chem. Rev*, 114:33693380, 2014.

[21] G. Reguera, K.D. McCarthy, T. Metha, J.S. Nicoll, M.T. Tuominen, and D.R. Lovley. Extracellur electron transfer via microbial nanowires. *Nature*, 435:1098–1101, 2005.

[22] N.S. Malvankar, M. Vargas, K.P. Nevin, A.E. Franks, C. Leang, B.C. Kim, K. Inoue, T Mester, S.F. Covalla, J.P. Johnson, V. M. Rotello, M.T. Tuominen, and D.R. Lovley. Tunable metallic-like conductivity in microbial nanowire networks. *Nature Nanotechnology*, 6:573 – 579, 2011.

[23] N.S. Malvankar, S.E. Yalcin, M.T. Tuominen, and D.R. Lovley. Visualization of charge propagation along individual pili proteins using ambient electrostatic force microscopy. *Nature Nanotechnology*, 9:1012 – 1017, 2014.

[24] N.S. Malvankar, M. Vargas, K.P. Nevin, P.L. Tremblay, K. Evans-Lutterodt, D. Nykypanchuke, E. Martz, M.T. Tuominen, and D.R. Lovley. Structural basis for metallic-like conductivity in microbial nanowires. *mBio*, 6(2):e00084, 2015.

[25] K. Xiao, N.S. Malvankar, C. Shu, E. Martz, D.R. Lovley, and X. Suna. Low energy atomic models suggesting a pilus structure that could account for electrical conductivity of *Geobacter sulfurreducens* pili. *Sci. Rep.*, 6:23385, 2016.

[26] G. Reguera, K.D. McCarthy, T. Mehta, J.S. Nicoll, M.T. Tuominen, and D.R. Lovley. Extracellular electron transfer via microbial nanowires. *Nature*, 435:1098 – 1101, 2005.

[27] J.P. Veazey, G. Reguera, and S.H. Tessmer. Electronic properties of conductive pili of the metal-reducing bacterium geobacter sulfurreducens probed by scanning tunneling microscopy. *Phys. Rev. E*, 84:060901, 2011.

[28] D.R. Lovley. Bug juice: harvesting electricity with microorganisms. *Nat. Rev. Microbio.*, 4(7):497–508, 2006.

[29] N.S. Malvankar and D.R. Lovley. Microbial nanowires: a new paradigm for biological electron transfer and bioelectronics. *ChemSusChem*, 5(6):1039–46, 2012.

[30] D.R. Lovley and N.S. Malvankar. Seeing is believing: novel imaging techniques help clarify microbial nanowire structure and function. *Environ Microbiol*, 17(7):2209–15, 2015.

[31] A.A. Tseng, K. Chen, C.D. Chen, and K.J. Ma. Electron beam lithography in nanoscale fabrication: recent development. *IEEE Transactions on Electronics Packaging and Manufacturing*, 26(2):141–149, 2003.

[32] EPFL. Resists for liftoff, April 2016.

[33] R.Y. Adhikari, N.S. Malvankar, M.T. Tuominen, and D.R. Lovley. Conductivity of individual geobacter pili. *RSC Adv.*, 6:8354–8357, 2016.

[34] N.S. Malvankar, M.T. Tuominen, and D.R. Lovley. Biofilm conductivity is a decisive variable for high-current-density geobacter sulfurreducens microbial fuel cells. *Energy Environ. Sci.*, 5(2):5790, 2012.

[35] C. Leang, N.S. Malvankar, A.E. Franks, K. P. Nevin, and D.R. Lovley. Engineering geobacter sulfurreducens to produce a highly cohesive conductive matrix with enhanced capacity for current production. *Energy Environ. Sci.*, 6:1901–1908, 2013.

[36] Keithley Instruments, Inc. *Optimizing Low Current Measurements with Model 4200-SCS Semiconductor Characterization System.* Keithley Application Note Series.

[37] T.W. Ebbesen, H.J. Lezec, H. Hiura, J.W. Bennett, H.F. Ghaemi, and T. Thio. Electrical conductivity of individual carbon nanotubes. *Nature*, 382:54–56, 1996.

[38] Yan. H., C. Chuang, A. Zhugayevych, S. Tretiak, F.W. Dahlquist, and G.C. Bazan. Inter-aromatic distances in geobacter sulfurreducens pili relevant to biofilm charge transport. *Adv Mater*, 27(11):1908–11, 2015.

[39] P.S. Bonanni, D. Massazza, and J.P. Busalmen. Stepping stones in the electron transport from cells to electrodes in geobacter sulfurreducens biofilms. *Phys Chem Chem Phys*, 15(25):10300–6, 2013.

[40] P.N. Reardon and K.T. Muelle. Structure of the type iva major pilin from the electrically conductive bacterial nanowires of geobacter sulfurreducens. *J Biol Chem*, 288(41):29260–6, 2013.

[41] G.T. Feliciano, A.J.R. da Silva, G. Reguera, and E. Artacho. Molecular and electronic structure of the peptide subunit of geobacter sulfurreducens conductive pili from first principles. *J Phys Chem A*, 116(30):8023–30, 2012.

[42] R.H. Baughman, J.L. Bredas, R.R. Chance, R.L. Elsenbaumer, and L.W. Shacklette. Structural basis for semiconducting and metallic polymer/dopant systems. *Chemical Reviews*, 82(2):209–222, 1982.

[43] A.G. MacDiarmid. 'synthetic metals': A novel role for organic polymer (nobel lecture). *Angew. Chem.*, 40:2581–2590, 2001.

[44] D.R. Lovley. Electromicrobiology. *Annu. Rev. Microbiol*, 66:391–409, 2012.

[45] N.S. Malvankar and D.R. Lovley. Microbial nanowires for bioenergy applications. *Current Opinion in Biotechnology*, 27:88–95, 2014.

[46] Y. Li and H. Li. Type iv pili of acidithiobacillus ferrooxidans can transfer electrons from extracellular electron donors. *J. Basic Microbiol.*, 54(3):226–31, 2014.

[47] L. Castro, M. Vera, J.. Muoz, M.L. Blzquez, F. Gonzlez, W. Sand, and A. Ballester. Aeromonas hydrophila produces conductive nanowires. *Res Microbiol.*, 165(9):794–802, 2014.

[48] M.Y. El-Naggara, G. Wangerb, K.M. Leung, T.D. Yuzvinsky, G. Southame, J. Yang, W.M. Lau, K.H. Nealson, and Y.A. Gorby. Electrical transport along bacterial nanowires from shewanella oneidensis mr-1. *PNAS*, 107(42):18127–18131, 2010.

[49] S. Pirbadian, S.E. Barchinger, K.M. Leung, H.S. Byun, Y. Jangir, R.A. Bouhenni, S.B. Reed, M.F. Romine, D.A. Saffarini, L. Shi, Y.A. Gorby, J.H. Golbeck, and M.Y. El-Naggar. Shewanella oneidensis mr-1 nanowires are outer membrane and periplasmic extensions of the extracellular electron transport components. *PNAS*, 111(35):12883–12888, 2014.

[50] A.C. Dohnalkova, M.J. Marshall, B.W. Arey, K. H. Williams, E.C. Buck, and J.K. Fredrickson. Imaging hydrated microbial extracellular polymers: Comparative analysis by electron microscopy. *Appl. Environ. Microbiol.*, 77(4):1254–1262, 2011.

[51] Adam Daire. *An Improved Method for Differential Conductance Measurements*. Keithley Instruments, Inc, 2005. Keithley Application Note Series.

[52] C. Shlizerman, A. Atanassov, I. Berkovich, G. Ashkenasy, and N. Ashkenasy. De novo designed coiled-coil proteins with variable conformations as components of molecular electronic devices. *J. Am. Chem. Soc.*, 132(14):5070–6, 2010.

[53] K. Kitagawa, T. Morita, and S. Kimura. Electron transport properties of helical peptide dithiol at a molecular level: Scanning tunneling microscope study. *Thin Solid Films*, 509(1-1):18–26, 2006.

[54] P.K. Kienker, W.F. DeGrado, and J.D. Lear. A helical-dipole model describes the single-channel current rectification of an uncharged peptide ion channel. *Proc. Natl. Acad. Sci. USA*, 91(11):4859–63, 1994.

[55] R.M. Metzger, B. Chen, U. Ho1pfner, M.V. Lakshmikantham, D. Vuillaume, T. Kawai, X. Wu, T.V. Tachibana, H.and Hughes, H. Sakurai, J. W. Baldwin, C. Hosch, M.P. Cava, L. Brehmer, and G. J. Ashwell. Unimolecular electrical rectification in hexadecylquinolinium tricyanoquinodimethanide. *J. Am. Chem. Soc.*, 119(43):10455–10466, 1997.

[56] Carl Branden and John Tooze. *Introduction to Protein Structure*. Garland Publiching, Inc., New York, 2 edition, 1999.

[57] J. Watanabe, T. Morita, and S. Kimura. Effects of dipole moment, linkers, and chromophores at side chains on long-range electron transfer through helical peptides. *J. Phys. Chem. B.*, 109(30):14416–14425, 2005.

[58] N.S. Malvankar, M.T. Tuominen, and D.R. Lovley. Lack of cytochrome involvement in long-range electron transport through conductive biofilms and nanowires of geobacter sulfurreducens. *Energy Environ. Sci.*, 5:8651–8659, 2012.

[59] S.H. Kim, C.Y. Jung, and H. Kim. Characterization of conduction mechanism in cu schottky contacts to p-type ge. *Trans. Electr. Electron. Mater.*, 15(6):324–327, 2014.

[60] S. Lee, J.S. Lim, and S.J. Baik. Integration of carbon nanotube interconnects for full compatibility with semiconductor technologies. *J. Electrochem. Soc.*, 158(11):K193–K197, 2011.

[61] P. Dallas, D. Stamopoulos, N. Boukos, V. Tzitzios, D. Niarchos, and D. Petridis. Characterization, magnetic and transport properties of polyaniline synthesized through interfacial polymerization. *Polymer*, 48(11):3162–69, 2007.

[62] K.D. Bozdaga, N.R. Chioua, V.N. Prigodina, and A.J. Epstein. Magnetic field, temperature and electric field dependence of magneto-transport for polyaniline nanofiber networks. *Synthethic Metals*, 160(3):271–274, 2010.

[63] W. Wu, G.Y. Jung, D.L. Olynick, J. Straznicky, Z. Li, X. Li, D.A.A. Ohlberg, Y. Chen, S.Y. Wang, J.A. Liddle, W.M. Tong, and R. S. Williams. One-kilobit cross-bar molecular memory circuits at 30-nm half-pitch fabricated by nanoimprint lithography. *Applied Physics A*, 80:1173–1178, 2005.

[64] G.Y. Jung, S. Ganapathiappan, D.A.A. Ohlberg, D.L.O. Olynick, Y. Chen, W. M. Tong, and R.S Williams. Fabrication of a 34 34 crossbar structure at 50 nm half-pitch by uv-based nanoimprint lithography. *Nano Letters*, 4:1225–1229, 2004.

[65] C. Shih, A.K. Museth, M. Abrahamsson, A.M. Blanco-Rodriguez, A.J. Di Bilio, J. Sudhamsu, B. R. Crane, K. L. Ronayne, M. Towrie, A. Vlcek Jr., J.H. Richards, J.R. Winkler, and H. B. Gray. Tryptophan-accelerated electron flow through proteins. *Science*, 320:1760–1762, 2008.

[66] N. Amdursky. Enhanced solid-state electron transport via tryptophan containing peptide networks. *Phys. Chem. Chem. Phys.*, 15:13479–13482, 2013.

[67] Y. Tan, R.Y. Adhikari, N.S. Malvankar, M.T. Tuominen, and D.R. Lovley. Synthetic biological protein nanowires with high conductivity. *Small*, 2016.

[68] Y. Nozaki and C. Tanford. The solubility of amino acids and two glycine peptides in aqueous ethanol and dioxane solutions. *The Journal of Biological Chemistry*, 246:2211–2217, 1971.

[69] P. Xua, Z. Chenga, Q. Pana, J. Xua, Q. Xianga, W. Yub, and Y. Chub. High aspect ratio in2o3 nanowires: Synthesis, mechanism and no2 gas-sensing properties. *Sensors and Actuators B*, 130:802–808, 2008.

[70] M.M. Mirza, H. Zhou, P. Velha, X. Li, K.E. Docherty, A. Samarelli, G. Ternent, and D.J. Paul. Nanofabrication of high aspect ratio (50:1) sub-10nm silicon nanowires using inductively coupled plasma etching. *J. Vac. Sci. Technol.*, 30:06FF02, 2012.

[71] L.P Johnson and J.G. Matisons. Synthesis of high aspect-ratio gold nanowires with highly porous morphology. *ISRN Nanomaterials*, 2012, 2012.

[72] H.A. Um, D.H. Lee, D.U. Heo, D.S. Yang, J. Shin, H. Baik, M.J. Cho, and D.H. Choi. High aspect ratio conjugated polymer nanowires for high performance field-effect transistors and phototransistors. *ACS Nano*, 9(5):5264–5274, 2012.

[73] W.I. Park, G. Zheng, X. Jiang, B. Tian, and C.M. Lieber. Controlled synthesis of millimeter-long silicon nanowires with uniform electronic properties. *Nano Letters*, 8(9):3004–3009, 2008.

[74] P. Tran, B. Alavi, and G. Gruner. Charge transport along the lambda-dna double helix. *Physical Review Letters*, 85(7):1564–1567, 2000.

[75] J. M. Kinsella and A. Ivanisevic. Dna-templated magnetic nanowires with different compositions: Fabrication and analysis. *Langmuir*, 23:3886–3890, 2007.

[76] A. Houlton, A.R. Pike, M.A. Galindo, and B.R. Horrocks. Dna-based routes to semiconducting nanomaterials. *Chem. Commun.*, pages 1797–1806, 2009.

[77] Y. Ma, J. Zhang, G. Zhang, and H. He. Polyaniline nanowires on si surfaces fabricated with dna templates. *J. Am. Chem. Soc.*, 126(22):7097–7101, 2004.

[78] H. Nakao, H. Hayashi, F. Iwata, H. Karasawa, K. Hirano, S. Sugiyama, and T. Ohtani. Fabricating and aligning -conjugated polymer-functionalized dna nanowires: atomic force microscopic and scanning near-field optical microscopic studies. *Langmuir*, 21(17):7945–7950, 2005.

[79] R. Mohammadzadegan, H. Mohabatkar, M.H. Sheikhi, A. Safavi, and M.B. Khajouee. Dna-templated gold nanowires. *Physica E*, 41:142–145, 2008.

[80] H. Nakao, H. Shiigi, Y. Yamamoto, S. Tokonami, T. Nagaoka, S. Sugiyama, and T. Ohtani. Highly ordered assemblies of au nanoparticles organized on dna. *Nano Letters*, 3(10):1391–1394, 2003.

[81] H. Nakao, S. Tokonami, T. Hamada, H. Shiigi, T. Nagaoka, F. Iwata, and Y. Takeda. Direct observation of one-dimensional plasmon coupling in metallic nanofibers prepared by evaporation-induced self-assembly with dna. *Nanoscale*, 4(21):6814–6822, 2012.

[82] A. Lakshmanan, S. Zhang, and C.A.E. Hauser. Short self-assembling peptides as building blocks for modern nanodevices. *Trends in Biotechnology*, 30(3):155–165, 2012.

[83] C. Chen and N.L. Rosi. Peptide-based methods for the preparation of nanostructured inorganic materials. *Angew. Chem. Int. Ed.*, 49(11):1924 1942, 2010.

[84] R.d.l. Rica, E. Mendoza, and H. Matsui. Bioinspired target-specific crystallization on peptide nanotubes for ultrasensitive pb ion detection. *Angew. Chem. Int. Ed.*, 49(11):1924 1942, 2010.

[85] A.S. Blum, C.M. Soto, K.E. Sapsford, C.D. Wilson, M.H. Moore, and B.R. Ratna. Molecular electronics based nanosensors on a viral scaffold. *Biosensors and Bioelectronics*, 26:2852 2857, 2011.

[86] S.J. Tans, M.H. Devoret, H. Dai, A. Thess, R.E. Smalley, L.J. Geerligs, and C. Dekker. Individual single-wall carbon nanotubes as quantum wires. *Nature*, 386:474–477, 1997.

[87] X. Guo, A.A. Gorodetsky, J. Hone, J.K. Barton, and C. Nuckolls. Conductivity of a single dna duplex bridging a carbon nanotube gap. *Nature Nanotechnology*, 3:163–167, 2008.

[88] G.I. Livshits, A. Stern, D. Rotem, N. Borovok, G. Eidelshtein, A. Migliore, E. Penzo, S.J. Wind, R.D. Felice, S.S. Skourtis, J.C. Cuevas, L. Gurevich, A.B. Kotlyar, and D. Porath. Long-range charge transport in single g-quadruplex dna molecules. *Nature Nanotechnology*, 9:1040–1046, 2014.

[89] Y.Z. Long, M.M. Li, C. Gub, M. Wan, J.L. Duvail, Z. Liu, and Z. Fan. Recent advances in synthesis, physical properties and applications of conducting polymer nanotubes and nanofibers. *Progress in Polymer Science*, 36:1415–1442, 2011.

[90] A. Care, P.L. Bergquist, and A. Sunna. Solid-binding peptides: smart tools for nanobiotechnology. *Trends in Biotechnology*, 33(5):259–268, 2015.

[91] P.Q. Nguyen, Z. Botyanszki, P.K.R. Tay, and N. Joshi. Programmable biofilm-based materials from engineered curli nanofibres. *Nature Communications*, 5:4945, 2014.

[92] W. Zhao, F. Liu, Y. Chen, J. Bai, and W. Gao. Synthesis of well-defined proteinepolymer conjugates for biomedicine. *Polymer*, 66:A1–A10, 2015.

[93] A.E. Rotarua, P.M. Shresthaa, F. Liua, B. Markovaitea, S. Chena, K.P. Nevin, and D.R. Lovley. Direct interspecies electron transfer between geobacter metallireducens and methanosarcina barkeri. *Appl. Environ. Microbiol.*, 80(15):4599–4605, 2014.

[94] Y. Tan, R.Y. Adhikari, N.S. Malvankar, J.E. Ward, K.P. Nevin, T.L. Woodard, J.A. Smith, A.E. Franks, M.T. Tuominen, and D.R. Lovley. The low conductivity of geobacter uraniireducens pili suggests a diversity of extracellular electron transfer mechanisms in the genus geobacter. *Frontiers in Microbiology*, 7:980, 2016.

[95] D.R. Lovley. Live wires: direct extracellular electron exchange for bioenergy and the bioremediation of energy-related contamination. *Energy Environ. Sci.*, 4:4896–4906, 2011.

[96] D.R. Lovley. Voltammetry and growth physiology of geobacter sulfurreducens biofilms as a function of growth stage and imposed electrode potential. *Electroanalysis*, 22(7-8):865–874, 2010.

[97] J.R. Lloyd, C. Leang, A.L.H. Myerson, M.V. Coppi, S. Cuifo, B. Methe, S.J. Sandler, and D.R. Lovely. Biochemical and genetic characterization of ppca, a periplasmic c-type cytochrome in geobacter sulfurreducens. *Biochem. J.*, 369:153–161, 2003.

[98] D.R. Lovley, T. Ueki, T. Zhang, N.S. Malvankar, P.M. Shrestha, K.A. Flanagan, M. Aklujkar, J.E. Butler, L. Giloteaux, A.E. Rotaru, D.E. Holmes, A.E. Franks, R. Orellana, C. Risso, and K.P. Nevin. Geobacter: the microbe electric's physiology, ecology, and practical applications. *Adv. Microb. Physiol.*, 59:1–100, 2011.

[99] Z.M. Summers, H.E. Fogarty, C. Leang, A.E. Franks, N.S. Malvankar, and D.R. Lovley. Direct exchange of electrons within aggregates of an evolved syntrophic coculture of anaerobic bacteria. *Science*, 330:1413 – 1415, 2010.

[100] Z.M. Summers, H.E. Fogarty, C. Leang, A.E. Franks, N.S. Malvankar, and D.R. Lovley. Direct exchange of electrons within aggregates of an evolved syntrophic coculture of anaerobic bacteria. *Science*, 330(6009):1413–1415, 2010.

[101] D.R. Bond and D.R. Lovley. Evidence for involvement of an electron shuttle in electricity generation by geothrix fermentans. *Appl. Environ. Microbiol.*, 71(4):2186–2189, 2005.

[102] N.J. Kotloskia and J.A. Gralnick. Flavin electron shuttles dominate extracellular electron transfer by shewanella oneidensis. *Appl. Environ. Microbiol.*, 4:e00553–12, 2013.

[103] A.E. Rotaru, T.L. Woodard, K.P. Nevin, and D.R. Lovley. Link between capacity for current production and syntrophic growth in geobacter species. *Front. Microbiol.*, 6:744, 2015.

[104] A.E. Rotaru, P.M. Shrestha, F. Liu, B. Marovaite, S. Chen, K.P. Nevin, and D.R. Lovley. Direct interspecies electron transfer between geobacter metallireducens and methanosarcina barkeri. *Appl. Environ. Microbiol.*, 80(15):4599–4605, 2014.

[105] L.Y. Wang, K.P. Nevin, T.L. Woodard, B.Z. Mu, and D.R. Lovley. Expanding the diet for diet: Electron donors supporting direct interspecies electron transfer (diet) in defined co-cultures. *Front. Microbiol.*, 7:236, 2016.

[106] X. Chena, L. Shenb, C.A. Yuanc, C.K.Y. Wong, and G. Zhang. Molecular model for the charge carrier density dependence of conductivity of polyaniline as chemical sensing materials. *Sensors and Actuators B*, 77:856–861, 2013.

[107] A.M. Katzenmeyer, F. Leonard, A.A. Talin, M.E. Toimil-Molares, J.G. Cederberg, J.Y. Huang, and J.L. Lensch-Falk. Observation of space-charge-limited transport in inas nanowires. *IEEE Transactions on Nanotechnology*, 10:1, 2011.

[108] M. Meyyappan and Mahendra Sunkara. *Inorganic Nanowires: Applications, Properties and Characterization*. CRC Press, Boca Raton, Florida, 2009.

[109] Y. Li and J.B. Lagowski. Charge carrier mobility in conjugated organic polymers case studies using multi-step computational approach. *Polymer*, 52(21):48414850, 2011.

[110] L. Kindera, J. Kanickia, and P. Petroffa. Structural ordering and enhanced carrier mobility in organic polymer thin film transistors. *Synthetic Metals*, 146(2):181–185, 2004.

[111] A.C. Prior. The field-dependence of carrier mobility in silicon and germanium. *Journal of Physics and Chemistry of Solids*, 12(2):175–180, 1960.

[112] I. McCulloch, M. Heeney, C. Bailey, K. Genevicius, I. MacDonald, M. Shkunov, D. Sparrowe, S. Tierney, R. Wagner, W. Zhang, M.L. Chabinyc, R.J. Kline, M.D. McGehee, and M.F. Toney. Liquid-crystalline semiconducting polymers with high charge-carrier mobility. *Nature Materials*, 5:328–333, 2006.

[113] H. Dong, X. Fu, J. Liu, Z. Wang, and W. Hu. 25th anniversary article: Key points for high-mobility organic field-effect transistors. *Advanced Materials*, 25:6158–6183, 2013.

[114] T. Lei, J.H. Dou, and J. Pei. Influence of alkyl chain branching positions on the hole mobilities of polymer thin-film transistors. *Advanced Materials*, 24:6457–6461, 2012.

[115] T.O. Yeates and S.B.H. Kent. Racemic protein crystallography. *Annual Review of Biophysics*, 41:41–61, 2012.

[116] L. Slabinski, L. Jaroszewski, A.P.C. Rodrigues, L. Rychlewski, I.A.W. Wilson, S.A. Lesley, and A. Godzik. The challenge of protein structure determination - lessons from structural genomics. *Protein Science*, 16(11):2472–2482, 2007.

[117] P.N. Reardon and K.T. Mueller. Structure of the type iva major pilin from the electrically conductive bacterial nanowires of geobacter sulfurreducens. *The Journal of Biological Chemistry*, 288(41):29260–29266, 2013.

[118] K. Lee, S. Cho, S.H. Park, A.J. Heeger, C.W. Lee, and S.H. Lee. Metallic transport in polyaniline. *Nature*, 441:65–68, 2006.

[119] C. Janiak. A critical account on pi-pi stacking in metal complexes with aromatic nitrogen-containing ligands. *J. Chem. Soc., Dalton Trans.*, page 38853896, 2000.

[120] X. Qian, T. Mester, L. Morgado, T. Arakawa, M.L. Sharma, K. Inoue, C. Joseph, C.A. Salgueiro, M.J. Maroney, and D.R. Lovley. Biochemical characterization of purified omcs, a c-type cytochrome required for insoluble fe(iii) reduction in geobacter sulfurreducens. *Biochimica et Biophysica Acta*, 1807:404412, 2011.

[121] F.X. Schmid. *Biological Macromolecules: UV-visible Spectrophotometry*. Encyclopedia of Life Sciences. Macmillan Publishers Ltd, 2001.

[122] N. Ghobadi. Band gap determination using absorption spectrum fitting procedure. *International Nano Letters*, 3(2), 2013.

[123] Joshua A. Russell. Measurement of optical bandgap energies of semiconductors. M.s. thesis, Oregon State University, 2011.

[124] M.D. Scafetta, A.M. Cordi, J.M. Rondinelli, and S.J. May. Band structure and optical transitions in lafeo3: theory and experiment. *J. Phys.: Condens. Matter*, 26:505502, 2014.

[125] S. Sarkar, N.S. Das, and K.K. Chattopadhyay. Optical constants, dispersion energy parameters and dielectric properties of ultra-smooth nanocrystalline bivo4 thin films prepared by rf-magnetron sputtering. *Solid State Sciences*, 33:5866, 2014.

[126] UC Davis SolarWiki. Indirect semiconductors, May 2016.

[127] A. Li. Interaction of nanoparticles with radiation. In A.N. Witt, G.C. Clayton, and B.T. Draine, editors, *Astrophysics of Dust*, volume 000, 2003.

[128] H. P. D. Lanyon and R. A. Tuft. Bandgap narrowing in heavily doped silicon. In *Electron Devices Meeting, 1978 International*, volume 24, pages 316–319, 1978.

[129] K.F. Derggren and B.E. Sernelius. Band-gap narrowing in heavily doped many-valley semiconductors. *Physical Review B*, 24, 1981.

[130] A. Shaker and A. Zerky. A new and simple model for plasma and doping induced band gap narrowing. *Journal of Electron Devices*, 8, 2010.

[131] J.L. Bredas and G.B. Street. Organic polymers based on aromatic rings (polyparaphenylene, polypyrole, polythiophene): Evolution of the electronic properties as a function of the torsion angle between adjacent rings. *J. Chem. Phys*, 83(3):1323–1329, 2006.

[132] H. Sirringhaus. 25th anniversary article: Organic field-effect transistors: The path beyond amorphous silicon. *Adv. Mater.*, 26:1319–1335, 2014.

[133] W. Huang, K. Besar, Y. Zhang, S. Yang, G. Wiedman, Y. Liu, W. Guo, J. Song, K., Hemker, K. Hristova, I.J. Kymissis, and H. E. Katz. A high-capacitance salt-free dielectric for self-healable, printable, and flexible organic field effect transistors and chemical sensor. *Adv. Funct. Mater.*, 25:3745–3755, 2015.

[134] C. Tanase, E.J. Meijer, P.W.M. Blom, and D.M. de Leeuw. Local charge carrier mobility in disordered organic field-effect transistors. *Organic Electronics*, 4:33–37, 2003.

[135] J.E. Anthony. Functionalized acenes and heteroacenes for organic electronics. *Chem. Rev.*, 106:5028–5048, 2006.

[136] C.R. Swartz, S.R. Parkin, J.E. Bullock, J.E. Anthony, A.C. Mayer, and G.G. Malliaras. Synthesis and characterization of electron-deficient pentacenes. *Org. Lett.*, 7(15):3163–3166, 2005.

[137] A.J. Apstein. Conducting polymers: Electrical conductivity. In J.E. Mark, editor, *Physical Properties of Polymers Handbook*, page 748. Springer New York, 2007.

[138] V.N. Prigodin, F.C. Hsu, J.H. Park, O. Waldmann, and A.J. Epstein. Electron-ion interaction in doped conducting polymers. *Physical Review B*, 78:035203, 2008.

[139] P. Kukic, D. Farrell, L.P. McIntosh, B. Garcia-Moreno E., K.S. Jensen, Z. Toleikis, K. Teilum, and J.E. Neilsen. Protein dielectric constants determied from nmr chemical shift perturbations. *J. Am. Chem. Soc.*, 135:16968–16976, 2013.

[140] V.N. Prigodin, F.C. Hsu, Y.M. Kim, J.H. Park, O. Waldmann, and A.J. Epstein. Electric field control of charge transport in doped polymers. *Syntheic Metals*, 153:157–160, 2005.

[141] F.C. Hsu, V.N. Prigodin, and A.J. Epstein. Electric-field-controlled conductance of metallic polymers in a transistor structure. *Physical Review B*, 74:235219, 2006.

[142] P. Trand, B. Alavi, and G. Gruner. Charge transport along the lambda-dna double helix. *Physics Review Letters*, 85(7):1564–1567, 2000.

[143] F.A. Hegmann, R.R. Tykwinski, K.P.H. Lui, J.E. Bullock, and J.E. Anthony. Picosecond transient photoconductivity in functionalized pentacene molecular crystals probed by terahertz pulse spectroscopy. *Physics Review Letters*, 89(22):227403, 2002.

[144] J.A. Reedijk, H.C.F. Martens, H.B. Brom, and M.A.J. Michels. Dopant-induced crossover from 1d to 3d charge transport in conjugated polymers. *Physics Review Letters*, 83(19):3904–3907, 1999.

[145] K. Lee and A.J. Heeger. Optical investigation of intra and interchain charge dynamics in conducting polymers. *Synthetic Metals*, 128:279–282, 2002.

[146] K. Lee, S. Cho, S.H. Park, A.J. Heeger, C.W. Lee, and S.H. Lee. Metallic transport in polyaniline. *Nature*, 441:65–68, 2006.

[147] L.T. Ngo, D. Almecija, J.E. Sader, B. Daly, N. Petkov, J.D. Holmes, D. Erts, and J.J. Boland. Ultimate-strength germanium nanowires. *Nano Letters*, 6(12):2964–2968, 2006.

[148] Y.S. Sohn, J. Park, G. Yoon, J. Song, S.W. Jee, J.H. Lee, S. Na, T. Kwon, and K. Eom. Mechanical properties of silicon nanowires. *Nanoscale Res. Lett.*, 5(1):211–216, 2010.

[149] S. Lampa-Pastrik, J.P. Veazey, K.A. Walsh, G.T. Feliciano, R.J. Steidl, S.H. Tessmer, and G. Reguera. Thermally activated charge transport in microbial protein nanowires. *Scientific Reports*, 6:23517, 2016.

[150] F. Chen, J. Xia, D.K. Ferry, and N. Tao. Dielectric screeing enhances performance in graphene fet. *Nano Letters*, 9(7):2571–2574, 2009.

[151] AK.M. Newaz, Y.S. Puzyrev, B. Wang, S.T. Pantelides, and K.I. Bolotin. Probing charge scattering mechanisms in suspended graphene by varying its dielectric environment. *Nature Communications*, 3(734), 2012.

[152] C.M. Hangarter and N.V. Myung. Magnetic alignment of nanowires. *Chem. Mater.*, 17:1320–1324, 2005.

[153] J.K. Park, O.P. Kwon, E.Y. Choi, C.K. Jung, and S.H. Lee. Enhanced electrical conductivity of polyaniline film by a low magnetic field. *Synthetic Metals*, 160:728–731, 2010.

[154] R.J.A. Hill, V.L. Sedman, S. Allen, P.M. Williams, M. Paoli, L.A. Abramovich, E. Gazit, L. Eaves, and S.J.B. Tendler. Alignment of aromatic peptide tubes in strong magnetic field. *Advanced Materials*, 19:4474–4479, 2007.

[155] N.S. Malvankar. *Investigation of electron transport and storage mechanism in microbial biofilms*. PhD thesis, University of Massachusetts Amherst, 2010.

[156] R. Krupke, F. Hennrich, H.B. Weber, M.M. Kappes, and H.V. Lohneysen. Simultaneous deposition of metallic bundles of single walled carbon nanotubes using ac-dielectrophoresis. *Nano Letter*, 3(8):1019–1023, 2003.

[157] C.L. Asbury, A.H. Diercks, and G.V.D. Engh. Trapping of dna by dielectrophoresis. *Electrophoresis*, 23:2658–2666, 2002.

[158] C.F. Chou, J.O. Tegenfeldt, O. Bakajin, S.S. Chan, E.C. Cox, N. Darnton, T. Duke, and R.H. Austin. Electrodeless dielectrophoresis of single and double stranded dna. *Biophysical Journal*, 83(4):2170–2179, 2002.

[159] J. Castillo, S. Tanzi, M. Dimaki, and W. Svendsen. Manipulation of self-assembly amyloid peptide nanotubes by dielectrophoresis. *Electrophoresis*, 29:5026–5032, 2008.